



seit 1558

QED CORRECTIONS TO THE HYPERFINE
SPLITTING AND g FACTOR OF
FEW-ELECTRON IONS

DISSERTATION

zur Erlangung des akademischen Grades
doctor rerum naturalium (Dr. rer. nat.)

vorgelegt dem Rat der
PHYSIKALISCH-ASTRONOMISCHEN FAKULTÄT
der
FRIEDRICH-SCHILLER-UNIVERSITÄT JENA

von

M. Sc. Valeriia Kosheleva

geboren am 14.12.1993 in Arkhangelsk

GUTACHTER:

1. Prof. Dr. Stephan Fritzsche (Friedrich-Schiller-Universität Jena)
2. PD Dr. Zoltán Harman (Max-Planck-Institut für Kernphysik (MPIK))
3. Prof. Dr. Andrzej Czarnecki (University of Alberta)

TAG DER DISPUTATION: 28. Juni 2022

ABSTRACT

Quantum electrodynamics (QED) is the first quantum field theory that describes all phenomena associated with electrically charged particles. Despite its mathematical complexity, it is quite effective in describing and predicting experimental results. With the introduction of lasers, atomic spectroscopy is constantly evolving, contributing to QED testing and continuous improvements in the precision of physical constants determination. Atomic systems offer many opportunities for high-precision QED tests. In the present dissertation, we focus on the magnetic sector of QED: the hyperfine structure and the Zeeman effect in few-electron ions.

We present the systematic QED treatment of the electron correlation effects in the ground-state hyperfine structure in lithiumlike ions for the wide range of nuclear charge numbers $Z = 7 - 82$. The one- and two-photon exchange corrections are evaluated rigorously within the QED formalism. The electron-correlation contributions due to the exchange by three and more photons are accounted for within the Breit approximation employing the recursive perturbation theory. The calculations are performed in the framework of the extended Furry picture, i.e., with the inclusion of the effective local screening potential in the zeroth-order approximation. In comparison to previous theoretical computations, we improve the accuracy of the interelectronic-interaction correction to ground-state hyperfine structure in lithiumlike ions.

The g factor of a bound electron is a rigorous tool for verifying the Standard Model and searching for new physics. Recently, a measurement of the g factor for lithiumlike silicon was reported and it disagrees by 1.7σ with theoretical prediction [D. A. Glazov *et al.*, *Phys. Rev. Lett.* **123**, 173001 (2019)]. Attempting to resolve this deviation another theoretical value for silicon has been delivered. It results in a 5σ disagreement with experimental value [V. A. Yerokhin *et al.*, *Phys. Rev. A* **102**, 022815 (2020)]. We perform large-scale high-precision computations of the interelectronic-interaction and many-electron QED corrections to determine the cause of this disagreement. Similar to the case of hyperfine splitting, we carry out the calculations within the extended Furry picture of QED. And we carefully analyze the final values' dependence on the binding potential. As a result, the agreement between theory and experiment for the g factor of lithiumlike silicon improves significantly. We also present the most accurate theoretical prediction for lithiumlike calcium too, which perfectly agrees with the experimental value.

ZUSAMMENFASSUNG

Die Quantenelektrodynamik (QED), die erste Quantenfeldtheorie, beschreibt alle Phänomene, die mit elektrisch geladenen Teilchen verbunden sind. Trotz ihrer mathematischen Komplexität ist sie sehr effektiv bei der Beschreibung und Vorhersage experimenteller Ergebnisse. Mit der Einführung von Lasern entwickelt sich die Atomspektroskopie ständig weiter und trägt zur Überprüfung der QED und zur kontinuierlichen Verbesserung der Präzision der Bestimmung physikalischer Konstanten bei. Atomare Systeme bieten viele Möglichkeiten für hochpräzise QED-Tests. In der vorliegenden Dissertation konzentrieren wir uns auf den magnetischen Sektor der QED: die Hyperfeinstruktur und den Zeeman-Effekt in Ionen mit wenigen Elektronen.

Wir präsentieren die systematische QED-Behandlung der Elektronenkorrelationseffekte in der Grundzustands-Hyperfeinstruktur in lithiumähnlichen Ionen für den weiten Bereich der Kernladungszahl $Z = 7 - 82$. Die Ein- und Zwei-Photonen-Austauschkorrekturen werden im Rahmen des QED-Formalismus rigoros bewertet. Die Beiträge der Elektronenkorrelation aufgrund des Austausches von drei und mehr Photonen werden innerhalb der Breit-Approximation unter Verwendung der rekursiven Störungstheorie berücksichtigt. Die Berechnungen werden im Rahmen des erweiterten Furry-Bildes durchgeführt, d.h. unter Einbeziehung des effektiven lokalen Abschirmungspotentials in der Näherung nullter Ordnung. Im Vergleich zu früheren theoretischen Berechnungen verbessern wir die Genauigkeit der interelektronischen Wechselwirkungskorrektur der Hyperfeinstruktur im Grundzustand in lithiumähnlichen Ionen.

Der g -Faktor eines gebundenen Elektrons ist ein rigoroses Werkzeug zur Überprüfung des Standardmodells und bei der Suche nach neuer Physik. Kürzlich wurde eine Messung des g -Faktors für lithiumähnliches Silizium berichtet, die mit der theoretischen Vorhersage um 1.7σ nicht übereinstimmt [D. A. Glazov *et al.*, *Phys. Rev. Lett.* **123**, 173001 (2019)]. Bei dem Versuch, diese Abweichung zu beheben, wurde ein weiterer theoretischer Wert für Silizium geliefert. Dieser führt zu 5σ Abweichung von dem experimentellen Wert [V. A. Yerokhin *et al.*, *Phys. Rev. A* **102**, 022815 (2020)]. Wir führen groß angelegte hochpräzise Berechnungen der interelektronischen Wechselwirkung und Viel-Elektronen-QED-Korrekturen durch, um die Ursache dieser Abweichung zu bestimmen. Ähnlich wie bei der Hyperfeinaufspaltung führen wir die Berechnungen innerhalb des erweiterten Furry-Bildes der QED durch. Zudem

analysieren wir sorgfältig die Abhängigkeit der Ergebnisse vom Bindungspotential. Als Resultat wurde die Übereinstimmung zwischen Theorie und Experiment für den g-Faktor lithiumähnlichen Siliziums signifikant verbessert. Zusätzlich präsentieren wir die bisher genaueste theoretische Vorhersage für lithiumähnliches Calcium, die perfekt mit dem experimentellen Wert übereinstimmt.

PUBLICATIONS

The list of publications which have been prepared during period of my PhD study is presented below.

- *Ground-state hyperfine splitting of B-like ions in the high-Z region*
D. A. Glazov, A. V. Volotka, O. V. Andreev, **V. P. Kosheleva**, S. Fritzsche, V. M. Shabaev, G. Plunien, and Th. Stöhlker
Phys. Rev. A **99**, 062503 (2019).
- *Atomic processes with twisted electrons*
V. A. Zaytsev, A. Surzhykov, V. G. Serbo, **V. P. Kosheleva**, M. E. Groshev, V. A. Yerokhin, V. M. Shabaev, and Th. Stöhlker
J. Phys.: Conf. Ser. **1412**, 052013 (2020).
- *Many-electron effects in the hyperfine splitting of lithiumlike ions*
V. P. Kosheleva, A. V. Volotka, D. A. Glazov, and S. Fritzsche
Phys. Rev. Research **2**, 013364 (2020).
- *Resonant two-photon ionization of atoms by twisted and plane-wave light*
V. P. Kosheleva, V. A. Zaytsev, R. A. Müller, A. Surzhykov, and S. Fritzsche
Phys. Rev. A **102**, 063115 (2020).
- *Redefined vacuum approach and gauge-invariant subsets in two-photon-exchange diagrams for a closed-shell system with a valence electron*
R. N. Soguel, A. V. Volotka, E. V. Tryapitsyna, D. A. Glazov, **V. P. Kosheleva**, and S. Fritzsche
Phys. Rev. A **103**, 042818 (2021).
- *g Factor of Lithiumlike Silicon and Calcium: Resolving the Disagreement between Theory and Experiment*
V. P. Kosheleva, A. V. Volotka, D. A. Glazov, D. V. Zinenko, and S. Fritzsche
accepted for publication in Phys. Rev. Lett. (2022); arXiv:2201.00612.
- *Electron-correlation effects in the g factor of lithiumlike ions*
V. P. Kosheleva, D. V. Zinenko, A. V. Volotka, D. A. Glazov, and S. Fritzsche
in preparation.

Посвящается моим родителям
Кошелевой Елене Александровне и Кошелеву Павлу Витальевичу.

CONTENTS

1	INTRODUCTION	1
1.1	Notations and conventions	6
2	FREE FIELDS IN A FURRY PICTURE	9
3	BOUND-STATE QED IN EXTERNAL FIELD APPROXIMATION	17
3.1	Interacting fields	17
3.2	Time-evolution operator	20
3.3	S-matrix formalism	21
3.3.1	Adiabatic S-matrix formalism of Gell-Mann, Low, and Sucher	22
3.4	Green's function and S-matrix of bound-state QED theory	25
3.4.1	One-particle Green's function: Exact electron and photon propagators	26
3.4.2	N-particle Green's function: two-time Green's function formalism	27
4	HYPERFINE STRUCTURE IN LITHIUMLIKE IONS	39
4.1	The hyperfine splitting in the lowest-order approximation	39
4.2	Electron correlation effects	42
4.2.1	Zeroth-order contribution	44
4.2.2	First-order contribution	45
4.2.3	Second-order contribution	46
4.2.4	Third- and higher-order contributions	50
4.3	Results and discussions	53
5	g FACTOR OF LITHIUMLIKE $^{28}\text{Si}^{11+}$ AND $^{40}\text{Ca}^{17+}$	61
5.1	Theory	61
5.2	Third-order correction $\Delta g^{(3+)}$: estimation of the higher order part $\Delta g_{\text{H}}^{(3+)}$	64
5.3	Interelectronic interaction: calculation	65
5.4	Interelectronic interaction: results	67
5.5	QED corrections: calculation	68
5.6	QED corrections: results	71
5.7	Total results and discussions	71
6	CONCLUSIONS AND OUTLOOK	75
7	APPENDIX	87
7.1	Three-electron contribution $X_{3\text{el}}^{(2)}$	87
7.2	Two-electron contribution $X_{2\text{el}}^{(2)}$	89

7.3	Reducible contribution $\chi_{\text{red}}^{(2)}$	90
7.4	Counterterm contribution $\chi_{\text{ct}}^{(2)}$	97
	DECLARATION	98
	Curriculum Vitae	101

LIST OF FIGURES

Figure 3.1	The N-particle two-time Green's function G is the amplitude for going from one state of N particles to another state. Here $N = 3$ and $G \equiv G(t', \mathbf{x}'_1, \mathbf{x}'_2, \mathbf{x}'_3; t, \mathbf{x}_1, \mathbf{x}_2, \mathbf{x}_3)$	28
Figure 4.1	Feynman diagrams representing the one-photon exchange correction to the hfs within the framework of the extended Furry picture. The photon propagator is indicated by the wavy line. The electron propagator in the effective potential V^{eff} is shown by the triple line. The magnetic interaction $\delta V = H_\mu$ is represented by the dashed line that ends with a triangle. The extra interaction term associated with the screening potential counterterm $-V^{\text{scr}}$ is represented by the symbol \otimes	45
Figure 4.2	Feynman diagrams illustrating the three-electron contribution to the two-photon-exchange correction $X_{3\text{el}}^{(2)}$ to the hfs. The notations are identical to those shown in Fig. 4.1	48
Figure 4.3	Feynman diagrams illustrating the two-electron part of the two-photon-exchange correction $X_{2\text{el}}^{(2)}$ to the hfs. The notations are identical to those shown in Fig. 4.1	48
Figure 4.4	Feynman diagrams illustrating the counterterm part of the two-photon-exchange correction $X_{\text{counterterms}}^{(2)}$ to the hfs, which appear in the framework of the extended Furry picture only. The notations are identical to those shown in Fig. 4.1	49
Figure 4.5	The two-photon-exchange correction $X_a^{(2)}$ to the ground-state hfs in Li-like ions scaled by a factor Z^2 as a function of the nuclear charge number Z . The rigorous QED calculation results (solid magneta) are compared to the Breit approximation calculations: no-pair (Breit _{no-ee+} , red dashed) and one-pair (Breit _{one-ee+} , dark blue dash-dotted). The Kohn-Sham starting potential is used to obtain all values.	56
Figure 5.1	Feynman diagrams illustrating the screened self-energy correction to the bound-electron g factor. The counterterm diagrams are shown in the second line. The notations are identical to those shown in Fig. 4.1 The only difference is that now the magnetic interaction δV is equal to the V^{magn} , i.e. $\delta V = V^{\text{magn}}$	69

Figure 5.2 Feynman diagrams illustrating the screened vacuum-polarization correction to the bound-electron g factor. The counterterm diagrams are shown in the second line. The notations are identical to those shown in Fig. 4.1. The only difference is that now the magnetic interaction δV is equal to the V^{magn} , i.e. $\delta V = V^{\text{magn}}$. 70

Figure 5.3 Theoretical (squares) and experimental (circles) g -factor values for Li-like silicon reported in this and previously published works. 73

Figure 5.4 Theoretical (squares) and experimental (circles) g -factor values for Li-like calcium reported in this and previously published works. 73

LIST OF TABLES

Table 4.1	Interelectronic-interaction contributions to the ground-state hfs in Li-like $^{15}\text{N}^{4+}$ with various starting potentials: Coulomb, Core-Hartree, and Kohn-Sham, in terms of X_a , defined by Eq. (4.19).	54
Table 4.2	Contributions to the ground-state hfs in Li-like $^{98}\text{Tc}^{40+}$ with different starting potentials: Coulomb, core-Hartree, and Kohn-Sham, in terms of X_a , as defined by Eq. (4.19).	54
Table 4.3	Contributions to the ground-state hfs in Li-like $^{209}\text{Pb}^{79+}$ with different starting potentials: Coulomb, core-Hartree, and Kohn-Sham, in terms of X_a , as defined by Eq. (4.19).	55
Table 4.4	Comparison of the one- $[X_a^{(1)}]$ and two-photon exchange $[X_a^{(2)}]$ corrections to the ground-state hfs in Li-like ions calculated using the rigorous QED approach and the Breit approximations: no-pair ($\text{Breit}_{\text{no-}ee^+}$) and one-pair ($\text{Breit}_{\text{no-}ee^+}$), see text for details. The values are calculated using the Kohn-Sham starting potential.	57
Table 4.5	Interelectronic-interaction contributions to the ground-state hfs in Li-like ions obtained with the Kohn-Sham potential, in terms of the hfs parameter X_a defined by Eq. (4.4). In the last two columns, the total value of X_a and the Bohr-Weisskopf correction ϵ_{sph} evaluated within the homogeneous sphere model are also presented. The uncertainty of the total value (numbers in parentheses) is determined as a root-sum-square of the numerical uncertainties of the individual corrections and the unknown QED contribution of the third order in $1/Z$ estimated as $(\alpha Z)^3/Z^3$. The total values are compared with the ones from Refs. (Volotka et al., 2008; Shabaev et al., 1998).	58
Table 5.1	Interelectronic-interaction contributions Δg_{int} to the ground-state g factor of $^{28}\text{Si}^{11+}$ and $^{40}\text{Ca}^{17+}$ for various starting potentials: Coulomb, core-Hartree (CH), Kohn-Sham (KS), Dirac-Hartree (DH), and Dirac-Slater (DS), in units of 10^{-6}	67

Table 5.2	<p>QED corrections Δg_{QED} to the ground-state g factor of of $^{28}\text{Si}^{11+}$ and $^{40}\text{Ca}^{17+}$ for various starting potentials: Coulomb, core-Hartree (CH), Kohn-Sham (KS), Dirac-Hartree (DH), and Dirac-Slater (DS), in units of 10^{-6}. Values for the Coulomb potential are taken from Refs. (Yerokhin et al., 2020; Yerokhin et al., 2021).</p>	72
Table 5.3	<p>Theoretical contributions to the ground-state g factor of Li-like $^{28}\text{Si}^{11+}$ and $^{40}\text{Ca}^{17+}$ ions. Total theoretical and experimental values are compared. The numbers in parentheses indicate the uncertainty of the last digit(s). All figures are significant unless an uncertainty is specified.</p>	72

INTRODUCTION

Quantum electrodynamics (QED) is a field theory that describes all of the phenomena associated with charged particles interacting via photon exchange. Since it describes the electromagnetic interaction from fundamental principles, it models other interactions included in the Standard Model of particle physics. Lamb and Retherford, [1947] discovered experimentally the difference in energy between the $2s_{1/2}$ and $2p_{1/2}$ states in hydrogen that was not predicted by the Dirac equation. This discovery marked the beginning of QED. Later, Kusch and Foley, [1948] experimentally observed the anomalous magnetic moment of the electron. As a result of these two discoveries, Bethe, [1947]; Feynman, [1949b]; Feynman, [1949a]; Schwinger, [1948a]; Schwinger, [1948b]; Schwinger, [1949b]; Schwinger, [1949a]; Tomonaga, [1946]; Koba et al., [1947a]; Koba et al., [1947b]; Dyson, [1949b]; Dyson, [1949a]; Dyson, [1952] and many others started to develop the QED theory as a physical description of the electromagnetic interaction that is consistent with both special relativity and quantum physics.

Atomic spectroscopy has advanced steadily since the invention of lasers, contributing to QED tests. Atomic systems offer a variety of possibilities for high-precision QED tests. In the present thesis we focus on the magnetic sector of QED: the hyperfine structure and the Zeeman effect in few-electron ions.

The interaction of bound electrons with the magnetic field of a nucleus with nonzero spin results in the hyperfine splitting (hfs) of atomic energy levels. The first measurements of hyperfine structure in hydrogenlike ions (Klaft et al., [1994]; Crespo López-Urrutia et al., [1996]; Crespo López-Urrutia et al., [1998]; Seelig et al., [1998]; Beiersdorfer et al., [2001]) sparked intense research into hfs in highly charged, few-electron ions. These ions offer unique opportunities to test QED in the most intense electric and magnetic fields. Indeed, in the case of hydrogenlike ^{209}Bi , the electron in the $1s$ state is exposed to a magnetic field of about 10^4 T on average. Such a magnetic field is several orders of magnitude stronger than that produced by the most powerful superconducting magnets.

We note that at the origin, the hyperfine interaction operator is singular. As a result, the hfs is extremely sensitive to the magnetization distributions of the nucleus (the so-called Bohr-Weisskopf effect). The uncertainty of the theoretical value of the hfs is

determined by a lack of understanding of nuclear characteristics, and it defines the limit for any precision QED testing. Therefore, direct comparisons between theory and experiment for H-like ions can not be used to assess QED effects on the hfs. To get around this issue, it was suggested by Shabaev et al., [2001] to consider a specific difference in hfs values in hydrogenlike, $\Delta E^{(1s)}$, and lithiumlike, $\Delta E^{(2s)}$, of the same heavy isotope

$$\Delta'E = \Delta E^{(2s)} - \xi_{\text{hfs}} \Delta E^{(1s)}. \quad (1.1)$$

Here parameter ξ_{hfs} is calculated theoretically in such a way that the Bohr-Weisskopf effect in the specific difference $\Delta'E$ is canceled. It was demonstrated by Shabaev et al., [2001] that both the parameter ξ_{hfs} and the specific difference are very stable in terms of possible modifications of nuclear models and nuclear parameters. This implies that both ξ_{hfs} and $\Delta'E$ can be accurately assessed. Thus, in the case of ^{209}Bi , precise calculation by Volotka et al., [2012] yields $\xi_{\text{hfs}} = 0.16886$. As a result of studying the specific difference, stringent tests of QED in strong fields can be achieved.

This proposal marked the beginning of precise experiments on hfs in H- and Li-like bismuth ions, the accuracy of which has already reached less than 0.002% (Lochmann et al., [2014]; Ullmann et al., [2015]; Sánchez et al., [2017]; Ullmann et al., [2017]). However, it was only recently discovered that there is a 7σ discrepancy between experimental (Ullmann et al., [2017]) and theoretical (Volotka et al., [2012]) values of the specific difference in ^{209}Bi . In the meantime, the inaccurate value of the nuclear magnetic moment of ^{209}Bi has been identified as the cause of this discrepancy. A new value of the magnetic moment, obtained in a recent NMR experiment along with elaborated magnetic shielding calculations, differs considerably from the tabular value (Skripnikov et al., [2018]). Even though the current value brings a specific difference into agreement, the test of QED in ^{209}Bi is limited by the present value's substantially higher uncertainty. The uncertainty caused by the magnetic moment, in particular, is approximately one order of magnitude greater than other uncertainties in the theoretical value of the specific difference (Nörtershäuser et al., [2019]). In this thesis, we expand the computations to other Li-like ions to advance the QED test with the hfs.

The interaction of the bound electron with an external constant magnetic field causes another effect, known as Zeeman splitting of the energy levels. The Zeeman effect in highly charged ions has been the focus of extensive theoretical and experimental research over the last several decades. In hydrogenlike carbon and silicon ions, the bound electron g factor is now measured with a relative precision of a few parts in 10^{11} (Sturm et al., [2011]; Sturm et al., [2013]; Sturm et al., [2014]). These measurements, together with excellent theoretical studies (Blundell et al., [1997];

Persson et al., [1997]; Beier, [2000]; Karshenboim, [2000]; Karshenboim et al., [2001]; Glazov and Shabaev, [2002]; Shabaev and Yerokhin, [2002]; Nefiodov et al., [2002]; Yerokhin et al., [2002]; Yerokhin et al., [2004]; Pachucki et al., [2005b]; Pachucki et al., [2005a]; Lee et al., [2005]; Jentschura, [2009]; Yerokhin and Harman, [2013]; Czarnecki and Szafron, [2016]; Yerokhin and Harman, [2017]; Czarnecki et al., [2018]; Czarnecki et al., [2020], have resulted in the most exact electron mass value to date (Sturm et al., [2014]; Köhler et al., [2015]; Zatorski et al., [2017]). Furthermore, the current experimental methods allow for high-precision g -factor measurements in few-electron ions (Wagner et al., [2013]; Lindenfels et al., [2013]; Köhler et al., [2016]; Glazov et al., [2019a]; Arapoglou et al., [2019]). Thus, recent experiments with Li-like ions have reported results with eleven significant digits (Köhler et al., [2016]; Glazov et al., [2019a]), achieving an accuracy equivalent to that of H-like ions.

The bound-electron g factor joins the group of observables that define our understanding of fundamental physics due to the extraordinary accuracy reached in both experiments and theory. The measurement of the g -factor isotope shift with Li-like calcium ions (Köhler et al., [2016]), for example, has allowed the relativistic nuclear recoil theory to be tested in the presence of a magnetic field. This measurement made it possible to investigate bound-state QED effects in the strong-field domain beyond the Furry picture (Shabaev et al., [2017]; Malyshev et al., [2017b]). The fine structure constant α is anticipated to be determined independently using high-precision bound-electron g -factor experiments and theoretical analyses (Shabaev et al., [2006]; Volotka and Plunien, [2014]; Yerokhin et al., [2016]). Furthermore, one can look for effects beyond the Standard Model (Debievre et al., [2020]). While calcium is the heaviest system measured to date, the most fascinating effects, such as new physics, tend to become more apparent as the nuclear charge number Z increases. As a result, the middle- Z ions are primarily used as a prototype to test theoretical methodologies, which still need to be improved to meet experimental precision and finally implement these exciting concepts.

With an uncertainty of about 10^{-9} , the first measurements of the g -factor were carried out using a Penning trap with Li-like silicon (Wagner et al., [2013]) and calcium (Köhler et al., [2016]) ions. The 15-fold improved experimental result for $^{28}\text{Si}^{11+}$ was just reported by Glazov et al., [2019a] making it the most precise g -factor value for few-electron ions at the moment. A variety of QED and nuclear effects should be thoroughly taken into account in theory to match the experimental accuracy.

The most precise theoretical g -factor value for $^{28}\text{Si}^{11+}$ at the time was determined by Glazov et al., [2019a] $g_{\text{th},2019} = 2.000\,889\,894\,4(34)$, and it was found to be 1.7σ away from the experimental value, $g_{\text{exp},2019} = 2.000\,889\,888\,45(14)$, provided *ibid.* The higher-order many-electron effects were accurately treated within the perturba-

tion theory, which contributed to the improvement of the final result. The calculations were done using the extended Furry picture, which includes an effective screening potential in the Dirac equation. Yerokhin et al., [2020] conducted an independent evaluation of the screened QED diagrams in an attempt to resolve the discrepancy. Unlike Glazov et al., [2019a], the calculations were carried out using the usual Furry picture, i.e., based on the Dirac equation with the Coulomb potential. The non-relativistic quantum electrodynamics (NRQED) approach was used to assess the higher-order many-electron effects to the leading order in αZ . As a consequence, $g_{\text{th},2020} = 2.000\,889\,896\,3(15)$ Yerokhin et al., [2020] was discovered to be a new theoretical value for $^{28}\text{Si}^{11+}$. The theoretical error bar for $g_{\text{th},2019}$ and $g_{\text{th},2020}$ is determined by estimating the unknown higher-order many-electron QED effects and the numerical uncertainty of the computed contributions. Even though higher-order many-electron effects in the original Furry picture are usually more significant than in the extended Furry picture, the corresponding uncertainty indicated by Yerokhin et al., [2020] is half as much as defined by Glazov et al., [2019a]. Overall, within the given error bars, $g_{\text{th},2019}$ and $g_{\text{th},2020}$ are in fair agreement. However, the theoretical value from Ref. (Yerokhin et al., [2020]) differs from the experiment by about 5.2σ , implying that the g -factor "puzzle" has only gotten worse. Yerokhin et al., [2021] recently completed an independent assessment of the two-photon-exchange contribution and provided new results for Li-like silicon and calcium. The 3.1σ disagreement for silicon remains, however slightly less than in Ref. (Yerokhin et al., [2020]). In the case of calcium, there is a 4.2σ discrepancy between theoretical and experimental (Köhler et al., [2016]) g -factor values.

The screened QED and interelectronic-interaction effects represent one of the most challenging theoretical contributions. So far, only two groups have conducted a rigorous assessment of these contributions. In this thesis, we examine the many-electron QED effects in greater depth to shed light on the ongoing discrepancy. We present large-scale QED computations in the extended Furry picture for various screening potentials and found that our current g -factor values for silicon and calcium are in good agreement with the experiment.

This dissertation is organized as follows. We start with the description of the non-interacting electron-positron and electromagnetic fields in the external field approximation. In Chap. [2] the main building blocks of the QED are given: we introduce the Lagrangian of the theory, define the concepts of the original Furry picture and construct electron and photon propagators.

In Chap. [3] we add the interaction between quantized electron-positron and electromagnetic fields. We construct the QED perturbation theory: define the evolution operator in Sec. [3.2] and scattering S -matrix in Sec. [3.3]. Subsequently, we focus on the

perturbation theory for the bound-state QED. Here we begin with a short description of the historically first approach introduced by Gell-Mann, Low and Sucher (Sec. 3.3.1). Finally, in Sec. 3.4 we formulate the two-time Green's function formalism used in the present dissertation.

The last two chapters constitute the main part of the thesis, where we consider the magnetic sector of the QED theory. In Chap. 4 we investigate the hfs in lithium-like ions, we focus on the many-electron effects in the hfs, namely, interelectronic-interaction corrections. We perform the calculations within the extended Furry picture. As a result, we substantially improve the accuracy of the interelectronic-interaction contribution to the ground-state hfs in lithiumlike ions in the range $Z = 7 - 82$.

In Chap. 5 we consider the g factor of lithiumlike silicon and calcium. We improve the theoretical value of the g factor as well as explain the reasons for the discrepancy between theory and experiment, established by Glazov et al., 2019a and Yerokhin et al., 2020. As a result, our new theoretical values are in a much better agreement with the experimental values: the difference is just 1.4σ and 0.6σ for silicon and calcium, respectively.

Finally, in Chap. 6 conclusions and an outlook to future work are given.

1.1 NOTATIONS AND CONVENTIONS

The relativistic units ($\hbar = c = m_e = 1$) and the Heaviside charge unit, where $\alpha = e^2/(4\pi)$ is a fine structure constant and $e < 0$ is the electron charge are used throughout the thesis. When it appears to be convenient, the electron mass m_e is restored in the expressions. In addition, we use the following definitions: χ^μ for contravariant four-vector, $\chi_\mu = g_{\mu\nu}\chi^\nu$ for covariant four-vector, $g_{\mu\nu}$ is the metric tensor

$$g_{\mu\nu} = g^{\mu\nu} = \begin{pmatrix} 1 & 0 & 0 & 0 \\ 0 & -1 & 0 & 0 \\ 0 & 0 & -1 & 0 \\ 0 & 0 & 0 & -1 \end{pmatrix},$$

and $\alpha^\mu = \gamma^0\gamma^\mu$ are the Dirac matrices in their standard representation

$$\alpha^0 = \begin{pmatrix} \mathbb{1} & 0 \\ 0 & \mathbb{1} \end{pmatrix}, \quad \alpha = \begin{pmatrix} 0 & \boldsymbol{\sigma} \\ \boldsymbol{\sigma} & 0 \end{pmatrix},$$

$$\gamma^0 \equiv \beta = \begin{pmatrix} \mathbb{1} & 0 \\ 0 & -\mathbb{1} \end{pmatrix}, \quad \boldsymbol{\gamma} = \begin{pmatrix} 0 & \boldsymbol{\sigma} \\ -\boldsymbol{\sigma} & 0 \end{pmatrix},$$

and the 2×2 Pauli matrices

$$\sigma_1 = \begin{pmatrix} 0 & 1 \\ 1 & 0 \end{pmatrix}, \quad \sigma_2 = \begin{pmatrix} 0 & -i \\ i & 0 \end{pmatrix}, \quad \sigma_3 = \begin{pmatrix} 1 & 0 \\ 0 & -1 \end{pmatrix}.$$

Here $\mathbb{1}$ is a unit 2×2 matrix

$$\mathbb{1} = \begin{pmatrix} 1 & 0 \\ 0 & 1 \end{pmatrix}.$$

We should note that throughout the thesis, we will use the notation $\mathbb{1}$ for unitary matrices of other dimensions; for example, see Sec. [3.2](#) where $\mathbb{1}$ is a 4×4 matrix.

- We use the Roman style (p) for scalars, boldface (\mathbf{p}) for three vectors, and italic style p for four-vectors and their components. Four vectors have the form $p = (p_0, \mathbf{p})$ and in coordinate space are also denoted as $\chi = (t_\chi, \mathbf{x})$.
- The scalar product of four-vectors is defined as $k p = k^\mu p_\mu = k^0 p_0 - \mathbf{k} \cdot \mathbf{p}$. The summing over repeated indices is assumed by default.

- In expressions containing integrals, the dimension is indicated by style, i.e., four-dimensional integrals are given by $\int dx$ and three-dimensional by $\int d\mathbf{x}$.
- Superscript \wedge also denotes second quantization field operators, which usually referred to as just *quantized* field operators: quantized electromagnetic field operator $\hat{A}_\mu(x)$ and quantized electron-positron field operator $\hat{\psi}(x)$.
- We use superscript (0) to denote free fields. We note, that we understand under the free electron-positron field operator $\widehat{\psi}^{(0)}(x)$ the field operator describes bound electrons. This means the electron is considered in the external field of a nucleus (Furry picture) or effective potential which is a sum of nucleus potential and screening potentials formed by core electrons (extended Furry picture). This interaction is accounted for non-perturbatively.

 FREE FIELDS IN A FURRY PICTURE

The QED theory describes the interaction between charged particles which is mediated by the exchange of the photon. But firstly, let us start from the description of the noninteracting matter and light. The total Lagrangian density of free fields \mathcal{L}_0 is given by

$$\mathcal{L}_0 = \mathcal{L}_0^\gamma + \mathcal{L}_0^{ee^+}, \quad (2.1)$$

where \mathcal{L}_0^γ describes free photons and $\mathcal{L}_0^{ee^+}$ refers to the free electrons and positrons. Each term in Eq. (2.1) can be expressed through free electromagnetic field $A_\mu^{(0)}(x)$ and free Dirac field $\psi^{(0)}(x)$ as follows

$$\begin{aligned} \mathcal{L}_0^\gamma &= -\frac{1}{4} F_{\mu\nu}^{(0)}(x) F^{\mu\nu, (0)}(x), \\ \mathcal{L}_0^{ee^+} &= \bar{\psi}^{(0)}(x) (i\gamma^\mu \partial_\mu - m_e) \psi^{(0)}(x). \end{aligned} \quad (2.2)$$

Here $F_{\mu\nu}^{(0)}(x) = \partial_\mu A_\nu^{(0)}(x) - \partial_\nu A_\mu^{(0)}(x)$ denotes the electromagnetic field tensor and $\bar{\psi}^{(0)}(x) \equiv [\psi^{(0)}(x)]^\dagger \gamma^0$.

In the present thesis we consider ionic systems with the nucleus being a source of the binding potential V^{nucl} . To describe such a system one needs to construct a total Lagrangian density \mathcal{L} in the form

$$\mathcal{L} = \mathcal{L}_0^\gamma + \mathcal{L}_0^{ee^+} + \mathcal{L}_{\text{int}}^{\text{nucl}}, \quad (2.3)$$

where the term $\mathcal{L}_{\text{int}}^{\text{nucl}}$ describes the interaction between electrons and nucleus

$$\mathcal{L}_{\text{int}}^{\text{nucl}} = -e \bar{\psi}^{(0)}(x) \gamma^\mu \psi^{(0)}(x) A_\mu^{\text{nucl}}(x). \quad (2.4)$$

Here $A_\mu^{\text{nucl}} = \left(\frac{V^{\text{nucl}}}{e}, \mathbf{0} \right)$ is a vector potential associated with the electric field generated by the nucleus¹. We note here, that now $\psi^{(0)}(x)$ is a Dirac field in the

¹We note that one should make the following substitution in \mathcal{L}_0^γ term: $A_\nu^{(0)}(x) \rightarrow A_\nu^{(0)}(x) + A_\nu^{\text{nucl}}$.

presence of the external potential.

Usually, the Lagrangian density with a subscript $_0$ (free fields) can be treated exactly, and any interaction is considered using perturbation theory. But this approach does not work for the case of ions with high Z , where Z is the nuclear charge number. Indeed, the binding potential has a form $V^{\text{nucl}} \sim -\alpha Z$, therefore the interaction between bound electron and nucleus is proportional to the αZ . For the case, for example, of uranium $Z = 92$ this expansion parameter reads as $\alpha Z \approx 0.67$. Therefore a perturbation expansion in αZ becomes meaningless, and the interaction between electrons and nucleus has to be considered non-perturbatively. This effectively means that the interaction term $\mathcal{L}_{\text{int}}^{\text{nucl}}$ has to be added to the unperturbed Lagrangian density $\mathcal{L}_0^{ee^+}$ which now would describe to the zeroth-order the bound electrons. This is called the external field approximation, or Furry picture (Furry, 1951). Therefore, in the framework of the Furry picture Lagrangian density from Eq. (2.3) is nothing else as unperturbed Lagrangian density $\mathcal{L}_{0,F}$

$$\mathcal{L}_{0,F} \equiv \mathcal{L}_0^\gamma + \mathcal{L}_0^{ee^+} + \mathcal{L}_{\text{int}}^{\text{nucl}}, \quad (2.5)$$

and noninteracting (with photon field) electrons and positrons are now defined as

$$\mathcal{L}_{0,F}^{ee^+} \equiv \mathcal{L}_0^{ee^+} + \mathcal{L}_{\text{int}}^{\text{nucl}}. \quad (2.6)$$

and the free photon field is defined as before by $\mathcal{L}_{0,F}^\gamma \equiv \mathcal{L}_0^\gamma$. Then the equation of motion for free fermion field $\psi^{(0)}(x)$ is

$$\left(i\gamma^\mu \partial_\mu - m_e - e\gamma^\mu A_\mu^{\text{nucl}}(x) \right) \psi^{(0)}(x) = 0, \quad (2.7)$$

and for free photon field $A_\mu^{(0)}(x)$ in Feynman gauge (Peskin and Schroeder, 1995) is

$$\square A_\mu^{(0)}(x) = 0, \quad (2.8)$$

with $\square \equiv \frac{\partial^2}{\partial t^2} - \Delta$ being d'Alembert operator.

One can solve these Euler-Lagrange equations (2.7)-(2.8) and perform the quantization procedure of the corresponding field. Quantization means the transition from fields to the corresponding operators acting on the state Φ . By analogy with ordinary quantum mechanics, the state vector completely characterizes the physical state of the system of quantized fields. For further details see, i.e. (Itzykson and Zuber, 1980; Berestetsky et al., 1982).

Here we perform canonical (second) quantization, i.e., represent field operators

through creation and annihilation operators. Then corresponding free Dirac field operator $\widehat{\psi}^{(0)}$ in Heisenberg picture is defined as

$$\widehat{\psi}^{(0)}(t, \mathbf{x}) = \sum_n^{\varepsilon_n > 0} a_n \phi_n(\mathbf{x}) e^{-i\varepsilon_n t} + \sum_n^{\varepsilon_n < 0} b_n^\dagger \phi_n(\mathbf{x}) e^{-i\varepsilon_n t}, \quad (2.9)$$

where $\phi_n(\mathbf{x})$ are the solutions of the following stationary Dirac equation

$$h_D \phi_n(\mathbf{x}) = [-i\boldsymbol{\alpha} \cdot \boldsymbol{\nabla} + V^{\text{nucl}}(\mathbf{x}) + \beta] \phi_n(\mathbf{x}) = \varepsilon_n \phi_n(\mathbf{x}), \quad (2.10)$$

and ε_n are corresponding eigenvalues. All quantum numbers required to characterize the state are specified by the multi-index n . We note that in the case when these quantum numbers are continuous, the sums in Eq. (2.9) must be interpreted as integrals with proper normalizations. The electron annihilation operator for an electron in state n is denoted by a_n , while the positron creation operator for a positron in state m is denoted by b_m^\dagger . The anticommutation relations are implied by the canonical equal-time anticommutators for field operators,

$$\begin{aligned} \{a_n, a_m^\dagger\} &= \delta_{nm}, & \{a_n, a_m\} &= \{a_n^\dagger, a_m^\dagger\} = 0, \\ \{b_n, b_m^\dagger\} &= \delta_{nm}, & \{b_n, b_m\} &= \{b_n^\dagger, b_m^\dagger\} = 0, \\ \{a_n, b_m\} &= \{a_n, b_m^\dagger\} = \{a_n^\dagger, b_m\} = \{a_n^\dagger, b_m^\dagger\} = 0. \end{aligned} \quad (2.11)$$

The free photon field operator $\widehat{A}_\mu^{(0)}(x)$ in Heisenberg picture can be written as

$$\widehat{A}_\mu^{(0)}(x) = \int \frac{d\mathbf{k}}{\sqrt{2k^0(2\pi)^3}} \sum_{\lambda=0}^3 \left[c(\mathbf{k}, \lambda) A_{\mathbf{k}, \lambda}^\mu(\mathbf{x}) e^{-ik^0 t} + c^\dagger(\mathbf{k}, \lambda) A_{\mathbf{k}, \lambda}^{\mu*}(\mathbf{x}) e^{ik^0 t} \right], \quad (2.12)$$

where the Feynman gauge is used, and the plane waves $A_{\mathbf{k}, \lambda}^\mu(\mathbf{x})$ have the following form

$$A_{\mathbf{k}, \lambda}^\mu(\mathbf{x}) = \frac{\epsilon^\mu(\mathbf{k}, \lambda) e^{-i\mathbf{k}\mathbf{x}}}{\sqrt{2k^0(2\pi)^3}}. \quad (2.13)$$

Here \mathbf{k} and $\omega \equiv k^0 = |\mathbf{k}|$ are momentum and energy of the photon, respectively, $\epsilon^\mu(\mathbf{k}, \lambda)$ is its polarisation vector which is characterized by helicity λ . And, finally,

$c(\mathbf{k}, \lambda)$ and $c^\dagger(\mathbf{k}, \lambda)$ annihilates and creates, respectively, a photon with momentum \mathbf{k} and the helicity λ . They are subject to the following commutation relations

$$\begin{aligned} [c(\mathbf{k}, \lambda), c^\dagger(\mathbf{k}', \lambda')] &= -g^{\lambda\lambda'} 2\omega(2\pi)^3 \delta^3(\mathbf{k} - \mathbf{k}'), \\ [c(\mathbf{k}, \lambda), c(\mathbf{k}', \lambda')] &= [c^\dagger(\mathbf{k}, \lambda), c^\dagger(\mathbf{k}', \lambda')] = 0. \end{aligned} \quad (2.14)$$

We note that the case of $\lambda = 0, 3$ refers to the unphysical timelike and longitudinal photons, respectively. Due to the presence of these photons, the theory starts to have some problems, for example, the norm of the photon state with timelike polarisation ($\lambda = 0$) is negative which breaks one of the main postulates of quantum mechanics and lead to the negative probability to find such a photon! As long as we're talking about the free case, the situation isn't as bad as it appears, simply because a free electromagnetic field doesn't exist in nature. However, when moving on to the theory of interacting fields (Sec. 3.1), one must be careful that interaction does not excite these unphysical states. To overcome this issue one can use the Gupta-Bleuler approach (Itzykson and Zuber, 1980) and construct the physical subspace of state vectors that have positive norm and only the transverse photons ($\lambda = 1, 2$) contribute to observable quantities.

For both electron-positron $\widehat{\psi}^{(0)}(x)$ and electromagnetic $\widehat{A}_\mu^{(0)}(x)$ field operators, one can introduce *propagators*, which are nothing more than functions that characterize the propagation of these fields (or their quantum²) from one act of interaction to another. The vacuum expectation value of the time-ordered product determines the free propagator of the electron-positron field

$$\begin{aligned} iS_F(t_x - t_y, \mathbf{x}, \mathbf{y}) &= \langle 0 | T [\widehat{\psi}^{(0)}(x) \widehat{\bar{\psi}}^{(0)}(y)] | 0 \rangle \\ &= \frac{i}{2\pi} \int dE e^{-iE(t_x - t_y)} \sum_n \frac{\phi_n(\mathbf{x}) \bar{\phi}_n(\mathbf{y})}{E - \epsilon_n(1 - i\delta)}, \end{aligned} \quad (2.15)$$

where T denotes the time-ordering operator, $\bar{\phi}_n(x) \equiv [\phi_n(x)]^\dagger \gamma^0$, and δ is a small positive real number and in the final result, we need to take a limit as δ approaches zero. The propagator of the electron-positron field can be expressed as a function of energy E and coordinates using the Fourier transform with respect to the time variables, i. e. $S_F(t_x - t_y, \mathbf{x}, \mathbf{y}) \rightarrow S_F(E, \mathbf{x}, \mathbf{y})$. The explicit form of $S_F(E, \mathbf{x}, \mathbf{y})$ is given by

$$S_F(E, \mathbf{x}, \mathbf{y}) = \sum_n \frac{\phi_n(\mathbf{x}) \bar{\phi}_n(\mathbf{y})}{E - \epsilon_n(1 - i\delta)}. \quad (2.16)$$

²Electrons (positrons) and photons for $\widehat{\psi}^{(0)}(x)$ and $\widehat{A}_\mu^{(0)}(x)$, respectively.

From Eq. (2.15), one can see that $S_F(t_x - t_y, \mathbf{x}, \mathbf{y})$ has poles at the bound states of the electron and branch cuts from $(-\infty, -m_e]$ and $[m_e, +\infty)$. And this is not surprising because the $S_F(t_x - t_y, \mathbf{x}, \mathbf{y})$ is a *one-particle Green function* of the Dirac equation (2.7), i. e. satisfies the following equation

$$\left(\gamma^\mu \partial_\mu - m_e - e\gamma^\mu A_\mu^{\text{nucl}}(x)\right) S_F(t_x - t_y, \mathbf{x}, \mathbf{y}) = \delta(x - y). \quad (2.17)$$

Similarly, one can define the free photon propagator $D_{\mu\nu}(t_x - t_y, \mathbf{x} - \mathbf{y})$ as the vacuum expectation value of time-ordered product

$$\begin{aligned} -iD_{\mu\nu}(t_x - t_y, \mathbf{x} - \mathbf{y}) &= \left\langle 0 \left| T \left[\widehat{A}_\mu^{(0)}(x) \widehat{A}_\nu^{(0)}(y) \right] \right| 0 \right\rangle \\ &= \frac{i}{2\pi} \int d\omega e^{-i\omega(t_x - t_y)} D_{\mu\nu}(\omega, \mathbf{x} - \mathbf{y}). \end{aligned} \quad (2.18)$$

The temporal Fourier-transformed photon propagation function $D_{\mu\nu}(\omega, \mathbf{x} - \mathbf{y})$ is given by (Beier, 2000; Soguel et al., 2021)

$$D_{\mu\nu}^F(\omega, \mathbf{x} - \mathbf{y}) = \frac{g_{\mu\nu}}{4\pi|\mathbf{x} - \mathbf{y}|} e^{i\tilde{\omega}|\mathbf{x} - \mathbf{y}|}, \quad (2.19)$$

in the Feynman gauge, and by

$$\begin{aligned} D_{00}^C(\omega, \mathbf{x} - \mathbf{y}) &= \frac{1}{4\pi|\mathbf{x} - \mathbf{y}|}, \\ D_{i0}^C(\omega, \mathbf{x} - \mathbf{y}) &= D_{0j}^C(\mathbf{x} - \mathbf{y}; \omega) = 0, \\ D_{ij}^C(\omega, \mathbf{x} - \mathbf{y}) &= -\frac{\delta_{ij} e^{i\tilde{\omega}|\mathbf{x} - \mathbf{y}|}}{4\pi|\mathbf{x} - \mathbf{y}|} - \nabla_i^{(x)} \nabla_j^{(y)} \frac{1 - e^{i\tilde{\omega}|\mathbf{x} - \mathbf{y}|}}{4\pi\omega^2|\mathbf{x} - \mathbf{y}|}, \end{aligned} \quad (2.20)$$

in the Coulomb gauge. Here $\tilde{\omega} = \sqrt{\omega^2 + i\eta}$, the branch of the square root is fixed by the condition $\text{Im}(\tilde{\omega}) > 0$, indexes $i, j = 1, 2, 3$, and δ_{ij} is a usual Kronecker delta.

For later purposes we introduce the operator $I(\omega, \mathbf{x} - \mathbf{y})$ representing the interelectronic interaction mediated via the exchange of virtual photons

$$I(\omega, \mathbf{x} - \mathbf{y}) = e^2 \alpha^\mu \alpha^\nu D_{\mu\nu}(\omega, \mathbf{x} - \mathbf{y}). \quad (2.21)$$

The interelectronic-interaction operator $I(\omega, \mathbf{x} - \mathbf{y})$ regardless the gauge has the following properties

$$\begin{aligned} I(\omega, \mathbf{x} - \mathbf{y}) &= I(-\omega, \mathbf{x} - \mathbf{y}), \\ I'(\omega, \mathbf{x} - \mathbf{y}) &= -I'(-\omega, \mathbf{x} - \mathbf{y}), \\ I'(0, \mathbf{x} - \mathbf{y}) &= 0, \end{aligned} \tag{2.22}$$

with

$$I'(\omega, \mathbf{x} - \mathbf{y}) \equiv \frac{dI(\omega, \mathbf{x} - \mathbf{y})}{d\omega}. \tag{2.23}$$

Inserting Eq. (2.19) into Eq. (2.21) one can express $I(\omega, \mathbf{x} - \mathbf{y})$ in Feynman gauge as

$$I^F(\omega, \mathbf{x} - \mathbf{y}) = \alpha \frac{1 - \boldsymbol{\alpha}_x \cdot \boldsymbol{\alpha}_y}{|\mathbf{x} - \mathbf{y}|} e^{i\tilde{\omega}|\mathbf{x} - \mathbf{y}|}, \tag{2.24}$$

and using Eqs. (2.20) and (2.21) one obtains $I(\omega, \mathbf{x} - \mathbf{y})$ in Coulomb gauge

$$\begin{aligned} I^C(\omega, \mathbf{x} - \mathbf{y}) &= \alpha \left(\frac{1 - \boldsymbol{\alpha}_x \cdot \boldsymbol{\alpha}_y e^{i\tilde{\omega}|\mathbf{x} - \mathbf{y}|}}{|\mathbf{x} - \mathbf{y}|} \right. \\ &\quad \left. + \left[(\boldsymbol{\alpha}_x \cdot \nabla_x), \left[(\boldsymbol{\alpha}_y \cdot \nabla_y), \frac{e^{i\tilde{\omega}|\mathbf{x} - \mathbf{y}|} - 1}{\omega^2 |\mathbf{x} - \mathbf{y}|} \right] \right] \right). \end{aligned} \tag{2.25}$$

We want to stress that one-particle Green's functions and propagators are frequently used interchangeably in the literature. Thus, Green's function $G'(x, y)$ of some operator \hat{B} is defined as its impulse response, i.e. $\hat{B}G'(x, y) = \delta(x - y)$. Green's function $G'(x, y)$ has a physical meaning: it describes the system's response to an instant point source $\delta(x - y)$, which is why it is also known as the *source function*. In the present thesis, we define free electron $S_F(t_x - t_y, \mathbf{x}, \mathbf{y})$ and photon $D_{\mu\nu}(t_x - t_y, \mathbf{x} - \mathbf{y})$ propagators in a way that they coincide with the definition of one-particle Green's function (here we use the term one-particle because in our case operator \hat{B} describes one particle only) given above. Thus, electron propagator $S_F \equiv G'(x, y)$, where $G'(x, y)$ is a Green's function of Dirac equation (2.7). Similarly, photon propagator $D_{\mu\nu} \equiv G'(x, y)$ with $G'(x, y)$ (for Feynman gauge) being a Green's function of the wave equation (2.8). Note that our definition of propagators coincide with one introduced by Berestetsky et al., [1982]; Weinberg, [2005].

However, it is more convenient to interpret Green's function as a correlation function and give a different definition. Therefore, we will understand under one-particle **Green's function** $G(x, y)$ a vacuum expectation of the time-ordered product of either

two electron-positron or two electromagnetic field operators (in the notation of Peskin and Schroeder, 1995) it is propagators of electron and photon, respectively)

$$G(x, y) \equiv \begin{cases} \langle 0 | T [\widehat{\psi}^{(0)}(x) \widehat{\bar{\psi}}^{(0)}(y)] | 0 \rangle & \text{for electron} \\ \langle 0 | T [\widehat{A}_\mu^{(0)}(x) \widehat{A}_\nu^{(0)}(y)] | 0 \rangle & \text{for photon} \end{cases} \quad (2.26)$$

We note that one particle Green's function $G(x, y)$ coincide with $G'(x, y)$ within a constant factor $\pm i$. The generalization of the G for the case of N particles will be made later in Subsec. 3.4.2

 BOUND-STATE QED IN EXTERNAL FIELD APPROXIMATION

In this chapter, we consider interacting electron-positron and electromagnetic fields and construct the QED perturbation theory. Namely, we build the time-evolution operator in Sec. 3.2 and present its Dyson series. Then in Sec. 3.3 we define the central object of the quantum field theory, the S -matrix. In the following Sec. 3.3.1, we consider the bound-state QED theory. We describe the formalism that Gell-Mann, Low, and Sucher first introduced for calculating the energy shifts of states from the discrete spectrum, the adiabatic S -matrix approach. And we conclude this chapter by formulating the two-time Green's function formalism that is used in the current dissertation for computations of the QED corrections to the hyperfine splitting and g factor of few-electron ions.

3.1 INTERACTING FIELDS

We start this subsection with a note that from now on we will work in the framework of an external field approximation (Furry picture) unless otherwise stated. We saw in the previous subsection, that any interaction with external classical electromagnetic field is introduced by the minimal coupling scheme, see Eq. (2.4). One can do the same for the case of the second-quantized operators of Dirac $\hat{\psi}(x)$ and electromagnetic field $\hat{A}_\mu(x)$ and construct the corresponding Lagrangian density $\hat{\mathcal{L}}_{\text{int}}$,

$$\hat{\mathcal{L}}_{\text{int}} = -e\hat{\psi}(x)\gamma^\mu\hat{\psi}(x)\hat{A}_\mu(x), \quad (3.1)$$

we note that now $\hat{\psi}(x)$ and $\hat{A}_\mu(x)$ are interacting fields, therefore index (0) is omitted. Then the total QED Lagrangian density $\hat{\mathcal{L}}_{\text{QED}}$ reads as ^{1,2}

$$\hat{\mathcal{L}}_{\text{QED}} = \hat{\mathcal{L}}_{0,F}^\gamma + \hat{\mathcal{L}}_{0,F}^{ee^+} + \hat{\mathcal{L}}_{\text{int}}. \quad (3.2)$$

Here $\hat{\mathcal{L}}_{0,F}^\gamma \equiv \hat{\mathcal{L}}_0^\gamma$ and $\hat{\mathcal{L}}_{0,F}^{ee^+}$ are given by Eqs. (2.2), (2.6) where one needs to make the following replacement

$$\begin{aligned} \psi^{(0)}(x) &\longrightarrow \hat{\psi}(x), \\ A^{(0)}(x) &\longrightarrow \hat{A}(x). \end{aligned} \quad (3.3)$$

One can see that the dynamics of both field operators $\hat{\psi}(x)$ and $\hat{A}(x)$ are included in the same Lagrangian (3.2) density so that each can change under the influence of the other. This results in a non-linear system which is usually only solved using perturbative techniques. These are the Feynman diagrams which we will discuss later. Since we are generally unable to find an exact expression for $\hat{\psi}(x)$ and $\hat{A}(x)$, we rely on a perturbative method, with $\hat{\mathcal{L}}_{\text{int}}$ considered as a small perturbation to $\hat{\mathcal{L}}_{0,F}$. Indeed, $\hat{\mathcal{L}}_{\text{int}}$ depends on the coupling constant e and the perturbative expansion will be a power series of coupling constant α ³.

From $\hat{\mathcal{L}}_{\text{QED}}$ one can obtain the corresponding full QED Hamiltonian \hat{H}_{QED}

$$\hat{H}_{\text{QED}} = \hat{H}_{0,F} + \hat{H}_{\text{int}}, \quad (3.4)$$

where the first term, $\hat{H}_{0,F}$, is unperturbed Hamiltonian, and the second one, \hat{H}_{int} , is the interaction Hamiltonian. Then usual Schrödinger equation reads as ⁴

$$i \frac{\partial \Psi(t)}{\partial t} = (\hat{H}_{0,F} + \hat{H}_{\text{int}}) \Psi(t). \quad (3.5)$$

¹We note that we did not include in $\hat{\mathcal{L}}_{\text{QED}}$ mass and charge counterterms, therefore the derivations should be understood on a formal level.

²Strictly speaking, one needs to consider *normal ordered* QED Lagrangian density $\hat{\mathcal{L}}_{\text{QED}} \rightarrow: \hat{\mathcal{L}}_{\text{QED}} :$, when all creation operators are to the left of all annihilation operators in the product. This is usually done to remove divergence arising from the infinite energy of the vacuum E_{vac} . Since the absolute energies are not measured observables one can safely subtract the infinite constant E_{vac} , which is automatically done by introducing the *normal product* $::$ (Bjorken and Drell, 1965). Later, when we introduce the interaction Hamiltonian, we will write it explicitly.

³One can show that the perturbation series has the form $\sum_{L=0}^{\infty} e^{E-2+2L} a_L = e^{E-2} \sum_{L=0}^{\infty} \alpha^L a_L$, where L is number of loops, and E is number of external lines (Peskin and Schroeder, 1995).

⁴Here the operators $\hat{H}_{0,F}$ and \hat{H}_{int} are operators in Schrödinger representation. Therefore, one first needs to transform field operators in $\hat{\mathcal{L}}_{\text{QED}}$ (3.2) from the Heisenberg picture to Schrödinger one. We also notice that the Hamiltonian is expressed in the same way in terms of the field operators in the Schrödinger and Heisenberg representations.

In the absence of interaction, i.e., for $\hat{H}_{\text{int}} = 0$, the state vector $\Psi \equiv \Phi$ describes the motion of a given number of free particles with definite momenta and spins. The \hat{H}_{int} operator describes how these particles interact with one another and with themselves. Now let us introduce the following state vector

$$\Psi^{\text{IR}}(t) = e^{i\hat{H}_{0,F}t}\Psi(t). \quad (3.6)$$

It is simple to demonstrate that $\Psi^{\text{IR}}(t)$ meets the following condition

$$i\frac{\partial\Psi^{\text{IR}}(t)}{\partial t} = e^{i\hat{H}_{0,F}t}\hat{H}_{\text{int}}e^{-i\hat{H}_{0,F}t}\Psi^{\text{IR}}(t), \quad (3.7)$$

or

$$i\frac{\partial\Psi^{\text{IR}}(t)}{\partial t} = \hat{H}_{\text{int}}^{\text{IR}}(t)\Psi^{\text{IR}}(t), \quad (3.8)$$

where

$$\hat{H}_{\text{int}}^{\text{IR}}(t) = e^{i\hat{H}_{0,F}t}\hat{H}_{\text{int}}e^{-i\hat{H}_{0,F}t}, \quad (3.9)$$

is the perturbation Hamiltonian in some new representation. In contrast to the Schrödinger operator \hat{H}_{int} , this operator explicitly depends on time. In general, in this so-called *interaction representation*, an arbitrary operator $Q^{\text{IR}}(t)$ is related to the Schrödinger operator Q^{S} as follows

$$Q^{\text{IR}}(t) = e^{i\hat{H}_{0,F}t}Q^{\text{S}}e^{-i\hat{H}_{0,F}t}. \quad (3.10)$$

This implies that in the representation of the interaction, the time dependence of the operators is determined by the Hamiltonian of free particles because differentiating [\(3.10\)](#) with respect to t yields

$$i\frac{\partial Q^{\text{IR}}(t)}{\partial t} = [Q^{\text{IR}}(t), \hat{H}_{0,F}], \quad (3.11)$$

where we used that $\hat{H}_0^{\text{IR}} = \hat{H}_{0,F}$. Thus, in the interaction representation, the field operators satisfy the equations of motion of the free field, whereas the time dependence of the system's state vector $\Psi(t)$ is determined solely by the interaction Hamiltonian (in interaction picture), according to [\(3.8\)](#). Therefore, in the interaction picture, the interacting field operators $\hat{\psi}^{\text{IR}}(x)$ and $\hat{A}_\mu^{\text{IR}}(x)$ have the same spectral representation as the free field operators, see Eqs. [\(2.9\)](#) and [\(2.12\)](#), respectively. Furthermore, the propagators for $\hat{\psi}^{\text{IR}}(x)$ and $\hat{A}_\mu^{\text{IR}}(x)$ correspond to the definitions given by Eqs. [\(2.15\)](#)

and (2.18) for free electron-positron $\widehat{\psi}^{(0)}(x)$ and free electromagnetic $\widehat{A}_\mu^{(0)}(x)$ field operators.

3.2 TIME-EVOLUTION OPERATOR

The effect of the interaction is hidden in the state vector $\Psi^{\text{IR}}(t)$. As a result, the Schrödinger equation (3.8) serves as the starting point for a perturbative approach to the problem of interacting fields. We define the time-evolution operator (also known as the Dyson operator) $\hat{U}^{\text{IR}}(t, t_0)$ to describe the connection between the state vectors at t_0 and t_1 as

$$\Psi^{\text{IR}}(t) = \hat{U}^{\text{IR}}(t, t_0) \Psi^{\text{IR}}(t_0). \quad (3.12)$$

Inserting Eq. (3.12) into Eq. (3.8) one obtains the following equation for the evolution operator $\hat{U}^{\text{IR}}(t, t_0)$

$$i \frac{\partial}{\partial t} \hat{U}^{\text{IR}}(t, t_0) = \hat{H}_{\text{int}}^{\text{IR}}(t) \hat{U}^{\text{IR}}(t, t_0), \quad (3.13)$$

with the boundary condition

$$\hat{U}^{\text{IR}}(t_0, t_0) = \mathbb{1}.$$

The differential equation (3.13) is equivalent to the integral equation

$$\hat{U}^{\text{IR}}(t, t_0) = \mathbb{1} - i \int_{t_0}^t dt_1 \hat{H}_{\text{int}}^{\text{IR}}(t_1) \hat{U}^{\text{IR}}(t_1, t_0), \quad (3.14)$$

which can be solved by the iteration procedure (Dyson, 1949b)

$$\begin{aligned} \hat{U}^{\text{IR}}(t, t_0) = & \mathbb{1} - i \int_{t_0}^t dt_1 \hat{H}_{\text{int}}^{\text{IR}}(t_1) + \\ & + (-i)^2 \int_{t_0}^t dt_1 \int_{t_0}^{t_1} dt_2 \hat{H}_{\text{int}}^{\text{IR}}(t_1) \hat{H}_{\text{int}}^{\text{IR}}(t_2) + \dots \end{aligned} \quad (3.15)$$

Then the perturbation series for the time-evolution operator can be found using Eq. (3.15)

$$\hat{U}^{\text{IR}}(t, t_0) = \mathbb{1} + \sum_{n=1}^{\infty} \frac{(-i)^n}{n!} \int_{t_0}^t dt_1 \cdots \int_{t_0}^t dt_n T \left[\hat{H}_{\text{int}}^{\text{IR}}(t_1) \cdots \hat{H}_{\text{int}}^{\text{IR}}(t_n) \right], \quad (3.16)$$

where T is the time-ordered product operator. This expansion provides a basis for QED calculations by perturbation theory in α .

We observe that the series (3.16) can be formally summed up, yielding the time-ordered exponential function

$$\hat{U}^{\text{IR}}(t, t_0) = T \left[e^{-i \int_{t_0}^t dt \hat{H}_{\text{int}}^{\text{IR}}(t)} \right]. \quad (3.17)$$

However, in essence, this is merely a more compact version of the Eq. (3.16). The Hamiltonian $\hat{H}_{\text{int}}^{\text{IR}}$ may be written in any local field theory as an integral over the Hamilton density $\hat{\mathcal{H}}_{\text{int}}^{\text{IR}}$, which consists of field operator products and perhaps their derivatives. Thus, one can rewrite Eq. (3.17) as

$$\hat{U}^{\text{IR}}(t, t_0) = T \left[e^{-i \int_{t_0}^t dx \hat{\mathcal{H}}_{\text{int}}^{\text{IR}}(x)} \right]. \quad (3.18)$$

In Eq. (3.18) the time and the coordinates appear on an equal footing and, as a result, $\hat{U}^{\text{IR}}(t, t_0)$ is clearly relativistically invariant.

The time-evolution operator $\hat{U}^{\text{IR}}(t, t_0)$ is most commonly used in scattering processes. However, by using the adiabatic S-matrix formalism of Gell-Mann, Low, and Sucher or the two-time Green's function method, $\hat{U}^{\text{IR}}(t, t_0)$ can be used to calculate the energy shift of a bound level under the influence of interaction, see Secs. 3.3.1 and 3.4.2 respectively.

3.3 S-MATRIX FORMALISM

The scattering matrix (S-matrix) is an important concept in both quantum field theory and ordinary quantum mechanics. It describes the probability amplitude for a process in which the system transitions from an initial to a final state as a result of an interaction. When working in the interaction picture, the time-evolution operator is the best tool for evaluating the scattering matrix. We introduce the time-dependent state vector $\Psi^{\text{IR}}(t)$, which in the limit $t \rightarrow -\infty$ has evolved from the "free" initial state Φ_i

$$\lim_{t \rightarrow -\infty} \Psi^{\text{IR}}(t) = \Phi_i, \quad (3.19)$$

where Φ_i is eigenfunction of the operator $\hat{H}_{0,F}$. We should point out that such a consideration has a flaw: the vacuum fluctuations caused by the interaction between quantum fields do not completely disappear in the asymptotical region. As a result,

this approach to constructing the S-matrix is somewhat naive. This is on purpose: the approach works in practice, and technical issues can be addressed when a slightly more rigorous approach is used, with so-called in and out fields introduced (Greiner and Reinhardt, 1996; Schweber, 1961; Bjorken and Drell, 1965). The end result is, of course, the same as when taking the shorter route.

According to the definition, the S-matrix element is a projection of the state vector $\Psi^{\text{IR}}(t)$ on the final state Φ_f , in the limit $t \rightarrow +\infty$

$$S_{fi} = \lim_{t \rightarrow +\infty} \langle \Phi_f | \Psi^{\text{IR}}(t) \rangle = \langle \Phi_f | \hat{S} | \Phi_i \rangle, \quad (3.20)$$

where the final state Φ_f similarly to the Φ_i also describes free (bare) particles. Making use of Eqs. (3.12) and (3.19) one can express S-matrix element in terms of the time-evolution operator as follows

$$S_{fi} = \lim_{t_2 \rightarrow +\infty} \lim_{t_1 \rightarrow -\infty} \langle \Phi_f | \hat{U}^{\text{IR}}(t_2, t_1) | \Phi_i \rangle. \quad (3.21)$$

Comparing Eq. (3.21) with Eq. (3.20), we get the following definition of the \hat{S} -operator

$$\hat{S} = \hat{U}^{\text{IR}}(\infty, -\infty), \quad (3.22)$$

or according to Eq. (3.15)

$$\hat{S} = \mathbb{1} + \sum_{n=1}^{\infty} \frac{(-i)^n}{n!} \int dt_1 \cdots \int dt_n T \left[\hat{H}_{\text{int}}^{\text{IR}}(t_1) \cdots \hat{H}_{\text{int}}^{\text{IR}}(t_n) \right] = T \left[e^{-i \int dt \hat{H}_{\text{int}}^{\text{IR}}(t)} \right]. \quad (3.23)$$

Calculating the S-matrix element observable quantities, one can derive, e. g., scattering cross sections and decay rates by taking the square and doing certain kinematical manipulations.

3.3.1 Adiabatic S-matrix formalism of Gell-Mann, Low, and Sucher

In earlier sections, we showed how to get the perturbation series for the time-evolution operator $\hat{U}^{\text{IR}}(t, t_0)$ within the framework of the interaction picture. This gives a systematic way to build the S-matrix for scattering problems. Furthermore, the approach allows for the calculation of the energy shifts of states from the discrete spectrum.

Here we start consideration again within Schrödinger picture, the moment when another representation is considered we will denote wave-functions and operators

with the corresponding label. Let us introduce a discrete eigenstate Φ of the unperturbed Hamiltonian

$$\hat{H}_{0,F}\Phi = E_0\Phi. \quad (3.24)$$

And we want to find the eigenstate Ψ of the full Hamiltonian

$$\hat{H} = \hat{H}_{0,F} + \lambda\hat{H}_{int}, \quad (3.25)$$

containing some perturbation operator \hat{H}_{int}

$$\hat{H}\Psi = E\Psi. \quad (3.26)$$

The coupling constant λ determines the strength of the perturbation, which helps us keep track of the terms in the perturbation series. If \hat{H}_{int} is a stationary perturbation, the time-evolution operator may appear to be the wrong tool to use to describe the system at first glance. However, the adiabatic switching of the interaction comes to the rescue here. By modifying the Hamiltonian, the stationary problem is transformed into a time-dependent one

$$\hat{H}_\epsilon(t=0) = \hat{H} \quad , \quad \lim_{t \rightarrow \pm\infty} \hat{H}_\epsilon(t) = \hat{H}_{0,F}. \quad (3.27)$$

An explicit prescription for accomplishing this can be expressed in terms of a switching function

$$\hat{H}_\epsilon(t) = \hat{H}_{0,F} + \lambda e^{-\epsilon|t|}\hat{H}_{int}. \quad (3.28)$$

At asymptotic times $t \rightarrow \pm\infty$, the perturbation operator \hat{H}_{int} is exponentially dampened off. Of course, because the procedure's implementation is arbitrary, physical observables should not be dependent on it. As a result, at the end of the calculation, it must be possible to take the limit $\epsilon \rightarrow 0$.

Let us now move on to the interaction representation. According to Eq. (3.8), the equation of motion for the "adiabatic" state vector is given by

$$i\frac{\partial\Psi_\epsilon^{IR}(t)}{\partial t} = \lambda e^{-\epsilon|t|}\hat{H}_{int}^{IR}(t)\Psi_\epsilon^{IR}(t), \quad (3.29)$$

with the perturbation operator $\hat{H}_{\text{int}}^{\text{IR}}(t)$ given by Eq. (3.9). Similarly to Sec. 3.2, one can obtain the following differential equation for the adiabatic time-evolution operator \hat{U}_ϵ

$$i \frac{\partial}{\partial t} \hat{U}_\epsilon^{\text{IR}}(t, t_0) = \lambda e^{-\epsilon|t|} \hat{H}_{\text{int}}^{\text{IR}}(t) \hat{U}_\epsilon^{\text{IR}}(t, t_0). \quad (3.30)$$

According to the Eq. (3.29), the state $\Psi_\epsilon^{\text{IR}}(t)$ in the limit $t \rightarrow \infty$ is a constant. As an initial condition, we require that the state vector approach the unperturbed state (3.24)

$$\lim_{t \rightarrow -\infty} \Psi_\epsilon^{\text{IR}}(t) = \Phi. \quad (3.31)$$

Also we know, that at $t = 0$, $\hat{H}_\epsilon(0) = \hat{H}$, see Eq. (3.27). With all this in mind, one can conclude that the state

$$\Psi_\epsilon \equiv \Psi_\epsilon^{\text{IR}}(0) = \hat{U}_\epsilon^{\text{IR}}(0, -\infty) \Phi, \quad (3.32)$$

in some way is related to the desired solution of the full Hamiltonian (3.26). We note that this is only true if the perturbation operator is turned on "slowly enough", otherwise the switching-on will cause artificial dynamical excitations. However, it can be shown that limit of arbitrarily slow switching, $\lim_{\epsilon \rightarrow 0} \Psi_\epsilon^{\text{IR}}(0)$, does not exist mathematically! Despite this limitation, Gell-Mann and Low, [1951] demonstrated how to obtain a meaningful result for the energy of an interacting system. Let us now outline the main results of their work.

1. The state

$$\Psi = \lim_{\epsilon \rightarrow 0} \frac{\hat{U}_\epsilon^{\text{IR}}(0, -\infty) \Phi}{\langle \Phi | \hat{U}_\epsilon^{\text{IR}}(0, -\infty) | \Phi \rangle} \equiv \lim_{\epsilon \rightarrow 0} \frac{\Psi_\epsilon}{\langle \Phi | \Psi_\epsilon \rangle}, \quad (3.33)$$

is an eigenstate of the full Hamiltonian, i.e.,

$$(\hat{H} - E) \lim_{\epsilon \rightarrow 0} \frac{\Psi_\epsilon}{\langle \Phi | \Psi_\epsilon \rangle} = 0. \quad (3.34)$$

This holds true if the limit (3.33) exists and the perturbation series of Ψ in powers of the coupling constant λ is well defined.

2. The following formula can be used to calculate the *energy shift* of the state Ψ with respect to Φ caused by the interaction

$$\Delta E = E - E_0 = \lim_{\epsilon \rightarrow 0} i \epsilon \lambda \frac{\partial}{\partial \lambda} \ln \langle \Phi | \hat{U}_\epsilon^{\text{IR}}(0, -\infty) | \Phi \rangle. \quad (3.35)$$

Let us note, that the Gell-Mann-Low theorem does not guarantee the existence of Ψ defined in (3.33). However, if this state can be constructed, the interacting problem is solved.

Sucher, [1957] later presented the symmetrized form of Eq. (3.35), which became widely used for the calculations of level shifts for a state Φ

$$\Delta E = \lim_{\substack{\varepsilon \rightarrow 0 \\ \lambda \rightarrow 1}} \frac{i \varepsilon \lambda (\partial/\partial \lambda) \langle \Phi | \hat{S}_{\varepsilon, \lambda} | \Phi \rangle}{2 \langle \Phi | \hat{S}_{\varepsilon, \lambda} | \Phi \rangle}, \quad (3.36)$$

with $\hat{S}_{\varepsilon, \lambda}$ being an adiabatic \hat{S} -operator

$$\begin{aligned} \hat{S}_{\varepsilon, \lambda} &= \text{T} \left[e^{(-i\lambda \int dx e^{-\varepsilon|t|} \hat{H}_{\text{int}}^{\text{IR}}(x))} \right] \\ &= 1 + \sum_{j=1}^{\infty} \frac{(-i\lambda)^j}{j!} \int x_j \dots \int x_1 e^{-\varepsilon|t_j|} \dots e^{-\varepsilon|t_1|} \text{T} \left[\hat{H}_{\text{int}}^{\text{IR}}(x_j) \dots \hat{H}_{\text{int}}^{\text{IR}}(x_1) \right]. \end{aligned} \quad (3.37)$$

3.4 GREEN'S FUNCTION AND S-MATRIX OF BOUND-STATE QED THEORY

The exact scattering amplitudes, on the other hand, are more conveniently expressed in terms of field operators in the Heisenberg representation, where the time dependence is governed by the full QED Hamiltonian $\hat{H}_{\text{QED}} = \hat{H}_{\text{o,F}} + \hat{H}_{\text{int}}$ of a system of interacting particles. We emphasize once more that the full Hamiltonian in Heisenberg and Schrödinger is the same. Let us determine the relationship between the operators in the Heisenberg interaction representations. To simplify the discussion, we again make the assumption (which will not affect the final result) that the interaction is adiabatically "switched off" when $t = -\infty$, i. e. $\hat{H}_{\text{int}}^{\text{IR}}(t) = 0$. Then, for $t \rightarrow -\infty$, the Heisenberg and interaction representations coincide, and the wave functions of the system, Φ^{H} ⁵ and Ψ^{IR} , are the same

$$\Psi^{\text{IR}}(t = -\infty) = \Phi^{\text{H}}. \quad (3.38)$$

The wave function in the Heisenberg representation, on the other hand, has no time dependence (all time dependence on operators!), whereas in the interaction representation, the time dependence of the wave function has the form (see Eq. (3.12))

$$\Psi^{\text{IR}}(t) = \hat{U}^{\text{IR}}(t, -\infty) \Psi^{\text{IR}}(-\infty). \quad (3.39)$$

⁵Throughout this section label H refers to the Heisenberg picture.

Here \hat{U}^{IR} is given by Eq. (3.17). Comparing Eqs. (3.38) and (3.39), one can get the following equation

$$\Psi^{\text{IR}}(t) = \hat{U}^{\text{IR}}(t, -\infty)\Phi^{\text{H}}, \quad (3.40)$$

as the relation between the wave functions in the two representations. The corresponding formula for transforming the field operators, i.e., electron-positron field operators, has a similar form

$$\begin{aligned} \hat{\psi}(t, \mathbf{x}) &= (\hat{U}^{\text{IR}})^{-1}(t, -\infty)\hat{\psi}^{\text{IR}}(t, \mathbf{x})\hat{U}^{\text{IR}}(t, -\infty) \\ &= \hat{U}^{\text{IR}}(-\infty, t)\hat{\psi}^{\text{IR}}(t, \mathbf{x})\hat{U}^{\text{IR}}(t, -\infty), \end{aligned} \quad (3.41)$$

and likewise for field operators $\hat{\psi}$ and \hat{A}_μ in Heisenberg representation ⁶.

3.4.1 One-particle Green's function: Exact electron and photon propagators

In QED theory, invariant functions, particularly propagators of electron-positron and electromagnetic fields, play an important role. They are defined in terms of field operator products and can be calculated in closed form for free fields (see Chap. 2). For interacting fields, the exact electron \mathcal{S}_F and photon $\mathcal{D}_{\mu\nu}$ propagators can also be constructed as a vacuum expectation value of the time-ordered product

$$i\mathcal{S}_F(t_x - t_y, \mathbf{x}, \mathbf{y}) = \langle 0 | \text{T} [\hat{\psi}(x)\hat{\psi}(y)] | 0 \rangle, \quad (3.42)$$

$$-i\mathcal{D}_{\mu\nu}(t_x - t_y, \mathbf{x} - \mathbf{y}) = \langle 0 | \text{T} [\hat{A}_\mu(x)\hat{A}_\nu(y)] | 0 \rangle. \quad (3.43)$$

We note that the spectral representations (2.15) and (2.18)–(2.20) are not valid because an exact solution for the interacting fields is no longer available. However, using the transformation formulas for the field operators discussed above (3.41), the following formula can be obtained for the exact electron \mathcal{S}_F propagator

$$i\mathcal{S}_F(t_x - t_y, \mathbf{x}, \mathbf{y}) = \frac{\langle 0 | \text{T} [\hat{\psi}^{\text{IR}}(x)\hat{\psi}^{\text{IR}}(y)] | 0 \rangle}{\langle 0 | \hat{S} | 0 \rangle}, \quad (3.44)$$

⁶Here and throughout the thesis the label H for the field operators in Heisenberg representation is omitted.

and photon propagator $\mathcal{D}_{\mu\nu}$

$$-i\mathcal{D}_{\mu\nu}(t_x - t_y, \mathbf{x} - \mathbf{y}) = \frac{\langle 0 | T [\hat{A}_\mu^{\text{IR}}(\mathbf{x}) \hat{A}_\nu^{\text{IR}}(\mathbf{y})] | 0 \rangle}{\langle 0 | \hat{S} | 0 \rangle}. \quad (3.45)$$

For detailed description see, i.e., (Berestetsky et al., 1982; Peskin and Schroeder, 1995). By substituting the expansion (3.23) for \hat{S} -operator in the numerator and denominator and averaging using Wick's theorem (see Sec. 3.4.2), we get an expansion of $\mathcal{D}_{\mu\nu}$ and \mathcal{S}_F in the power series of α . The formulas (3.44) and (3.45) illustrate the relationship between the one-particle Green's function and the \hat{S} -operator. Later in Sec. 3.4.2 we adopt the definition (3.44) for the case of N-particle Green's function formalism used for calculating QED corrections to the energy shifts of few-electron ions.

3.4.2 N-particle Green's function: two-time Green's function formalism

We are now ready to talk about the actual calculations of the QED corrections to the energy shift of few-electron ions. Historically, the method given in Sec. 3.3.1 was the first approach suited for obtaining formal equations for the energy shift of a bound-state level (Gell-Mann and Low, 1951; Sucher, 1957). This approach has been employed in investigations involving high-Z few-electron systems, such as, e. g., Refs. (Labzowsky et al., 1993; Sapirstein, 1998). However, practical application of this method revealed that it has several serious drawbacks: the formal expressions for the so-called reducible diagrams⁷ are derived in a very complicated manner, this method requires a special investigation of the renormalization procedure because the adiabatic $\hat{S}_{\varepsilon,\lambda}$ suffers from ultraviolet divergences⁸, and it does not provide a proper treatment of quasi-degenerate levels.

Another approach to developing a perturbation theory for high-Z few-electron systems is to use Green's functions, which solves these issues far more elegantly. We remark that many variants of Green's function formalism have been created up to this point, with the techniques of extracting physical information from Green's functions, namely the energy levels and transition and scattering amplitudes, differing from one another. In the present thesis, we will work within the two-time Green's-function method (TTGF). This technique was developed by Shabaev Shabaev, 2002 and due to its ease of use in actual computations, the TTGF formalism has gained popularity in studies involving the energy shift of high-Z few-electron systems [see, for example,

⁷We refer to "reducible diagrams" as diagrams in which an atom's intermediate-state energy coincides with the reference-state energy.

⁸Because the adiabatically damped component, $\exp(-\varepsilon|t|)$, is non-covariant, the ultraviolet divergences in $\hat{S}_{\varepsilon,\lambda}$ can not be eliminated if $\varepsilon \neq 0$.

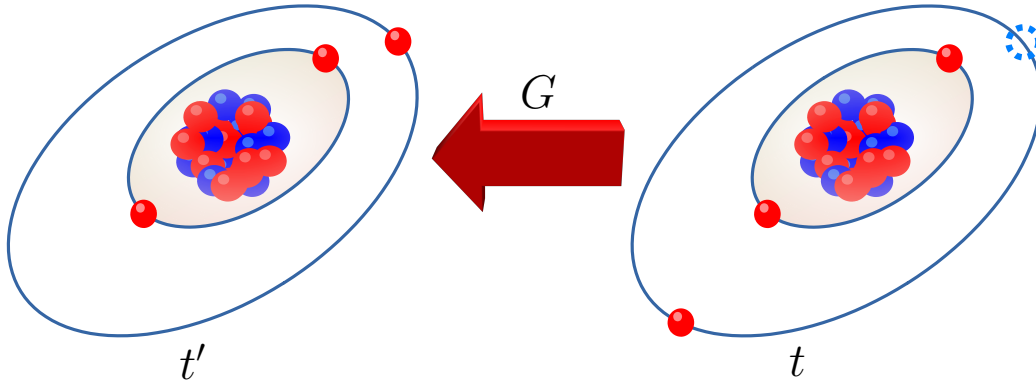


Figure 3.1: The N -particle two-time Green's function G is the amplitude for going from one state of N particles to another state. Here $N = 3$ and $G \equiv G(t', \mathbf{x}'_1, \mathbf{x}'_2, \mathbf{x}'_3; t, \mathbf{x}_1, \mathbf{x}_2, \mathbf{x}_3)$.

Refs. (Yerokhin et al., [1998]; Yerokhin et al., [2021]; Sikora et al., [2020]; Cakir et al., [2020]; Glazov et al., [2019a]; Glazov et al., [2006]; Volotka et al., [2014]; Oreshkina et al., [2008]). The method is based on using contour integral formalism to generate perturbation theories for the energy shift of some bound state, which was first developed in operator theory by Szökefalvi-Nagy and Kato (Kato, [1949]; Kato, [1950a]; Sz-Nagy, [1946]; Kato, [1950b]). Logunov and Tavkhelidze (Logunov and Tavkhelidze, [1962]) were the first to use two-time Green's functions in quantum field theory to formulate a quasipotential method. TTGF method, contrary to the Gell-Mann-Low-Sucher formalism, includes a straightforward procedure for calculating the energy of degenerate and quasi-degenerate states. The following sections summarize the method's main ideas in the case of a single level. For a more complete description see Ref. (Shabaev, [2002]).

As shown in Fig. [3.1] the two-time Green's function represents the probability amplitude for N fermions to move from one position to the other. A typical N -particle correlation function between two times t and t' is the corresponding mathematical object

$$G \equiv G(t', \mathbf{x}'_1, \dots, \mathbf{x}'_N; t, \mathbf{x}_1, \dots, \mathbf{x}_N) = \langle 0 | T [\hat{\psi}(t', \mathbf{x}'_1) \cdots \hat{\psi}(t', \mathbf{x}'_N) \times \hat{\bar{\psi}}(t, \mathbf{x}_N) \cdots \hat{\bar{\psi}}(t, \mathbf{x}_1)] | 0 \rangle. \quad (3.46)$$

We note that the two-time Green function G , like the usual Green function $G' \equiv G((\mathbf{x}'_1, t'_1), \dots, (\mathbf{x}'_N, t'_N); (\mathbf{x}_1, t_1), \dots, (\mathbf{x}_N, t_N))$ that depends on $2(N - 1)$ relative times, contains all of the information about the atomic system's energy levels (Shabaev, [2002]). However, G is easier to extract information about energy levels from, so Shabaev (Shabaev, [2002]) suggested working with TTGF rather than G' .

To demonstrate that it is possible to extract energies from TTGF, G , we should

make the following steps. Firstly, let us introduce the Fourier transform of the TTGF \mathcal{G} in time

$$\begin{aligned} & \mathcal{G}(E; \mathbf{x}'_1, \dots, \mathbf{x}'_N; \mathbf{x}_1, \dots, \mathbf{x}_N) \delta(E - E') \\ &= \frac{1}{2\pi i} \frac{1}{N!} \int_{-\infty}^{\infty} dt dt' \exp(iE't' - iEt) \\ & \quad \times \left\langle 0 \left| T \left[\hat{\psi}(t', \mathbf{x}'_1) \cdots \hat{\psi}(t', \mathbf{x}'_N) \hat{\bar{\psi}}(t, \mathbf{x}_N) \cdots \hat{\bar{\psi}}(t, \mathbf{x}_1) \right] \right| 0 \right\rangle. \end{aligned} \quad (3.47)$$

The spectral representation of \mathcal{G} reads as (Shabaev, 2002)

$$\begin{aligned} & \mathcal{G}(E; \mathbf{x}'_1, \dots, \mathbf{x}'_N; \mathbf{x}_1, \dots, \mathbf{x}_N) \\ &= \sum_n \frac{\Pi_n(\mathbf{x}'_1, \dots, \mathbf{x}'_N) \bar{\Pi}_n(\mathbf{x}_1, \dots, \mathbf{x}_N)}{E - E_n + i\delta} + (-1)^N \sum_n \frac{\Xi_n(\mathbf{x}'_1, \dots, \mathbf{x}'_N) \bar{\Xi}_n(\mathbf{x}_1, \dots, \mathbf{x}_N)}{E + E_n - i\delta}, \end{aligned} \quad (3.48)$$

with

$$\begin{aligned} \Pi_n(\mathbf{x}_1, \dots, \mathbf{x}_N) &= \frac{1}{\sqrt{N!}} \langle 0 | \hat{\psi}(0, \mathbf{x}_1) \cdots \hat{\psi}(0, \mathbf{x}_N) | \Omega_n \rangle, \\ \Xi_n(\mathbf{x}_1, \dots, \mathbf{x}_N) &= \frac{1}{\sqrt{N!}} \langle \Omega_n | \hat{\psi}(0, \mathbf{x}_1) \cdots \hat{\psi}(0, \mathbf{x}_N) | 0 \rangle. \end{aligned} \quad (3.49)$$

Here $|\Omega_n\rangle$ denotes the states with the exact energy eigenvalues E_n ,

$$\hat{H}_{\text{QED}} |\Omega_n\rangle = E_n |\Omega_n\rangle, \quad (3.50)$$

where \hat{H}_{QED} is a full QED Hamiltonian given by Eq. (3.4). The summation in Eq. (3.48) encompasses all bound and continuum states of the system of the interacting fields. It was assumed for the vacuum energy $E_0 = 0$ without loss of generality. One can rewrite Eq. (3.48) in terms of functions A_1 and B_1 as

$$\begin{aligned} & \mathcal{G}(E; \mathbf{x}'_1, \dots, \mathbf{x}'_N; \mathbf{x}_1, \dots, \mathbf{x}_N) \\ &= \int_{E_{\min}^{(+)}}^{\infty} dE' \frac{A_1(E'; \mathbf{x}'_1, \dots, \mathbf{x}'_N; \mathbf{x}_1, \dots, \mathbf{x}_N)}{E - E'} \\ & \quad - (-1)^N \int_{E_{\min}^{(-)}}^{\infty} dE' \frac{B_1(E'; \mathbf{x}'_1, \dots, \mathbf{x}'_N; \mathbf{x}_1, \dots, \mathbf{x}_N)}{E + E'}, \end{aligned} \quad (3.51)$$

where

$$\begin{aligned} A_1 &\equiv A_1(E; \mathbf{x}'_1, \dots, \mathbf{x}'_N; \mathbf{x}_1, \dots, \mathbf{x}_N) = \sum_n \delta(E - E_n) \Pi_n(\mathbf{x}'_1, \dots, \mathbf{x}'_N) \bar{\Pi}_n(\mathbf{x}_1, \dots, \mathbf{x}_N), \\ B_1 &\equiv B_1(E; \mathbf{x}'_1, \dots, \mathbf{x}'_N; \mathbf{x}_1, \dots, \mathbf{x}_N) = \sum_n \delta(E - E_n) \Xi_n(\mathbf{x}'_1, \dots, \mathbf{x}'_N) \bar{\Xi}_n(\mathbf{x}_1, \dots, \mathbf{x}_N). \end{aligned} \quad (3.52)$$

In Eq. (3.51) $E_{\min}^{(+)}$ is the minimal energy of states with electric charge eN and $E_{\min}^{(-)}$ is the minimal energy of states with electric charge $-eN$. Function $\mathcal{G}(E)$ (we omitted $\mathbf{x}'_1, \dots, \mathbf{x}'_N; \mathbf{x}_1, \dots, \mathbf{x}_N$) is an analytical continuation of the Green's function to the complex E -plane with the cuts $(-\infty, E_{\min}^{(-)})$ and $[E_{\min}^{(+)}, \infty)$. The system's bound states are of interest to us. The energies of the states with charge eN , which are physically the atomic eigenstates of an ion with N orbiting electrons, are the poles of $\mathcal{G}(E)$ on a positive real part, according to Eq. (3.51). We note, that in the total charge of the system, the charge of the nucleus is not included. For the case of noninteracting fields, $\widehat{\psi}^{(0)}$ and $\widehat{A}_\mu^{(0)}$, the poles corresponding to bound states are isolated. The isolated poles become branch points when the interaction between the fields is turned on since the photon has a zero mass. To develop the perturbation theory for energy level computations, we must separate these poles from the corresponding cuts. To accomplish so, we introduce the nonzero photon mass μ in such a manner that it is bigger than the level's energy shift (or energy splitting) and considerably smaller than the distance between levels. After performing the calculations we must put $\mu \rightarrow 0$. We should also mention that we ignore the instability of excited states and thus assume that the corresponding poles lie on the real axis.

Energy of a single level of N-electron atom

Now let us derive the formulas for the energy ΔE_a of a single isolated level a of an N -electron atom. The unperturbed energy level $E_a^{(0)}$ neglecting the perturbation is given by

$$E_a^{(0)} = \varepsilon_{a_1} + \dots + \varepsilon_{a_N}, \quad (3.53)$$

where ε_{a_N} is the one-electron Dirac energy,

$$h_D \phi_{a_N}(\mathbf{x}) = \left[-i\boldsymbol{\alpha} \cdot \boldsymbol{\nabla} + V^{\text{nucl}}(\mathbf{x}) + \beta \right] \phi_{a_N}(\mathbf{x}) = \varepsilon_{a_N} \phi_{a_N}(\mathbf{x}). \quad (3.54)$$

Here h_D is a Dirac Hamiltonian, see Eq. (2.10). The corresponding unperturbed N -electron wave function $u_a(\mathbf{x}_1, \dots, \mathbf{x}_N)$ is a one-determinant function

$$u_a(\mathbf{x}_1, \dots, \mathbf{x}_N) = \frac{1}{\sqrt{N!}} \sum_P (-1)^P \phi_{P a_1}(\mathbf{x}_1) \cdots \phi_{P a_N}(\mathbf{x}_N), \quad (3.55)$$

where P is the permutation operator giving rise to the sign $(-1)^P$ according to the parity of the permutation.

Let us introduce the function $g_{aa}(E)$

$$\begin{aligned} g_{aa}(E) &= \langle u_a | \mathcal{G}(E) \gamma_1^0 \cdots \gamma_N^0 | u_a \rangle \\ &\equiv \int d\mathbf{x}_1 \cdots d\mathbf{x}_N d\mathbf{x}'_1 \cdots d\mathbf{x}'_N u_a^\dagger(\mathbf{x}'_1, \dots, \mathbf{x}'_N) \\ &\quad \times \mathcal{G}(E, \mathbf{x}'_1, \dots, \mathbf{x}'_N; \mathbf{x}_1, \dots, \mathbf{x}_N) \gamma_1^0 \cdots \gamma_N^0 u_a(\mathbf{x}_1, \dots, \mathbf{x}_N). \end{aligned} \quad (3.56)$$

Using spectral representation for $\mathcal{G}(E)$ (3.51), where from the sum we consider only one bound state a , i. e. $n = a$ and $E' = E_a > 0$, one can show that

$$g_{aa}(E) = \frac{A_a}{E - E_a} + \text{terms that are regular at } E \sim E_a, \quad (3.57)$$

where according to Eqs. (3.49), (3.52)

$$\begin{aligned} A_a &= \frac{1}{N!} \int d\mathbf{x}_1 \cdots d\mathbf{x}_N d\mathbf{x}'_1 \cdots d\mathbf{x}'_N u_a^\dagger(\mathbf{x}'_1, \dots, \mathbf{x}'_N) \Pi_a(\mathbf{x}'_1, \dots, \mathbf{x}'_N) \\ &\quad \times \Pi_a^\dagger(\mathbf{x}_1, \dots, \mathbf{x}_N) u_a(\mathbf{x}_1, \dots, \mathbf{x}_N) \\ &= \frac{1}{N!} \int d\mathbf{x}_1 \cdots d\mathbf{x}_N d\mathbf{x}'_1 \cdots d\mathbf{x}'_N u_a^\dagger(\mathbf{x}'_1, \dots, \mathbf{x}'_N) \langle 0 | \hat{\psi}(0, \mathbf{x}'_1) \cdots \hat{\psi}(0, \mathbf{x}'_N) | \Omega_a \rangle \\ &\quad \times \langle \Omega_a | \hat{\psi}^\dagger(0, \mathbf{x}_N) \cdots \hat{\psi}^\dagger(0, \mathbf{x}_1) | 0 \rangle u_a(\mathbf{x}_1, \dots, \mathbf{x}_N). \end{aligned} \quad (3.58)$$

We remind that when a non-zero photon mass μ is introduced, the pole corresponding to the bound state a is isolated. As a result, the contour integral method is useful for generating the perturbation series for E_a . Let us choose a contour Γ in the complex E -plane that surrounds the pole corresponding to the level a while remaining outside of all other singularities. Then, according to the residue theorem

$$\frac{1}{2\pi i} \oint_{\Gamma} dE E g_{aa}(E) = E_a A_a, \quad (3.59)$$

and

$$\frac{1}{2\pi i} \oint_{\Gamma} dE g_{aa}(E) = A_a, \quad (3.60)$$

where the contour Γ is oriented anticlockwise. From Eqs. (3.59) and (3.60), one can get the following formula for energy E_a

$$E_a = \frac{\frac{1}{2\pi i} \oint_{\Gamma} dE E g_{aa}(E)}{\frac{1}{2\pi i} \oint_{\Gamma} dE g_{aa}(E)}. \quad (3.61)$$

For our purposes, it is more convenient to transform Eq.(3.61) in a way that directly yields the energy shift $\Delta E_a = E_a - E_a^{(0)}$,

$$\Delta E_a = \frac{\frac{1}{2\pi i} \oint_{\Gamma} dE \left(E - E_a^{(0)} \right) \Delta g_{aa}(E)}{1 + \frac{1}{2\pi i} \oint_{\Gamma} dE \Delta g_{aa}(E)}, \quad (3.62)$$

where $\Delta g_{aa} = g_{aa} - g_{aa}^{(0)}$ and $g_{aa}^{(0)} = \frac{1}{E - E_a^{(0)}}$.

One can build the function $\Delta g_{aa}(E)$ by perturbation theory

$$\Delta g_{aa}(E) = \Delta g_{aa}^{(1)}(E) + \Delta g_{aa}^{(2)}(E) + \dots, \quad (3.63)$$

where the superscript denotes the order in α . Accordingly, one can construct perturbation series in α for the energy shift ΔE_a

$$\Delta E_a = \Delta E_a^{(1)} + \Delta E_a^{(2)} + \dots, \quad (3.64)$$

where

$$\Delta E_a^{(1)} = \frac{1}{2\pi i} \oint_{\Gamma} dE \Delta E \Delta g_{aa}^{(1)}(E), \quad (3.65)$$

$$\begin{aligned} \Delta E_a^{(2)} = & \frac{1}{2\pi i} \oint_{\Gamma} dE \Delta E \Delta g_{aa}^{(2)}(E) \\ & - \left(\frac{1}{2\pi i} \oint_{\Gamma} dE \Delta E \Delta g_{aa}^{(1)}(E) \right) \left(\frac{1}{2\pi i} \oint_{\Gamma} dE \Delta g_{aa}^{(1)}(E) \right), \end{aligned} \quad (3.66)$$

$$\begin{aligned} \Delta E_a^{(3)} = & \frac{1}{2\pi i} \oint_{\Gamma} dE \left(E - E_a^{(0)} \right) \Delta g_{aa}^{(3)}(E) \\ & - \frac{1}{2\pi i} \oint_{\Gamma} dE \left(E - E_a^{(0)} \right) \Delta g_{aa}^{(2)}(E) \frac{1}{2\pi i} \oint_{\Gamma} dE' \Delta g_{aa}^{(1)}(E') \\ & - \frac{1}{2\pi i} \oint_{\Gamma} dE \left(E - E_a^{(0)} \right) \Delta g_{aa}^{(1)}(E) \\ & \times \left\{ \frac{1}{2\pi i} \oint_{\Gamma} dE' \Delta g_{aa}^{(2)}(E') - \left[\frac{1}{2\pi i} \oint_{\Gamma} dE' \Delta g_{aa}^{(1)}(E') \right]^2 \right\}, \end{aligned} \quad (3.67)$$

with $\Delta E \equiv E - E_a^{(0)}$. We should note that the terms in the second line of Eq. (3.66) and the last three lines of Eq. (3.67) are referred to as disconnected contributions, and they are usually merged with the corresponding irreducible diagrams.

Perturbation series for two-time Green's function

Let us discuss the procedure of calculating the perturbation series of function g_{aa} (3.63). If one finds the perturbation expansion for the Fourier transform of the TTGF, \mathcal{G} , or the TTGF, G , itself, one finds the perturbation series of function g_{aa} , according to definition (3.56).

Let us return to the definition of TTGF (3.46). When Eq. (3.46) is compared to Eq. (3.42), it is clear that the two-time Green's function is nothing more than an exact electron propagator for $N = 1$. Therefore, similarly to Eq. (3.44), exact TTGF can be represented in terms of corresponding fields in interaction representation

$$G(t', \mathbf{x}'_1, \dots, \mathbf{x}'_N; t, \mathbf{x}_1, \dots, \mathbf{x}_N) = \frac{\langle 0 | T \left[\hat{\psi}^{\text{IR}}(t', \mathbf{x}'_1) \cdots \hat{\psi}^{\text{IR}}(t', \mathbf{x}'_N) \hat{\psi}^{\text{IR}}(t, \mathbf{x}_N) \cdots \hat{\psi}^{\text{IR}}(t, \mathbf{x}_1) e^{-i \int dz \hat{\mathcal{H}}_{\text{int}}^{\text{IR}}(z)} \right] | 0 \rangle}{\langle 0 | T \left[e^{-i \int dz \hat{\mathcal{H}}_{\text{int}}^{\text{IR}}(z)} \right] | 0 \rangle}. \quad (3.68)$$

Here $\hat{\mathcal{H}}_{\text{int}}^{\text{IR}}(z)$ is Hamiltonian density describing the interaction

$$\hat{\mathcal{H}}_{\text{int}}^{\text{IR}}(z) = -\hat{\mathcal{L}}_{\text{int}}^{\text{IR}}(z) = e : \hat{\psi}^{\text{IR}}(z) \gamma_\mu \hat{\psi}^{\text{IR}}(z) \hat{A}_\mu^{\text{IR}}(z) :, \quad (3.69)$$

with $:$ being normal product. The perturbation expansion for TTGF (with fine structure constant α being an expansion parameter) is obtained by replacing the exponents in Eq. (3.68) with the Taylor series

$$G(t', \mathbf{x}'_1, \dots, \mathbf{x}'_N; t, \mathbf{x}_1, \dots, \mathbf{x}_N) = \left\{ \sum_{m=0}^{\infty} \frac{(-i)^m}{m!} \int dz_1 \cdots dz_m \langle 0 | T \left[\hat{\psi}^{\text{IR}}(t', \mathbf{x}'_1) \cdots \hat{\psi}^{\text{IR}}(t', \mathbf{x}'_N) \times \hat{\psi}^{\text{IR}}(t, \mathbf{x}_N) \cdots \hat{\psi}^{\text{IR}}(t, \mathbf{x}_1) \hat{\mathcal{H}}_{\text{int}}^{\text{IR}}(z_1) \cdots \hat{\mathcal{H}}_{\text{int}}^{\text{IR}}(z_m) \right] | 0 \rangle \right\} \times \left\{ \sum_{l=0}^{\infty} \frac{(-i)^l}{l!} \int d^4 z_1 \cdots d^4 z_l \langle 0 | T \left[\hat{\mathcal{H}}_{\text{int}}^{\text{IR}}(z_1) \cdots \hat{\mathcal{H}}_{\text{int}}^{\text{IR}}(z_l) \right] | 0 \rangle \right\}^{-1}. \quad (3.70)$$

As a result, the perturbation series for the function g_{aa} (3.63) and thus the energies E_a (3.64) are defined.

The function on the right side of the Eq. (3.68) can be constructed using Wick's theorem (Wick, 1950). It allows rewriting the time-ordered product of several operators

$ABCD \dots$ into a sum of normal-ordered products with all conceivable contractions \overline{AB} between two operators,

$$\begin{aligned} T[ABCD \dots] = & :ABCD \dots: + : \overline{AB}CD \dots: + : \overline{AC}BD \dots: + : \overline{AD}BC \dots: \\ & + : \overline{ABCD} \dots: + \dots + : \overline{AB}CD \dots: + : \overline{ABCD} \dots: + : \overline{ABCD} \dots: \\ & + : \overline{ABCD} \dots: + \dots \text{ all possible contractions ,} \end{aligned} \quad (3.71)$$

where the contraction between two neighboring operators is just a C-number defined as

$$\overline{AB} \equiv T[AB] - :AB: . \quad (3.72)$$

The following propagators result from contractions between the electron-positron fields $\hat{\psi}^{\text{IR}}(\mathbf{x})$ and between the photon fields $\hat{A}_{\mu}^{\text{IR}}(\mathbf{x})$

$$\begin{aligned} \overline{\hat{\psi}^{\text{IR}}(\mathbf{x})\hat{\psi}^{\text{IR}}(\mathbf{y})} &= \langle 0 | T [\hat{\psi}^{\text{IR}}(\mathbf{x})\hat{\psi}^{\text{IR}}(\mathbf{y})] | 0 \rangle \\ &= \frac{i}{2\pi} \int dE e^{-iE(t_x - t_y)} \sum_n \frac{\Phi_n(\mathbf{x})\bar{\Phi}_n(\mathbf{y})}{E - \varepsilon_n(1 - i\eta)} , \end{aligned} \quad (3.73)$$

and

$$\begin{aligned} \overline{\hat{A}_{\mu}^{\text{IR}}(\mathbf{x})\hat{A}_{\nu}^{\text{IR}}(\mathbf{y})} &= \langle 0 | T [\hat{A}_{\mu}^{\text{IR}}(\mathbf{x})\hat{A}_{\nu}^{\text{IR}}(\mathbf{y})] | 0 \rangle \\ &= \frac{i}{2\pi} \int d\omega e^{-i\omega(t_x - t_y)} D_{\mu\nu}(\omega, \mathbf{x} - \mathbf{y}). \end{aligned} \quad (3.74)$$

The temporal Fourier-transformed photon propagation function $D_{\mu\nu}(\omega, \mathbf{x} - \mathbf{y})$ is given by Eq. (2.19) in Feynman gauge and by Eq. (2.20) in Coulomb gauge. In Eq. (3.73), the sum runs over all bound and continuum electron states.

Extended Furry picture

We have previously formulated the QED perturbation theory within the framework of the extended Furry picture, in which the interaction of bound electrons with the nucleus is accounted for up to all orders in αZ and the interaction with the quantized electromagnetic field $\hat{A}_{\mu}(\mathbf{x})$ is accounted for perturbatively. As can be seen from the previous section, the construction of perturbation expansion is very convenient

within the interaction picture, so we will continue working within it unless otherwise specified. In what follows the total QED Hamiltonian $\hat{H}_{\text{QED}}^{\text{IR}}$ reads as

$$\hat{H}_{\text{QED}}^{\text{IR}} = \hat{H}_{0,\text{F}} + \hat{H}_{\text{int}}^{\text{IR}}, \quad (3.75)$$

here we used the fact that $\hat{H}_{0,\text{F}} = \hat{H}_{0,\text{F}}^{\text{IR}}$. In Eq. (3.75) the unperturbed normal-ordered Hamiltonian $\hat{H}_{0,\text{F}}$ is given by Beier et al., 2000

$$\hat{H}_{0,\text{F}} = \int d\mathbf{x} : \widehat{\psi^{(0)\dagger}}(\mathbf{x}) h_{\text{D}}(\mathbf{x}) \widehat{\psi^{(0)}}(\mathbf{x}) : = \sum_n^{\varepsilon_n > 0} \varepsilon_n a_n^\dagger a_n - \sum_n^{\varepsilon_n < 0} \varepsilon_n b_n^\dagger b_n, \quad (3.76)$$

and the interaction Hamiltonian $\hat{H}_{\text{int}}^{\text{IR}}$ reads as

$$\hat{H}_{\text{int}}^{\text{IR}} = \int d\mathbf{x} \hat{\mathcal{H}}_{\text{int}}^{\text{IR}}(\mathbf{x}) = \int d\mathbf{x} : \left(\hat{\psi}^{\text{IR}}(\mathbf{x}) \right)^\dagger h_{\text{int}}(\mathbf{x}) \hat{\psi}^{\text{IR}}(\mathbf{x}) :. \quad (3.77)$$

The interaction term $h_{\text{int}}(\mathbf{x})$ according to Eq. (3.69) is given by

$$h_{\text{int}}(\mathbf{x}) = e\alpha^\mu \hat{A}_\mu^{\text{IR}}(\mathbf{x}), \quad (3.78)$$

here we used the identity $\alpha^\mu = \gamma^0 \gamma^\mu$.

However, in the case of few-electron ions, it is possible to accelerate the perturbation theory by accounting for the part interelectronic interaction already in the zeroth order. To do so, one needs to add local screening potential $V^{\text{scr}}(\mathbf{x})$, which models the screening of the nuclear potential by bound electrons, to the unperturbed Dirac Hamiltonian

$$h_{\text{D}} \rightarrow h_{\text{D,eF}} = -i\boldsymbol{\alpha} \cdot \boldsymbol{\nabla} + V^{\text{eff}}(\mathbf{x}) + \beta, \quad (3.79)$$

where

$$V^{\text{eff}}(\mathbf{x}) = V^{\text{nucl}}(\mathbf{x}) + V^{\text{scr}}(\mathbf{x}). \quad (3.80)$$

It is called extended Furry picture (eF). Within the framework of this formalism, the unperturbed normal-ordered Hamiltonian $\hat{H}_{0,\text{eF}}$ is given now by

$$\begin{aligned} \hat{H}_{0,\text{F}} \rightarrow \hat{H}_{0,\text{eF}} &= \int d\mathbf{x} : \widehat{\psi_{\text{eF}}^{(0)\dagger}}(\mathbf{x}) h_{\text{D,eF}}(\mathbf{x}) \widehat{\psi_{\text{eF}}^{(0)}}(\mathbf{x}) : \\ &= \sum_n^{\varepsilon_{n,\text{eF}} > 0} \varepsilon_{n,\text{eF}} a_n^\dagger a_n - \sum_n^{\varepsilon_{n,\text{eF}} < 0} \varepsilon_{n,\text{eF}} b_n^\dagger b_n, \end{aligned} \quad (3.81)$$

where the electron-positron field operator $\widehat{\psi}_{eF}^{(0)}$ is given by the Eq. (2.9) but one need to replace ϕ_n and ε_n by the eigenfunctions and eigenvalues of the operator $h_{D,eF}$.

We note that the total QED Hamiltonian $\hat{H}_{\text{QED}}^{\text{IR}}$ (3.75) should not change since we do not change the system, only rearrange the terms. Therefore, since we add the term $V^{\text{scr}}(\mathbf{x})$ to the $\hat{H}_{\text{QED}}^{\text{IR}}$ we need to subtract it from $\hat{H}_{\text{QED}}^{\text{IR}}$ as well. We refer to this term as a counterpotential and include it to the interaction term $h_{\text{int},eF}$

$$h_{\text{int}}(\mathbf{x}) \rightarrow h_{\text{int},eF}(\mathbf{x}) = e\alpha^\mu \hat{A}_\mu^{\text{IR}}(\mathbf{x}) - V^{\text{scr}}(\mathbf{x}), \quad (3.82)$$

with the corresponding normal-ordered interaction Hamiltonian $\hat{H}_{\text{int},eF}^{\text{IR}}$

$$\hat{H}_{\text{int}}^{\text{IR}} \rightarrow \hat{H}_{\text{int},eF}^{\text{IR}} = \int d\mathbf{x} : \left(\hat{\psi}_{eF}^{\text{IR}}(\mathbf{x}) \right)^\dagger h_{\text{int},eF}(\mathbf{x}) \hat{\psi}_{eF}^{\text{IR}}(\mathbf{x}) : . \quad (3.83)$$

Here as in a case of the usual Furry picture, the spectral representations of $\hat{\psi}_{eF}^{\text{IR}}$ and $\widehat{\psi}_{eF}^{(0)}$ coincide.

In the present thesis, we perform calculations within the extended Furry picture, which has been already successfully applied to the QED calculations of various atomic properties (Sapirstein and Cheng, 2001; Oreshkina et al., 2007; Sapirstein and Cheng, 2006; Oreshkina et al., 2008; Glazov et al., 2019b; Sapirstein and Cheng, 2008; Sapirstein and Cheng, 2003; Ginges et al., 2017; Glazov et al., 2006; Kozhedub et al., 2007; Malyshev et al., 2014; Kozhedub et al., 2019). We note that the framework of extended Furry picture allows not only to accelerate the perturbation theory but also to relieve the quasidegeneracy of the $1s^2 2s$ and $1s^2 2p_{1/2}$ states already at the zeroth-order level and improve the energy level scheme of the first excited states. In the present thesis, we employ 5 starting potentials: Coulomb, core-Hartree (CH), Kohn-Sham (KS), Dirac-Hartree (DH), and Dirac-Slater (DS). We restrict our consideration to the Li-like ions in a ground state, i. e. configuration $(1s)^2 2s$. Therefore screening spherically symmetric potential V^{scr} partly takes into account the interelectronic interaction between the valence $2s$ electron and the core electrons of the $(1s)^2$ shell. The simplest choice of $V^{\text{scr}}(\mathbf{x})$ among mentioned above potentials is the core-Hartree (CH) potential

$$V^{\text{scr}}(\mathbf{x}) = \alpha \int_0^\infty dx' \frac{\rho_c(x')}{x_{>}}, \quad (3.84)$$

$$\rho_c(x) = 2 \left[G_{1s}^2(x) + F_{1s}^2(x) \right], \quad \int_0^\infty \rho_c(x) dx = 2,$$

where ρ_c is the radial charge density of the two core $1s$ electrons, $x_{>} = \max(x, x')$ with $x = |\mathbf{x}|$, and G/x and F/x are large and small radial components of the Dirac

wave function (Malyshev et al., 2017a). The rest of screening potentials are derived from the density-functional theory (Indelicato and Desclaux, 1990; Sapirstein and Cheng, 2002)

$$\begin{aligned} V^{\text{scr}}(\mathbf{x}) &= \alpha \int_0^\infty dx' \frac{1}{x'} \rho_t(x') - x_\alpha \frac{\alpha}{x} \left(\frac{81}{32\pi^2} x \rho_t(x) \right)^{1/3}, \\ \rho_t(x) &= \rho_c(x) + \left[G_{2s}^2(x) + F_{2s}^2(x) \right], \quad \int_0^\infty \rho_t(x) dx = 3. \end{aligned} \quad (3.85)$$

Here ρ_t is the total radial charge density of all electrons in $(1s)^22s$ configuration. The parameter $x_\alpha = 0, 2/3, 1$ are referred to as the Dirac-Hartree (DH), the Kohn-Sham (KS) and the Dirac-Slater (DS) potentials, respectively. We note, that potentials from Eq. (3.85) have wrong asymptotic behavior, therefore we replace (Latter, 1955) them by $V^{\text{eff}}(\mathbf{x}) = \frac{2\alpha}{x}$ at large x . Iterations are used to create self-consistent potentials, which continue until the energies of the core and valence states stabilize at 10^{-9} . The core-Hartree potential is not self-consistent, therefore, it is created after just one iteration.

 HYPERFINE STRUCTURE IN LITHIUMLIKE IONS

In this chapter, we investigate the interelectronic corrections to the ground-state hyperfine splitting in lithiumlike ions in the framework of the bound-state QED theory. Firstly, in Sec. 4.1, we give the basic formulas for the hfs in the lowest-order approximation. Then in Secs. 4.2.2 and 4.2.3, we consider the corrections to the hfs due to one- and two-photon exchanges. The description of the higher-order interelectronic-interaction corrections is given in Sec. 4.2.4. We conclude this chapter with the numerical results for the mentioned above corrections as well as the comparison of the QED treatment of the interelectronic interaction with methods based on the Breit approximation, see Sec. 4.3.

This chapter is based on the following reference:

Many-electron effects in the hyperfine splitting of lithiumlike ions
 V. P. Kosheleva, A. V. Volotka, D. A. Glazov, and S. Fritzsche
 Phys. Rev. Research **2**, 013364 (2020).

4.1 THE HYPERFINE SPLITTING IN THE LOWEST-ORDER APPROXIMATION

The interaction of bound electrons with the magnetic field of the nucleus causes the hyperfine splitting of atomic energy levels. The Fermi-Breit operator H_μ characterizes this interaction in the dipole approximation

$$H_\mu = \frac{|e|}{4\pi} \boldsymbol{\mu} \cdot \mathbf{T}, \quad (4.1)$$

where μ denotes the nuclear magnetic moment operator acting in nuclear state space. Operator \mathbf{T} represents the electronic part of H_μ , implying that operator \mathbf{T} acts in the space of bound electrons

$$\mathbf{T} = \sum_i \frac{[\mathbf{n}_i \times \boldsymbol{\alpha}_i]}{x_i^2} F(x_i). \quad (4.2)$$

Here index i denotes the atom's i th electron, $\mathbf{n}_i = \mathbf{x}_i/x_i$, and $F(r_i)$ denotes the nuclear magnetization volume distribution function, which is discussed further below. The total angular momentum of atomic electrons \mathbf{J} and nuclear spin \mathbf{I} are not conserved independently as a result of this interaction, and only the total atomic angular momentum $\mathbf{F} = \mathbf{J} + \mathbf{I}$ is an integral of motion. As a result, the energy levels, which are defined by the quantum number J , split into sublevels that correspond to all conceivable total angular momentum F values

$$F = J + I, J + I - 1, \dots, |J - I|. \quad (4.3)$$

Hyperfine splitting is the name for this type of splitting. We focus on Li-like ions with the valence electron in state $|a\rangle = |j_a m_a\rangle$, total angular momentum $j_a = 1/2$, and its projection m_a . The valence electron $|a\rangle$ determines the angular quantum numbers of the electronic system in this case: $J = j_a$ and $M_J = m_a$, where M_J is the projection of J . The energy levels of lithiumlike ion are then split into two components, $F^+ = I + 1/2$ and $F^- = I - 1/2$, according to Eq. (4.3), and the ground-state hfs value in Li-like ions may be represented as follows

$$\Delta E_{\text{hfs}} = E(F^+) - E(F^-). \quad (4.4)$$

Here the energy level of the lithiumlike ion with total angular momentum F is denoted by $E(F)$. Ground-state hfs may be determined analytically in the nonrelativistic one-electron point-nucleus approximation (so-called Fermi energy E_F)

$$\Delta E_{\text{hfs}} \xrightarrow{\text{nonrel}} E_F = \frac{\alpha(\alpha Z)^3}{n_a^3} \frac{g_I}{m_p} \frac{2I + 1}{(j_a + 1)(2l_a + 1)} \frac{1}{\left(1 + \frac{m_e}{M}\right)^3}. \quad (4.5)$$

Here $l_a = j_a \pm 1/2$ is the parity of the state $|a\rangle$, n_a defines a valence electron's principal quantum number, $g_I = \frac{\mu}{\mu_N I}$ is the nuclear g factor, μ is the nuclear magnetic moment, $\mu_N = \frac{e\hbar}{2m_p}$ is the nuclear magneton, and m_p and M are the proton and nuclear masses, respectively.

The ground-state hfs in Li-like ions may be parametrized using Eq. (4.5)

$$\Delta E_{\text{hfs}} = E_F X_a (1 - \epsilon), \quad (4.6)$$

where ϵ is a Bohr-Weisskopf correction originating from the extended nuclear magnetization distribution, X_a is a dimensionless hfs factor encompassing the many-electron and QED effects.

The volume distribution function $F(x)$ takes the Bohr-Weisskopf correction ϵ into account (see Eq. (4.2)). In the case of point-like nuclear magnetic moment approximation, for example, $F(x) = 1$. In this thesis, we employ the homogeneous sphere model to account for the spatial nuclear magnetization distribution, which reads as follows

$$F(x) = \begin{cases} \left(\frac{x}{R_0}\right)^3, & x \leq R_0 \\ 1, & x > R_0 \end{cases}, \quad (4.7)$$

where $R_0 = \sqrt{\frac{5}{3}\langle r^2 \rangle}$ is the magnetization sphere radius, $\langle r^2 \rangle$ corresponds to the magnetic root-mean-square (rms) radius. We assume that magnetic rms equals nuclear charge rms radius. The sphere model, on the other hand, does not always effectively reflect the distribution of nuclear magnetization. For evaluating the Bohr-Weisskopf correction, the nuclear single-particle model approximation is commonly utilized (Shabaev, 1994; Shabaev et al., 1995; Shabaev et al., 1997a; Shabaev et al., 1997b; Shabaev et al., 1998; Zherebtsov and Shabaev, 2000; Tupitsyn et al., 2002). The total angular momentum of the unpaired nucleon (proton or neutron) is used to define nuclear magnetization in this model. The unpaired nucleon in nuclei with odd or even nuclear charge numbers is a proton or a neutron, respectively. Thus, for example, in Refs. (Shabaev et al., 1997b; Zherebtsov and Shabaev, 2000; Tupitsyn et al., 2002), the radially symmetric distribution function $F(x)$ was derived within the framework of the nuclear single-particle model. It was shown that the ratio of the Bohr-Weisskopf corrections calculated with different magnetization distribution models remains constant to a high degree of accuracy for Li-like ions (Shabaev et al., 2001) and even neutral atoms (Ginges and Volotka, 2018), as obtained for H-like ions. With this in mind, one can utilize the results for H-like ions obtained with the odd nucleon model, for example, to evaluate the Bohr-Weisskopf correction for the corresponding Li-like ion, i.e., $\epsilon_{\text{odd}}^{\text{Li}} = \epsilon_{\text{odd}}^{\text{H}} \left(\epsilon_{\text{sph}}^{\text{Li}} / \epsilon_{\text{sph}}^{\text{H}} \right)$.

In the one-electron approximation, the dimensionless hfs parameter X_a is given by

$$X_a = G_a \langle a | T_z | a \rangle, \quad (4.8)$$

with

$$G_a = \frac{n_a^3 (2l_a + 1) j_a (j_a + 1)}{2(\alpha Z)^3 m_a}. \quad (4.9)$$

Here, T_z is z component of the \mathbf{T} operator given by Eq. (4.2). In the nonrelativistic one-electron point-nucleus approximation, G_a^{-1} is the nonrelativistic value of the electron component of the Fermi energy, such that $X_a \rightarrow 1$.

4.2 ELECTRON CORRELATION EFFECTS

Let us now investigate the many-electron effects to the hfs in the framework of the QED perturbation theory. When considering the magnetic interaction, the interaction Hamiltonian must now include the following term

$$\hat{H}_{\text{magn}}^{\text{IR}} = \int d\mathbf{x} : \left(\hat{\psi}^{\text{IR}}(\mathbf{x}) \right)^\dagger \delta V(\mathbf{x}) \hat{\psi}^{\text{IR}}(\mathbf{x}) : . \quad (4.10)$$

Here $\delta V(\mathbf{x})$ denotes the external magnetic perturbing potential. Then the total interaction Hamiltonian $\hat{H}_{\text{int}}^{\text{IR}}$ reads as

$$\hat{H}_{\text{int}}^{\text{IR}} = \int d\mathbf{x} : \left(\hat{\psi}^{\text{IR}}(\mathbf{x}) \right)^\dagger h_{\text{int}}(\mathbf{x}) \hat{\psi}^{\text{IR}}(\mathbf{x}) : + \int d^3x \psi^\dagger(\mathbf{x}) \delta V(\mathbf{x}) \psi(\mathbf{x}), \quad (4.11)$$

in usual Furry picture and

$$\hat{H}_{\text{int}}^{\text{IR}} = \int d\mathbf{x} : \left(\hat{\psi}_{\text{eF}}^{\text{IR}}(\mathbf{x}) \right)^\dagger h_{\text{int,eF}}(\mathbf{x}) \hat{\psi}_{\text{eF}}^{\text{IR}}(\mathbf{x}) : + \int d^3x \psi^\dagger(\mathbf{x}) \delta V(\mathbf{x}) \psi(\mathbf{x}), \quad (4.12)$$

in the extended Furry picture. In this chapter we use interaction Hamiltonian defined by either Eq. (4.11) or Eq. (4.12) with $\delta V(\mathbf{x})$ being a Fermi-Breit operator

$$\delta V(\mathbf{x}) = H_\mu. \quad (4.13)$$

In such a case, the interaction Hamiltonian (4.11) or (4.12) operates in the electron and nuclear states' Fock spaces, but the nuclear states are limited to the ground-state subspace $|IM_I\rangle$ only with $M_I = -I, \dots, I$. To separate the contributions to the hfs, we limit ourselves to effects that are linear in H_μ . In other words, we only consider the Feynman diagrams of the first order in the hyperfine interaction. The hfs parameter X_a according to Eqs. (4.4) and (4.6) given by

$$X_a = \frac{E(F^+) - E(F^-)}{E_F}, \quad (4.14)$$

where $E(F)$ is the energy of a single isolated level of the Li-like ion and F is its total angular momentum. $E(F)$ can be found using the two-time Green's function method described in the previous Sec. 3.4.2, see Eq. (3.61)

$$E(F) = \frac{\oint_{\Gamma} d\varepsilon \varepsilon G_F(\varepsilon)}{\oint_{\Gamma} d\varepsilon G_F(\varepsilon)}. \quad (4.15)$$

The contour Γ only surrounds the pole $\varepsilon = E^{(0)}$, where $E^{(0)}$ is the unperturbed energy, which is, contrary to Sub. 3.4.2, the sum of the one-electron Dirac and nuclear energies, $G_F(\varepsilon) = \langle FM_F I j_a | \mathcal{G}(E) \gamma_1^0 \gamma_2^0 \gamma_3^0 | FM_F I j_a \rangle$, and $|FM_F I j_a \rangle$ is the wave function of the coupled system (nucleus + electrons)

$$|FM_F I j_a \rangle = \sum_{M_I m_a} C_{IM_I j_a m_a}^{FM_F} |IM_I \rangle |j_a m_a \rangle. \quad (4.16)$$

Here $|IM_I \rangle$ denotes the nuclear wave function with nuclear spin I and its projection M_I , whereas $|j_a m_a \rangle$ denotes the unperturbed 3-electron one-determinant wave function in the $1s^2 2s$ state with total angular momentum j_a and its projection m_a . The energy $E(F)$ and the function $G_F(\varepsilon)$ are to be expanded in the power series in α according to the perturbation theory

$$\begin{aligned} E(F) &= E^{(0)} + E^{(1)}(F) + \dots + E^{(i)}(F) + \dots, \\ G_F(\varepsilon) &= G^{(0)}(\varepsilon) + G_F^{(1)}(\varepsilon) + G_F^{(2)}(\varepsilon) + \dots + G_F^{(i)}(\varepsilon) + \dots \end{aligned} \quad (4.17)$$

It should be noted that there is no interaction of bound electrons with the magnetic field of the nucleus in the zeroth order in α , and thus the zeroth-order energy $E^{(0)}$ does not depend on the total angular momentum F . In this vein, the hfs parameter X_a can be expanded as follows

$$\begin{aligned} X_a &= X_a^{(0)} + X_a^{(1)} + X_a^{(2)} + X_a^{(3+)}, \\ X_a^{(3+)} &= X_a^{(3)} + \dots + X_a^{(i)} + \dots, \end{aligned} \quad (4.18)$$

where i denotes the i th order correction $X_a^{(i)}$ in α , which is written as

$$X_a^{(i)} = \frac{E^{(i+1)}(F^+) - E^{(i+1)}(F^-)}{E_F}. \quad (4.19)$$

All relevant corrections, such as the one-electron QED, screened QED, and interelectronic-interaction terms to the hfs, are included in each order in α . However, in this thesis, we only consider the interelectronic-interaction corrections. Then the terms in Eq. (4.18) pertain to the interelectronic-interaction corrections due to one-photon ex-

change $(X_a^{(1)})$, two-photon exchange $(X_a^{(2)})$, and three- and more-photon exchange $(X_a^{(3+)})$, respectively. In contrast to previous works (see, for example, (Volotka et al., 2008; Shabaev et al., 1998)), we explicitly separate out the two-photon-exchange term $X_a^{(2)}$, as it is now obtained within the rigorous QED framework. Then the first-order term $X_a^{(1)}$ corresponds to $B(\alpha Z)/Z$ in Refs. (Volotka et al., 2008; Shabaev et al., 1998), whereas the sum $X_a^{(2+)} = X_a^{(2)} + X_a^{(3+)}$ corresponds to $C(\alpha Z, Z)/Z^2$ in Refs. (Volotka et al., 2008; Shabaev et al., 1998).

4.2.1 Zeroth-order contribution

The lowest order term $X_a^{(0)}$ according to the Eq. (4.19) reads as

$$X_a^{(0)} = \frac{E^{(1)}(F^+) - E^{(1)}(F^-)}{E_F}, \quad (4.20)$$

where

$$E^{(1)}(F) = \frac{1}{2\pi i} \oint_{\Gamma} d\varepsilon (\varepsilon - E^{(0)}) G_F^{(1)}(\varepsilon), \quad (4.21)$$

and the Feynman rules are used to calculate $G_F^{(1)}(\varepsilon)$

$$G_F^{(1)}(\varepsilon) = \frac{\langle FM_F I j_a | H_{\mu} | FM_F I j_a \rangle}{(\varepsilon - E^{(0)})^2}. \quad (4.22)$$

Using Eqs. (4.21) and (4.22), we get

$$E^{(1)}(F) = \langle FM_F I j_a | H_{\mu} | FM_F I j_a \rangle. \quad (4.23)$$

When Eqs. (4.1), (4.16), and (4.23) are substituted into Eq. (4.20), an explicit form for $X_a^{(0)}$ can be found

$$X_a^{(0)} = G_a \langle a | T_z | a \rangle, \quad (4.24)$$

which is the same as Eq. (4.8), where this term was obtained in the one-electron approximation.

As was mentioned before in Subsection 3.4.2 we perform calculations within the extended Furry picture. In the present chapter, we employ three starting potentials: Coulomb, core-Hartree, and Kohn-Sham. It's worth noting that the original Furry picture was used in previous computations, therefore only the total value of X_a may

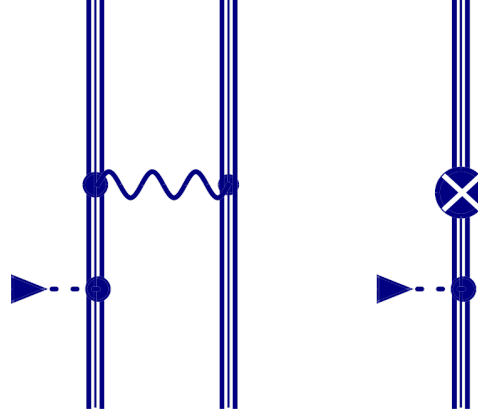


Figure 4.1: Feynman diagrams representing the one-photon exchange correction to the hfs within the framework of the extended Furry picture. The photon propagator is indicated by the wavy line. The electron propagator in the effective potential V^{eff} is shown by the triple line. The magnetic interaction $\delta V = H_\mu$ is represented by the dashed line that ends with a triangle. The extra interaction term associated with the screening potential counterterm $-V^{\text{scr}}$ is represented by the symbol \otimes .

be compared to the corresponding results from Refs. (Volotka et al., 2008; Shabaev et al., 1998). Here, we should note that in previous calculations (Volotka et al., 2008; Shabaev et al., 1998) the original Furry picture was used, and therefore, only the total value of χ_a can be compared with corresponding value from Refs. (Volotka et al., 2008; Shabaev et al., 1998).

4.2.2 First-order contribution

The next order correction $\chi_a^{(1)}$ to the hfs is given by

$$\chi_a^{(1)} = \frac{E^{(2)}(F^+) - E^{(2)}(F^-)}{E_F}, \quad (4.25)$$

where

$$E^{(2)}(F) = \frac{1}{2\pi i} \oint_{\Gamma} d\varepsilon (\varepsilon - E^{(0)}) G_F^{(2)}(\varepsilon) - \frac{1}{2\pi i} \oint_{\Gamma} d\varepsilon (\varepsilon - E^{(0)}) G_F^{(1)}(\varepsilon) \frac{1}{2\pi i} \oint_{\Gamma} d\varepsilon G_F^{(1)}(\varepsilon). \quad (4.26)$$

Fig. 4.1 depicts the one-photon exchange diagrams of the nucleus corresponding to $G_F^{(2)}(\varepsilon)$ in the presence of a magnetic field. The counterterm diagrams representing an additional interaction appear in the extended Furry picture, see Sec. 3.4.2. These diagrams are also depicted in Fig. 4.1 where the symbol \otimes stands for local screening potential counterterm $-V^{\text{scr}}$. Using the Feynman rules for the functions $G_F^{(2)}(\varepsilon)$ and

$G_F^{(1)}(\varepsilon)$, and keeping only the linear dependence on H_μ , the one-photon exchange correction to the hfs in Li-like ion $X_a^{(1)}$ is obtained in the form

$$X_a^{(1)} = 2G_a \sum_b \left[\sum_P (-1)^P (\langle \zeta_{b|P_aP_b} | T_z | a \rangle + \langle \zeta_{a|P_bP_a} | T_z | b \rangle) - \right. \quad (4.27)$$

$$\left. - \frac{1}{2} (\langle a | T_z | a \rangle - \langle b | T_z | b \rangle) \langle ab | I'(\varepsilon_a - \varepsilon_b) | ba \rangle \right] - 2G_a \langle \eta_a | T_z | a \rangle,$$

with

$$|\eta_a\rangle = \sum_n' \frac{\langle n | V^{\text{scr}} | a \rangle}{\varepsilon_a - \varepsilon_n}, \quad (4.28)$$

$$|\zeta_{a|P_bP_a}\rangle = \sum_n \frac{|n\rangle \langle na | I(\Delta) | P_bP_a \rangle}{\varepsilon_b - \varepsilon_n}, \quad |\zeta_{b|P_aP_b}\rangle = \sum_n \frac{|n\rangle \langle nb | I(\Delta) | P_aP_b \rangle}{\varepsilon_a - \varepsilon_n}.$$

Here, $\Delta = \varepsilon_a - \varepsilon_{P_a}$, ε_n denotes one-electron energies, $|b\rangle$ denotes the $1s$ state, and the sum over b takes into account two possible projections $m_b = \pm 1/2$ of total angular momentum j_b . The prime on the sums over the intermediate states n indicates that the terms with vanishing denominators are omitted. The interelectronic-interaction operator $I(\omega)$ is given by Eq. (2.21). We would like to point out that a rigorous evaluation of the one-photon exchange correction to the ground-state hfs in Li-like ions was previously performed in Refs. (Volotka et al., 2008; Shabaev et al., 1998; Oreshkina et al., 2007) in the framework of the original Furry picture and Ref. (Sapirstein and Cheng, 2001) in the framework of the extended Furry picture.

4.2.3 Second-order contribution

The second-order correction $X_a^{(2)}$ to the hfs reads as follows

$$X_a^{(2)} = \frac{E^{(3)}(F^+) - E^{(3)}(F^-)}{E_F}, \quad (4.29)$$

where

$$\begin{aligned}
E^{(3)}(F) = & \frac{1}{2\pi i} \oint_{\Gamma} d\varepsilon (\varepsilon - E^{(0)}) G_F^{(3)}(\varepsilon) \\
& - \frac{1}{2\pi i} \oint_{\Gamma} d\varepsilon (\varepsilon - E^{(0)}) G_F^{(2)}(\varepsilon) \frac{1}{2\pi i} \oint_{\Gamma} d\varepsilon G_F^{(1)}(\varepsilon) \\
& - \frac{1}{2\pi i} \oint_{\Gamma} d\varepsilon (\varepsilon - E^{(0)}) G_F^{(1)}(\varepsilon) \left[\frac{1}{2\pi i} \oint_{\Gamma} d\varepsilon G_F^{(2)}(\varepsilon) - \left(\frac{1}{2\pi i} \oint_{\Gamma} d\varepsilon G_F^{(1)}(\varepsilon) \right)^2 \right].
\end{aligned} \tag{4.30}$$

Figs. 4.2, 4.3, and 4.4 show diagrams of two-photon exchange in the presence of a magnetic field of the nucleus that correspond to the function $G_F^{(3)}(\varepsilon)$.

The $X_a^{(2)}$ can be formally written as

$$X_a^{(2)} = X_{3el}^{(2)} + X_{2el}^{(2)} + X_{red}^{(2)} + X_{ct}^{(2)}, \tag{4.31}$$

where $X_{3el}^{(2)}$ is three-electron, $X_{2el}^{(2)}$ is two-electron, $X_{ct}^{(2)}$ is counterterm, and $X_{red}^{(2)}$ is reducible contributions, respectively. The first term in Eq. 4.31 is written as follows

$$X_{3el}^{(2)} = X_{3el,A}^{(2)} + X_{3el,B}^{(2)} + X_{3el,C}^{(2)} + X_{3el,D}^{(2)}, \tag{4.32}$$

where each contribution is represented by the Feynman diagrams shown in Fig. 4.2. Three-electron diagrams correspond to a relatively simple subset of diagrams; its structure is very similar to $X_a^{(1)}$, but unlike $X_a^{(1)}$, we now deal with much large number of contributions.

The two-electron contribution $X_{2el}^{(2)}$, like the previous term $X_{3el}^{(2)}$, can be presented using the many-electron diagrams shown in Fig. 4.3. Therefore, $X_{2el}^{(2)}$ can be written as follows

$$X_{2el}^{(2)} = X_{2el,lad-W}^{(2)} + X_{2el,cr-W}^{(2)} + X_{2el,lad-S}^{(2)} + X_{2el,cr-S}^{(2)}. \tag{4.33}$$

As can be seen, $X_{2el}^{(2)}$ is comprised of a ladder ("lad") and a cross ("cr") part, with the additional labels "-S" and "-W" denoting cases where the magnetic interaction is inserted in the internal electron line or the external electron line, respectively. The two-electron term $X_{2el}^{(2)}$ involves integrating over the energy of the virtual photon ω , which is infrared-divergent in some terms. However, these infrared-divergent terms may be separated, and the divergences cancel each other out. We perform a Wick rotation with the integration contours chosen in Ref. (Mohr and Sapirstein, 2000) to avoid strong oscillations for large real values of ω .

The third term, $X_{red}^{(2)}$ in Eq. 4.31 is a reducible term, which corresponds to contri-

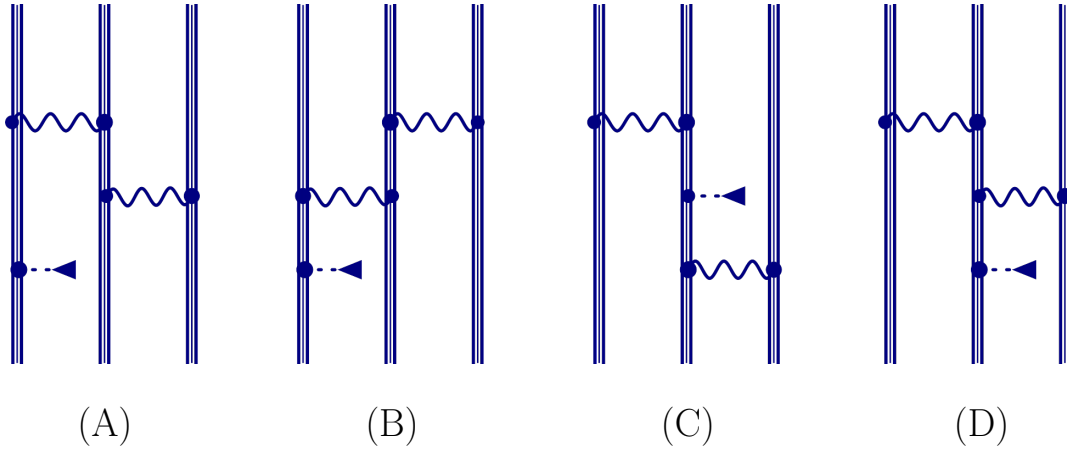


Figure 4.2: Feynman diagrams illustrating the three-electron contribution to the two-photon-exchange correction $\chi_{3\text{el}}^{(2)}$ to the hfs. The notations are identical to those shown in Fig. 4.1

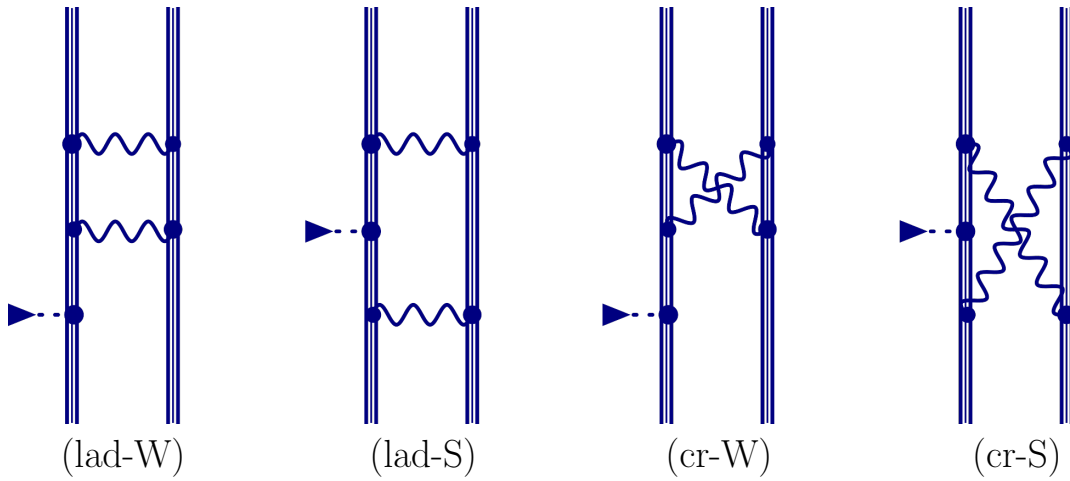


Figure 4.3: Feynman diagrams illustrating the two-electron part of the two-photon-exchange correction $\chi_{2\text{el}}^{(2)}$ to the hfs. The notations are identical to those shown in Fig. 4.1

butions with the system's intermediate energy equal to its initial energy as well as disconnected ones (lines 2 and 3 in Eq. (4.30)). Finally, the last term in Eq. (4.31) is a counterterm contribution $\chi_{\text{ct}}^{(2)}$, which appear only in the extended Furry picture formalism (see Fig. 4.4). Appendix 7 contains the formal expressions for all of the terms in Eqs. (4.31)–(4.33).

Furthermore, the formal expressions of the two-photon exchange correction $\chi_{\text{a}}^{(2)}$ involve infinite summations over the entire Dirac spectrum, including the infinite partial wave expansion. The dual-kinetic balance finite basis set method (Shabaev et al., 2004) for the Dirac equation is used to perform the summation over the intermediate states. We construct the basis functions from B-splines (Sapirstein and Johnson, 1996). To establish a clear convergence pattern of the calculated findings, we continuously increased the number of basis functions from $N = 92$ to $N = 212$, and then did the

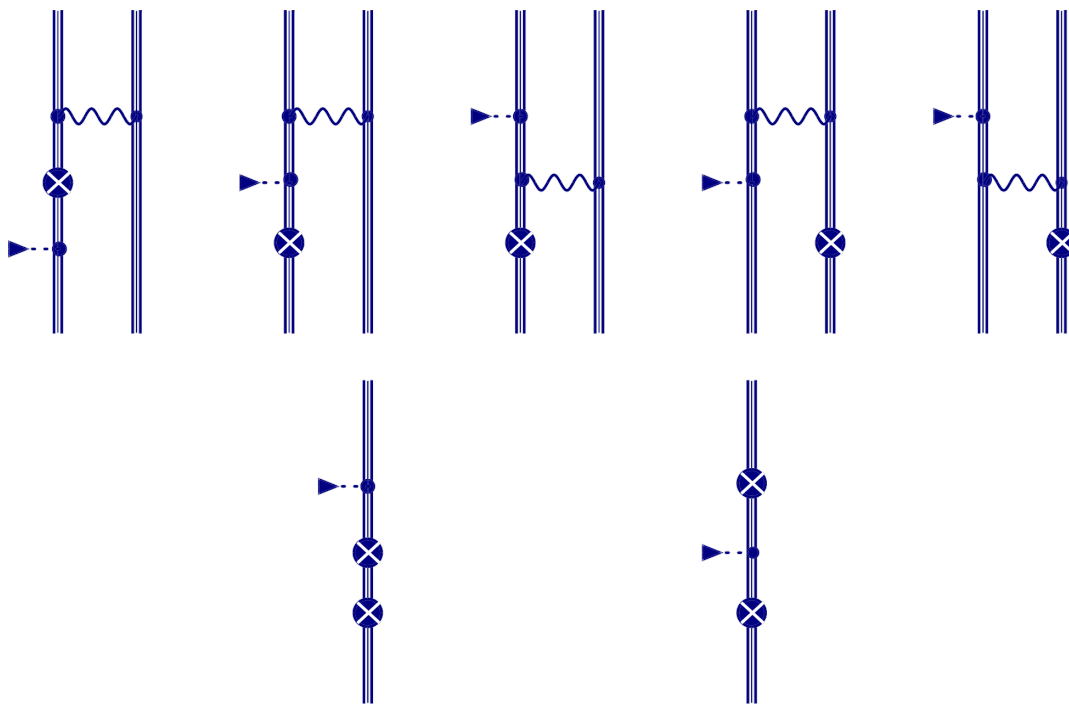


Figure 4.4: Feynman diagrams illustrating the counterterm part of the two-photon-exchange correction $\chi_{\text{counterterms}}^{(2)}$ to the hfs, which appear in the framework of the extended Furry picture only. The notations are identical to those shown in Fig. 4.1

extrapolation $N \rightarrow \infty$. The partial wave summation over the Dirac quantum number κ was stopped at $\kappa_{\text{max}} = 10$, and the remainder was estimated using least-squares inverse polynomial fitting. The absolute uncertainty of this estimation in $\chi_a^{(2)}$ is found to be around 3×10^{-7} in the case of $Z = 7$ and rapidly decreases to 10^{-7} or less as Z increases.

The two-photon exchange correction is calculated within the Feynman and Coulomb gauges as a consistency check, and the results are found to be gauge invariant to a very high degree of precision. As an additional consistency check, we compare the obtained results for the $\chi_a^{(2)}$ to the results evaluated within the Breit approximation (see the next section). The comparison includes both a numerical and an analytical check, which was performed by replacing the interelectronic-interaction operator $I(\omega)$ in the Breit approximation with its frequency-independent counterpart. All of this validates the accuracy of the current calculations.

4.2.4 *Third- and higher-order contributions*¹

While the rigorous QED approach is currently limited to the first and second orders of the interelectronic interaction, the third- and higher-order contributions ($X_a^{(3+)}$) are also significant at the current level of theoretical accuracy. As a result, these contributions are currently taken into account within the so-called Breit approximation, which is based on the Dirac-Coulomb Breit equation. The interelectronic-interaction operator $I(\omega)$ is substituted by its $\omega = 0$ -limit in the Coulomb gauge in this approximation

$$I(\omega, x_{12}) \rightarrow I_B(x_{12}) = \alpha \left(\frac{1}{x_{12}} - \frac{\alpha_1 \alpha_2}{x_{12}} + \frac{1}{2} [h_1^D, [h_2^D, x_{12}]] \right). \quad (4.34)$$

The projector on the space positive-energy states of the one-electron Dirac Hamiltonian is another important part of the Dirac-Coulomb-Breit method. Faustov, [1970] and Sucher, [1980] demonstrated the origin of this method. Because the use of this projector effectively suppresses processes involving virtual electron-positron pairs, it is also known as the "no-pair approximation" (Breit_{no-ee+}). However, mixing the large and small components of the Dirac wave functions by the Fermi-Breit operator (4.1) (or any other operator with α matrices) results in a significant increase in the negative-energy contributions. To account for these contributions, one needs either build the positive-energy projectors for to the Dirac Hamiltonian, which includes the Fermi-Breit operator, or evaluate them separately as the first-order perturbation in this operator. We employ the second approach, which entails incorporating processes involving a single virtual electron-positron pair (Breit_{one-ee+}).

Any of the available approaches can account for the interelectronic interaction, see, for example, Refs. (Boucard and Indelicato, [2000]; Dzuba et al., [1987]; Ginges and Volotka, [2018]; Shabaev et al., [1995]; Zherebtsov and Shabaev, [2000]; Yerokhin, [2008]; Blundell et al., [1989]; Glazov et al., [2017]; Bratzev et al., [1977]). Previously, to evaluate $X_a^{(3+)}$ (Volotka et al., [2012]) or $X_a^{(2+)}$ (Volotka et al., [2008]), the all-order CI-DFS method (Bratzev et al., [1977]) was used. In this dissertation, we use a recursive formulation of perturbation theory (Glazov et al., [2017]). This method efficiently accesses the individual terms of the perturbation expansion up to any order. It also guarantees that the zeroth-order Hamiltonian is the same for rigorous QED and Breit-approximation calculations. This approach has recently been successfully applied to analogous computations of higher-order contributions to the g factor of Li-like ions (Glazov

¹This section does not include work related to this thesis. The calculations outlined in this section have been carried out by D. A. Glazov in Ref. (Kosheleva et al., [2020]).

et al., 2019a).

We begin with the Dirac-Coulomb-Breit equation to formulate this approach,

$$\Lambda_+ (H_0 + H_1) \Lambda_+ |A\rangle = E_A |A\rangle. \quad (4.35)$$

Here Λ_+ is the positive-energy-states projection operator, which is built as the product of one-electron projectors. The zeroth-order Hamiltonian is constructed as a sum of the one-electron Dirac Hamiltonians,

$$H_0 = \sum_{j=1}^3 h_{D,eF}(\mathbf{x}_j), \quad (4.36)$$

where $h_{D,eF}$ is given by Eq. (3.79) and index j numerates the electrons. The orthogonal basis set of many-electron wave functions is formed by the Hamiltonian's eigenfunctions $|N^{(0)}\rangle$,

$$\Lambda_+ H_0 \Lambda_+ |N^{(0)}\rangle = E_N^{(0)} |N^{(0)}\rangle. \quad (4.37)$$

The Slater determinants of the one-electron solutions of the Dirac equation may be used to construct eigenfunctions $|N^{(0)}\rangle$. For the case of some reference state $|A\rangle$ in the zeroth approximation, we have

$$\Lambda_+ H_0 \Lambda_+ |A^{(0)}\rangle = E_A^{(0)} |A^{(0)}\rangle. \quad (4.38)$$

The term H_1 in Eq. (4.35) is the interelectronic interaction in the Breit approximation with the screening potential being subtracted,

$$H_1 = \sum_{j<k;j,k=1}^3 I_B(\mathbf{x}_{jk}) - \sum_{j=1}^3 V^{\text{scr}}(\mathbf{x}_j). \quad (4.39)$$

Then we build the perturbation theory with respect to H_1 , which yields the energy E_A and wave function $|A\rangle$ expansions shown below

$$E_A = \sum_{k=0}^{\infty} E_A^{(k)}, \quad (4.40)$$

$$|A\rangle = \sum_{k=0}^{\infty} |A^{(k)}\rangle = \sum_{k=0}^{\infty} \sum_N |N^{(0)}\rangle \langle N^{(0)} | A^{(k)} \rangle. \quad (4.41)$$

The recursive scheme for evaluating $E_A^{(k)}$ and $\langle N^{(0)} | A^{(k)} \rangle$ order by order was presented by Glazov et al., [2017]. Here we aim to construct the perturbation series for the hfs parameter, $X_a^{(k)}$. To do so we substitute Eq. (4.41) into the following relation

$$X_a = G_a \langle A | T_0 | A \rangle, \quad (4.42)$$

and find

$$\begin{aligned} X_a^{(k)} &= G_a \sum_{j=0}^k \langle A^{(j)} | T_z | A^{(k-j)} \rangle \\ &= G_a \sum_{j=0}^k \sum_{M,N} \langle A^{(j)} | M^{(0)} \rangle \langle M^{(0)} | T_z | N^{(0)} \rangle \langle N^{(0)} | A^{(k-j)} \rangle. \end{aligned} \quad (4.43)$$

It is worth noting that the normalization condition $\langle A | A \rangle = 1$, rather than the widely accepted intermediate normalization $\langle A^{(0)} | A \rangle = 1$, is used here. In the no-pair Breit approximation, Eq. (4.43) is utilized to calculate $X_a^{(k)}$. We include the contribution of negative-energy excitations within the one-pair Breit approximation, which is calculated as

$$X_{a[-]} = 2G_a \sum_{p,n} \frac{\langle p | T_z | n \rangle}{\varepsilon_p - \varepsilon_n} \langle \hat{a}_n^+ \hat{a}_p A | H_1 | A \rangle. \quad (4.44)$$

Here $|p\rangle$ and $|n\rangle$ denote the positive- and negative-energy one-electron states, respectively, and \hat{a}^+ and \hat{a} denote the corresponding creation and annihilation operators, respectively. Then the corresponding contribution of the k th order is

$$\begin{aligned} X_a^{(k)[-]} &= 2G_a \sum_{j=0}^{k-1} \sum_{M,N} \langle A^{(j)} | M^{(0)} \rangle \\ &\times \left[\sum_{p,n} \frac{\langle p | T_z | n \rangle \langle \hat{a}_n^+ \hat{a}_p M^{(0)} | H_1 | N^{(0)} \rangle}{\varepsilon_p - \varepsilon_n} \right] \langle N^{(0)} | A^{(k-j-1)} \rangle. \end{aligned} \quad (4.45)$$

We utilize Eqs. (4.43) and (4.45) to calculate the required third- and higher-order contributions from the wave-function coefficients $\langle N^{(0)} | A^{(k)} \rangle$ obtained within the recursive approach. We note that the formulas given above are valid for the case of the extended Furry picture. In order to obtain formulas in original Furry picture one just need to make the following substitutions

$$h_{D,eF} \rightarrow h_D, \quad (4.46)$$

and

$$H_1 \rightarrow \sum_{j < k; j, k=1}^3 I_B(x_{jk}). \quad (4.47)$$

4.3 RESULTS AND DISCUSSIONS

First, we will go over the nuclear models and nuclear parameters that were used in the calculations. The nucleus' finite size is accounted for in the Fermi model for nuclear charge density, with charge radii are taken from Ref. (Angeli and Marinova, 2013). The Bohr-Weisskopf correction ϵ is calculated within the homogeneous sphere model, i.e. $\epsilon \equiv \epsilon_{\text{sph}}$. According to the Eq. (4.6), ϵ_{sph} reads as

$$\epsilon_{\text{sph}} = 1 - \frac{X_{a,\text{sph}}}{X_a}, \quad (4.48)$$

where $X_{a,\text{sph}}$ denotes the dimensionless hfs factor calculated using the homogeneous sphere model to account for the spatial nuclear magnetization distribution Eq. (4.7) is considered, and X_a is calculated using the point-like nuclear magnetic moment approximation, i.e. $F(x) = 1$.

Tables 4.1, 4.2, and 4.3 present the interelectronic-interaction corrections to the ground state hfs in Li-like $^{15}\text{N}^{4+}$, $^{98}\text{Tc}^{40+}$, and $^{209}\text{Pb}^{79+}$ ions, respectively, including individual orders of the perturbation theory. The individual terms' uncertainties are determined by their convergence with respect to the number of basis functions and their maximum orbital momentum. The results were obtained using three different starting potentials: Coulomb, core-Hartree, and Kohn-Sham. The latter two correspond to the extended Furry picture and allow for partial consideration of interelectronic interaction in zeroth order. We also compare our results with the corresponding terms from the earlier theoretical computations (Volotka et al., 2008; Shabaev et al., 1998) for the case of the original Furry picture in Tables 4.1 and 4.3. The one-electron relativistic factor $X_a^{(0)}$ corresponds to the product $A(\alpha Z)(1 - \delta)$ from Refs. (Volotka et al., 2008; Shabaev et al., 1998), the one photon exchange correction $X_a^{(1)}$, and the higher-order terms $X_a^{(2+)}$, which correspond to the notations $B(\alpha Z)/Z$ and $C(\alpha Z, Z)/Z^2$ or $C(0)/Z^2$. We want to emphasize that we corrected the values from Refs. (Volotka et al., 2008; Shabaev et al., 1998) (see third column in Tables 4.1 and 4.3) to the Fermi model of the charge distribution with the radii from Ref. (Angeli and Marinova, 2013) and to the pointlike magnetization distribution as calculated in this thesis. As a result, we can conclude that the main reason for our

	Coulomb			Core-Hartree	Kohn-Sham
	This work	Volotka et al., 2008 ^a	Volotka et al., 2008	This work	This work
$X_a^{(0)}$	1.004 912	1.004 91	1.004 89	0.617 954	0.618 795
$X_a^{(1)}$	-0.381 459	-0.381 46	-0.381 01	0.023 225	0.019 646
$X_a^{(2)}$	0.018 867			0.000 249	0.003 200
$X_a^{(3)}$	-0.001 027(12)			0.000 085(3)	-0.000 172(3)
$X_a^{(4)}$	0.000 139(8)			-0.000 022(7)	0.000 033(4)
$X_a^{(5)}$	0.000 048(2)			0.000 006(3)	-0.000 006(1)
$X_a^{(6)}$	0.000 013(1)			-0.000 001(1)	0.000 001
$X_a^{(7)}$	0.000 003(1)			0.000 001	-0.000 000
$X_a^{(3+)}$	-0.000 825(15)			0.000 068(8)	-0.000 144(5)
$X_a^{(2+)}$	0.018 042(15)	0.018 00	0.017 98	0.000 317(8)	0.003 056(5)
Total	0.641 495(15)	0.641 45	0.641 86	0.641 496(8)	0.641 497(5)

^a Results from Volotka et al., 2008, recalculated to the nuclear models and nuclear parameters employed in this paper.

Table 4.1: Interelectronic-interaction contributions to the ground-state hfs in Li-like $^{15}\text{N}^{4+}$ with various starting potentials: Coulomb, Core-Hartree, and Kohn-Sham, in terms of X_a , defined by Eq. (4.19).

	Coulomb	core-Hartree	Kohn-Sham
$X_a^{(0)}$	1.233 403 0	1.145 748 3	1.148 599 7
$X_a^{(1)}$	-0.077 938 0	0.010 485 0	0.007 506 6
$X_a^{(2)}$	0.000 755 7	-0.000 022 3	0.000 106 1
$X_a^{(3)}$	-0.000 008 6	0.000 001 2	-0.000 000 5
$X_a^{(4)}$	0.000 000 1	-0.000 000 1	0.000 000 0
$X_a^{(3+)}$	-0.000 008 4	0.000 001 2	-0.000 000 5
Total	1.156 212 3	1.156 212 2	1.156 212 0

Table 4.2: Contributions to the ground-state hfs in Li-like $^{98}\text{Tc}^{40+}$ with different starting potentials: Coulomb, core-Hartree, and Kohn-Sham, in terms of X_a , as defined by Eq. (4.19).

	Coulomb		Core-Hartree This work	Kohn-Sham This work
	This work	Shabaev et al., 1998 ^a		
$X_a^{(0)}$	2.397 606 5	2.397 6	2.398 7	2.292 003 7
$X_a^{(1)}$	-0.085 899 5	-0.085 9	-0.081 7	0.020 407 4
$X_a^{(2)}$	0.000 736 3			0.000 023 5
$X_a^{(3)}$	-0.000 008 2			0.000 000 5
$X_a^{(4)}$	0.000 000 1			0.000 000 0
$X_a^{(3+)}$	-0.000 008 1			0.000 000 5
$X_a^{(2+)}$	0.000 728 2	0.000 1	0.000 1	0.000 024 0
Total	2.312 435 2	2.311 8	2.317 1	2.312 435 2

^a Results from Shabaev et al., 1998, recalculated to the nuclear models and nuclear parameters employed in this paper.

Table 4.3: Contributions to the ground-state hfs in Li-like $^{209}\text{Pb}^{79+}$ with different starting potentials: Coulomb, core-Hartree, and Kohn-Sham, in terms of X_a , as defined by Eq. (4.19).

values differing from those calculated in (Volotka et al., 2008; Shabaev et al., 1998) is due to the different treatment of the two-photon exchange $[X_a^{(2)}]$ and higher-order $[X_a^{(3+)}]$ terms. Indeed, Tables 4.1 and 4.3 show that $X_a^{(0)}$ and $X_a^{(1)}$ agree well with the values obtained in Refs. (Volotka et al., 2008; Shabaev et al., 1998). While the higher orders $X_a^{(2+)}$ are improved over Ref. (Volotka et al., 2008) due to the use of recursive perturbation theory in the current investigation, and over Ref. (Shabaev et al., 1998) due to the rigorous evaluation of the two photon-exchange correction. When compared to the perturbation theory based on the Coulomb starting potential, the framework of the extended Furry picture improves convergence (original Furry picture). As shown in Tables 4.1, 4.2, and 4.3, using the extended Furry picture improves the accuracy of interelectronic-interaction correction, particularly in the low- Z region. For example, in the case of nitrogen $^{15}\text{N}^{4+}$, the total value's uncertainty is reduced by a factor of four.

Table 4.4 and Figure 4.5 compare the Breit and QED treatments of the one- $[X_a^{(1)}]$ and two-photon exchange $[X_a^{(2)}]$ corrections to the ground-state hfs in Li-like ions. The values are obtained using the Kohn-Sham potential within the extended Furry picture. Within the Breit approximation, two results are distinguished: "no-pair" ($\text{Breit}_{\text{no-ee}^+}$) and "one-pair" ($\text{Breit}_{\text{one-ee}^+}$), as discussed in the previous Subsection. The results in Table 4.4 and Figure 4.5 show that for light ions, the difference between the QED approach and both Breit approximations ($\text{Breit}_{\text{no-ee}^+}/\text{Breit}_{\text{one-ee}^+}$) is less than 0.1%, but it grows rapidly as Z increases. For gold ($Z = 79$), the difference between the rigorous QED treatment and the $\text{Breit}_{\text{one-ee}^+}$ approximation for the two-photon exchange term is about 6%, while the QED-Breit no-ee^+ difference is more than 12%.

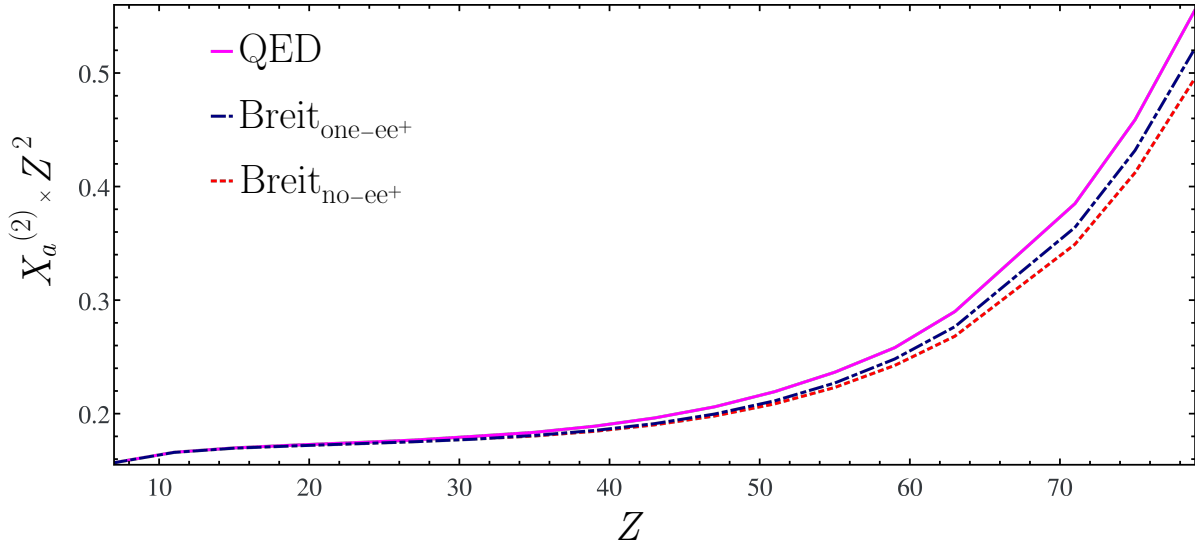


Figure 4.5: The two-photon-exchange correction $X_\alpha^{(2)}$ to the ground-state hfs in Li-like ions scaled by a factor Z^2 as a function of the nuclear charge number Z . The rigorous QED calculation results (solid magenta) are compared to the Breit approximation calculations: no-pair (Breit_{no-ee+}, red dashed) and one-pair (Breit_{one-ee+}, dark blue dash-dotted). The Kohn-Sham starting potential is used to obtain all values.

Table 4.5 displays the interelectronic-interaction contributions calculated with the Kohn-Sham starting potential in terms of the dimensionless hfs parameter X_α over a wide range of nuclear charge numbers $Z = 7 - 82$. The zeroth-order values $X_\alpha^{(0)}$ are displayed in the second column, while the contributions of the first ($X_\alpha^{(1)}$), second ($X_\alpha^{(2)}$), and higher orders ($X_\alpha^{(3+)}$) are displayed in columns three through five, respectively. The total value of X_α and the Bohr-Weisskopf correction ϵ_{sph} evaluated within the homogeneous sphere model are given in the last two columns. The total value's uncertainty is calculated by taking the root-sum-square of the numerical uncertainties of the individual corrections and the unknown QED contribution in the third order in $1/Z$. The third-order Breit approximation is only valid up to order $(\alpha Z)^2$, hence the treatment of the $X_\alpha^{(3+)}$ term in the context of recursive perturbation theory based on the Breit approximation is only valid up to order $(\alpha Z)^2$. Thus, in the current work, the unknown QED contribution of the third order in $1/Z$ is estimated to be $(\alpha Z)^3/Z^3$.

We also compare our total values of the interelectronic-interaction contribution to the corresponding results of the earlier theoretical calculations (Volotka et al., 2008; Shabaev et al., 1998) in Table 4.5. We would like to emphasize the values of the total interelectronic-interaction correction obtained in Refs. (Volotka et al., 2008; Shabaev et al., 1998) are corrected to the nuclear models and nuclear parameters used in this thesis. Unlike Refs. (Volotka et al., 2008; Shabaev et al., 1998), our results are obtained within the context of the extended Furry picture; thus, we can not compare

Ion		QED	Breit _{one-ee+}	Breit _{no-ee+}
¹⁵ N ⁴⁺	$X_a^{(1)}$	0.019 646 3(2)	0.019 645 9(2)	0.019 641 2(2)
	$X_a^{(2)}$	0.003 199 9(3)	0.003 198 2(3)	0.003 198 5(3)
⁹⁸ Tc ⁴⁰⁺	$X_a^{(1)}$	0.007 506 6	0.007 489 1	0.007 435 5
	$X_a^{(2)}$	0.000 106 1	0.000 103 5	0.000 102 8
¹⁹⁷ Au ⁷⁶⁺	$X_a^{(1)}$	0.011 326 4	0.011 169 9	0.011 224 4
	$X_a^{(2)}$	0.000 089 0	0.000 083 7	0.000 079 4

Table 4.4: Comparison of the one- $[X_a^{(1)}]$ and two-photon exchange $[X_a^{(2)}]$ corrections to the ground-state hfs in Li-like ions calculated using the rigorous QED approach and the Breit approximations: no-pair (Breit_{no-ee+}) and one-pair (Breit_{one-ee+}), see text for details. The values are calculated using the Kohn-Sham starting potential.

our results with Refs. (Volotka et al., 2008; Shabaev et al., 1998) term by term; instead, only total values (see column 6 in Table 4.5) can be compared.

Table 4.5 shows that for the light ions, for example, ¹⁵N⁴⁺, the difference between the current results and the ones given in Ref. (Volotka et al., 2008) is about 0.006% and decreases rapidly as the nuclear charge number Z increases. It is explained by the fact that the higher-order corrections $X_a^{(3+)}$ converge faster with increasing Z in the framework of perturbation theory within the extended Furry picture used in this investigation. For the high- Z region, we also compare our results to those of Ref. (Shabaev et al., 1998). As shown in Table 4.5 the difference between the current results and Ref. (Shabaev et al., 1998) is about 0.02% – 0.03%, which is significantly greater than in the middle- Z region. It is primarily explained by the fact that in the work (Shabaev et al., 1998), the correction $X_a^{(2)}$ was estimated by its nonrelativistic limit and the contribution $X_a^{(3+)}$ was ignored. Furthermore, in contrast to previous calculations (Volotka et al., 2008; Shabaev et al., 1998), we have more thoroughly examined all of the uncertainties, i.e., numerical error of the individual terms and unknown higher-order contributions. Because the uncertainty of the Bohr-Weisskopf correction dominates throughout the nuclear charge range under consideration, the current results do not improve the hfs values of Li-like ions. The specific differences in the hfs values for different charge states (Shabaev et al., 2001; Volotka and Plunien, 2014), on the other hand, can significantly reduce this uncertainty. To obtain the most accurate theoretical predictions for the specific differences, simultaneous evaluation of the screened QED corrections is also required.

Ion	$X_a^{(0)}$	$X_a^{(1)}$	$X_a^{(2)}$	$X_a^{(3+)}$	Total	ϵ_{sph}
$^{15}\text{N}^{4+}$	0.618 794 6	0.019 646 3(2)	0.003 199 9(3)	-0.000 144(5)	0.641 497(5) 0.641 45 ^a	0.000 268 0
$^{23}\text{Na}^{8+}$	0.758 442 6	0.015 527 7(1)	0.001 371 5(2)	-0.000 037 0(13)	0.775 304 9(14) 0.775 28 ^a	0.000 496 5
$^{31}\text{P}^{12+}$	0.833 026 7	0.012 682 5	0.000 754 8	-0.000 014 4(5)	0.846 449 6(6) 0.846 43 ^a	0.000 733 5
$^{39}\text{K}^{16+}$	0.884 885 5	0.010 832 6	0.000 476 9	-0.000 007 2(3)	0.896 187 8(5) 0.896 17 ^a	0.001 034 0
$^{51}\text{V}^{20+}$	0.927 883 1	0.009 600 0	0.000 329 6	-0.000 003 9(2)	0.937 808 8(4) 0.937 81 ^a	0.001 355 1
$^{55}\text{Mn}^{22+}$	0.948 019 4	0.009 141 2	0.000 280 9	-0.000 002 9(1)	0.957 438 5(4) 0.957 43 ^a	0.001 554 7
$^{57}\text{Fe}^{23+}$	0.957 971 8	0.008 942 9	0.000 260 6	-0.000 002 5(1)	0.967 173 1(4) 0.967 16 ^a	0.001 655 7
$^{59}\text{Co}^{24+}$	0.967 921 1	0.008 762 6	0.000 242 5	-0.000 002 3(1)	0.976 923 9(4)	0.001 753 4
$^{61}\text{Ni}^{25+}$	0.977 891 1	0.008 599 4	0.000 226 4	-0.000 002 0(1)	0.986 714 5(4) 0.986 71 ^a	0.001 859 6
$^{69}\text{Ga}^{28+}$	1.008 153 0	0.008 195 4	0.000 187 1	-0.000 001 4(1)	1.016 534 1(4)	0.002 230 8
$^{79}\text{Br}^{32+}$	1.050 690 7	0.007 824 2	0.000 149 7	-0.000 001 0	1.058 663 6(4)	0.002 776 1
$^{89}\text{Y}^{36+}$	1.097 198 8	0.007 605 1	0.000 124 2	-0.000 000 6	1.104 927 5(4)	0.003 352 3

^a Volotka et al., [2008] recalculated to the nuclear models and nuclear parameters employed in this thesis.

^b Shabaev et al., [1998] recalculated to the nuclear models and nuclear parameters employed in this thesis.

Table 4.5: Interelectronic-interaction contributions to the ground-state hfs in Li-like ions obtained with the Kohn-Sham potential, in terms of the hfs parameter X_a defined by Eq. (4.4). In the last two columns, the total value of X_a and the Bohr-Weisskopf correction ϵ_{sph} evaluated within the homogeneous sphere model are also presented. The uncertainty of the total value (numbers in parentheses) is determined as a root-sum-square of the numerical uncertainties of the individual corrections and the unknown QED contribution of the third order in $1/Z$ estimated as $(\alpha Z)^3/Z^3$. The total values are compared with the ones from Refs. (Volotka et al., [2008]; Shabaev et al., [1998]).

TABLE 4.5 (Continued.)

Ion	$X_a^{(0)}$	$X_a^{(1)}$	$X_a^{(2)}$	$X_a^{(3+)}$	Total	ϵ_{sph}
$^{98}\text{Tc}^{40+}$	1.148 599 7	0.007 506 6	0.000 106 1	-0.000 000 5	1.156 212 0(4)	0.004 094 4
$^{109}\text{Ag}^{44+}$	1.206 400 7	0.007 514 4	0.000 093 3	-0.000 000 3	1.214 008 1(4)	0.004 961 0
$^{121}\text{Sb}^{48+}$	1.272 127 8	0.007 619 3	0.000 084 3	-0.000 000 3	1.279 831 1(4)	0.005 937 6
					1.279 5 ^b	
$^{133}\text{Cs}^{52+}$	1.347 184 0	0.007 816 7	0.000 078 2	-0.000 000 2	1.355 078 7(4)	0.007 086 5
$^{141}\text{Pr}^{56+}$	1.433 721 5	0.008 109 6	0.000 074 7	-0.000 000 2	1.441 905 6(4)	0.008 410 4
					1.441 6 ^b	
$^{151}\text{Eu}^{60+}$	1.533 117 2	0.008 497 9	0.000 073 3	-0.000 000 2	1.541 688 2(4)	0.010 032 4
					1.541 4 ^b	
$^{165}\text{Ho}^{64+}$	1.648 631 7	0.008 994 7	0.000 074 0	-0.000 000 2	1.657 700 2(4)	0.011 958 0
					1.657 4 ^b	
$^{175}\text{Lu}^{68+}$	1.783 175 6	0.009 611 4	0.000 076 5	-0.000 000 2	1.792 863 3(4)	0.014 224 2
					1.792 6 ^b	
$^{185}\text{Re}^{72+}$	1.945 250 8	0.010 390 4	0.000 081 6	-0.000 000 2	1.955 722 6(4)	0.016 444 1
					1.955 4 ^b	
$^{197}\text{Au}^{76+}$	2.134 320 5	0.011 326 4	0.000 089 0	-0.000 000 3	2.145 735 7(4)	0.019 382 4
$^{209}\text{Pb}^{79+}$	2.300 174 6	0.012 164 4	0.000 096 6	-0.000 000 4	2.312 435 2(4)	0.021 811 3
					2.311 8 ^b	

^b Ref. Shabaev et al., 1998 recalculated to the nuclear models and nuclear parameters employed in this thesis.

g FACTOR OF LITHIUMLIKE $^{28}\text{Si}^{11+}$ AND $^{40}\text{Ca}^{17+}$

In this chapter, we aim to explain a persisting disagreement between theoretical and experimental values of a g factor of lithiumlike silicon and calcium established by Glazov et al., [2019a] and Yerokhin et al., [2020]. To do so, we analyse in details the many-electron QED correction to the g factor of lithiumlike ions: interelectron-interaction (Secs. [5.3] and [5.4]) and QED corrections (Secs. [5.5] and [5.6]). In Sec. [5.2] we carefully analyze the possible ways of estimation of the unknown high order part of the many-electron QED contributions. And finally, we provide a reader with the final theoretical values of the g factor of lithiumlike silicon and calcium (Sec. [5.7]).

This chapter is based on the following reference:

g Factor of Lithiumlike Silicon and Calcium: Resolving the Disagreement between Theory and Experiment

V. P. Kosheleva, A. V. Volotka, D. A. Glazov, D. V. Zinenko, and S. Fritzsche
Phys. Rev. Lett., accepted for publication (2022); arXiv:2201.00612.

5.1 THEORY

The interaction of the bound electron with the external magnetic field \mathbf{B} is represented by the operator

$$V^{\text{magn}}(\mathbf{x}) = -B\mu_z = -B\frac{e}{2}[\mathbf{x} \times \boldsymbol{\alpha}]_z, \quad (5.1)$$

where, without loss of generality, \mathbf{B} is assumed to be aligned in z -direction, μ_z is the z -projection of the electron magnetic moment. In the Li-like atom with a spinless nucleus, the magnetic field induces the energy shift

$$\Delta E_a = -\frac{e}{2}g m_a B, \quad (5.2)$$

where g is the electronic g factor and m_a is the z -projection of the total angular momentum j_a of the ground $(1s)^22s$ state. Within the independent-electron approximation, the energy shift ΔE_a is found as an expectation value of V^{magn} with the unperturbed three-electron one-determinant wave function $|a\rangle = |j_a m_a\rangle$. The corresponding lowest-order g -factor value is

$$g_C^{(0)} = -\frac{2 \langle a | \sum_i V^{\text{magn}}(x_i) | a \rangle}{e m_a B}, \quad (5.3)$$

where index i refers to the i th electron of the atom. We denote by $g_C^{(0)}$ the value obtained for the Coulomb nuclear potential (original Furry picture). Alternatively, one can introduce an effective screening potential in the Dirac equation (extended Furry picture), which leads to the corresponding "screened" value of $g^{(0)}$, see the discussion in Sec. 5.3

In the case when one-electron wave functions are solutions of the Dirac equation with the pointlike Coulomb potential of the nucleus, the lowest-order g factor is known analytically as g_D and given by the Breit formula (Breit, 1928) for the $2s$ state (Glazov et al., 2014)

$$g_D = \frac{2}{3}(1 + \sqrt{2 + 2\gamma}) = 2 - \frac{(\alpha Z)^2}{6} + \dots, \quad (5.4)$$

where $\gamma = \sqrt{1 - (\alpha Z)^2}$. The lowest-order result $g_C^{(0)}$ has to be supplemented by various QED corrections

$$g = g_C^{(0)} + \Delta g_{\text{int}} + \Delta g_{\text{QED}} + \Delta g_{\text{nuc}}. \quad (5.5)$$

So far, the interelectronic-interaction correction Δg_{int} was calculated rigorously (to all orders in αZ) up to the second order in $1/Z$ (Wagner et al., 2013; Volotka et al., 2012; Volotka et al., 2014; Yerokhin et al., 2021). The QED correction Δg_{QED} consists of one-electron and many-electron (screened) QED effects. The leading one-electron QED correction is represented by one-loop self-energy and vacuum polarization diagrams in the presence of magnetic field. This contribution was evaluated to all orders in αZ , e.g., in Refs. (Yerokhin et al., 2004; Glazov et al., 2006; Yerokhin and Harman, 2017; Cakir et al., 2020). The screened one-loop QED correction of the first order in $1/Z$ was rigorously calculated in Refs. (Volotka et al., 2014; Volotka et al., 2009; Glazov et al., 2010; Andreev et al., 2012). The higher-order QED contributions are known only within some approximation so far (Glazov et al., 2004; Pachucki et al., 2005b; Pachucki et al., 2005a; Jentschura, 2009; Yerokhin and Harman, 2013; Czarnecki and Szafron, 2016; Czarnecki et al., 2018; Czarnecki et al., 2020; Aoyama

et al., [2019]; Shabaev et al., [2002]. The contribution, Δg_{nuc} , stands for the nuclear effects, such as nuclear recoil and nuclear polarization. Recently, the nuclear recoil effect in Li-like ions was studied in Refs. (Shabaev et al., [2017]; Malyshev et al., [2017b]; Shabaev et al., [2018]). At the current level of experimental and theoretical accuracy, the nuclear polarization effect is negligible.

In the present thesis, we focus on Δg_{int} and Δg_{QED} corrections. These corrections are to be obtained within the framework of the bound-state QED perturbation theory. To accomplish this, the following steps must be taken:

1. In Eqs. (4.10)–(4.13), replace $\delta V(\mathbf{x})$ with $V^{\text{magn}}(\mathbf{x})$ to construct the interaction Hamiltonian in the original (4.12) or extended (4.13) Furry picture.
2. Evaluate the energy shift corrections $\Delta E_{\text{int/QED}}$ due to the interelectronic interaction (int) or QED effects (QED) using formulas (3.65)–(3.67) where Δg is built using the Feynman rules.
3. We limit ourselves to linear effects in V^{magn} , just as we did with hfs. To put it another way, we only consider the Feynman diagrams of the first order in the magnetic interaction.
4. The corresponding contribution to the g factor (see Eq. (5.3)) is given by

$$\Delta g_{\text{int/QED}} = -\frac{2\Delta E_{\text{int/QED}}}{(eBm_\alpha)}. \quad (5.6)$$

Within the framework of bound-state QED perturbation theory, each of the contributions Δg_{int} and Δg_{QED} can be expanded as follows

$$\Delta g = \Delta g^{(1)} + \Delta g^{(2)} + \Delta g^{(3+)}, \quad (5.7)$$

where the i th order in α is denoted by the superscript i and $\Delta g^{(3+)}$ denotes all higher orders. So far, only three terms have been rigorously evaluated, namely $\Delta g_{\text{int}}^{(1)}$, one-photon exchange, $\Delta g_{\text{int}}^{(2)}$, two-photon exchange, and $\Delta g_{\text{QED}}^{(1)}$, one-electron self-energy and vacuum polarization, to all orders in αZ without any additional approximations. The second order QED correction $\Delta g_{\text{QED}}^{(2)}$ is divided into two parts: the one-electron two-loop QED term $\Delta g_{\text{QED-1e}}^{(2)}$ and the many-electron (screened) QED term $\Delta g_{\text{QED-me}}^{(2)}$. While the latter has been independently calculated in Refs. (Volotka et al., [2009]; Glazov et al., [2010]) and (Yerokhin et al., [2020]), the former is currently being evaluated (Yerokhin and Harman, [2013]; Sikora et al., [2020]; Debierre et al., [2021]).

The terms that are not yet known to all orders in αZ are approximated, for example,

within the αZ expansion or by using certain efficient operators. These terms are presented as follows

$$\Delta g^{(i)} = \Delta g_{\text{L}}^{(i)} + \Delta g_{\text{H}}^{(i)}, \quad (5.8)$$

account, where $\Delta g_{\text{L}}^{(i)}$ is the leading-order part, which is taken into account, and $\Delta g_{\text{H}}^{(i)}$ stands for the currently unknown higher-order part, whose value must be approximated to assign the uncertainty to $\Delta g^{(i)}$. Note that depending on the computation technique, the leading-order terms $\Delta g_{\text{L}}^{(i)}$ might be defined in a variety of ways. So, in the NRQED approach, $\Delta g_{\text{L}}^{(i)}$ typically represents the contribution of the lowest order in αZ . Within the Breit approximation, $\Delta g_{\text{L}}^{(i)}$, on the other hand, contains higher orders in αZ , but only the leading order is complete. Generally, in comparison to $\Delta g_{\text{L}}^{(i)}$, the higher-order part $\Delta g_{\text{H}}^{(i)}$ is suppressed by the factor $(\alpha Z)^2$.

5.2 THIRD-ORDER CORRECTION $\Delta g^{(3+)}$: ESTIMATION OF THE HIGHER ORDER PART $\Delta g_{\text{H}}^{(3+)}$

As previously stated in the original Furry picture, the binding potential only includes the nucleus' Coulomb field, implying that the electron-electron interaction is completely ignored in the zeroth order. The perturbation theory is used to account for this interaction. In this case, the effective expansion parameter in Eq. (5.7) is $1/Z$. Because the rigorous treatment of $\Delta g^{(i)}$ is currently limited by the second order, the higher-order terms in αZ are evaluated to the leading order, i.e., only the $\Delta g_{\text{L}}^{(3+)}$ part. This can be accomplished in the NRQED approach by using accurate variational wave functions in the Hyleraas basis (Yerokhin et al., 2017), the configuration interaction method (Bratzev et al., 1977; Glazov et al., 2004), or the recursive perturbation theory (Glazov et al., 2019a; Glazov et al., 2017) in the Breit approximation.

The theoretical accuracy is currently limited primarily by the missing higher-order contributions $\Delta g_{\text{H}}^{(3+)}$, which can be estimated in a variety of ways. The first option is based on the higher-order term from the perturbation theory's previous order: (i) $\Delta g_{\text{H}}^{(3+)} \simeq \Delta g_{\text{H}}^{(2)}/Z$. The second option, on the other hand, is solely based on the leading-order term from the same order of perturbation theory: (ii) $\Delta g_{\text{H}}^{(3+)} \simeq \Delta g_{\text{L}}^{(3+)}(\alpha Z)^2$. Finally, the third method combines both schemes (i) and (ii), employing both the leading-order terms and the higher-order correction from the preceding order of perturbation theory: (iii) $\Delta g_{\text{H}}^{(3+)} \simeq \Delta g_{\text{H}}^{(2)} \left(\Delta g_{\text{L}}^{(3+)}/\Delta g_{\text{L}}^{(2)} \right)$. The estimations based on these schemes can differ by an order of magnitude. As a result, it is critical to choose wisely among these estimation schemes.

The higher-order contribution $g^{(3+)}$, including the currently unknown part $\Delta g_{\text{H}}^{(3+)}$,

can be significantly reduced by introducing an effective local screening potential into the Dirac equation, which is referred to as the extended Furry picture. The perturbation series is rearranged in such a way that the dominant part of each order is transferred to lower orders. This "rearrangement" is, of course, dependent on the screening potential chosen. When all orders of the perturbation theory are incorporated entirely, the total result should be independent of the zeroth-order approximation. In fact, the higher-order part $\Delta g_{\text{H}}^{(3+)}$ is missing at present. As a result, the difference in total values obtained with various screening potentials allows one to estimate the magnitude of this part.

In this chapter, we employ four types of screening potential: core-Hartree (CH), Kohn-Sham (KS), Dirac-Hartree (DH), and Dirac-Slater (DS). The expressions for these potentials can be found in Subsection [3.4.2](#).

5.3 INTERELECTRONIC INTERACTION: CALCULATION

The interelectronic-interaction correction Δg_{int} to the g factor can be expanded as

$$\Delta g_{\text{int}} = \Delta g_{\text{int}}^{(1)} + \Delta g_{\text{int}}^{(2)} + \Delta g_{\text{int}}^{(3+)} . \quad (5.9)$$

Here the i th order in α is denoted by the superscript i while $\Delta g_{\text{int}}^{(3+)}$ refers to all higher orders. In the framework of the extended Furry picture, one can obtain zeroth-order value $g^{(0)}$ using Eq. [\(5.3\)](#) with wave function $|a\rangle$ constructed from the one-electron wave-function being a solution of Dirac equation with some effective potential. We note, that $g^{(0)}$ already partially includes interelectronic-interaction effects, therefore, within extended Furry picture, the additional term $\Delta g^{(0)}$ in expansion Eq. [\(5.9\)](#) appears

$$\Delta g^{(0)} = g^{(0)} - g_{\text{C}}^{(0)} . \quad (5.10)$$

The contributions in Eq. [\(5.9\)](#) are defined by the set of diagrams depicted on Figs. [4.1-4.4](#). The only difference is that now the dashed line that ends with a triangle represent the interaction with the external magnetic field $\delta V = V^{\text{magn}}$. The first-order correction $\Delta g_{\text{int}}^{(1)}$ corresponds to the relatively straightforward one-photon exchange diagrams shown in Fig. [4.1](#). It was first computed in Ref. (Shabaev et al., [2002](#)), and now all that remains is to compute it with the required numerical accuracy for the screening potentials under consideration.

The two-photon-exchange contribution $\Delta g_{\text{int}}^{(2)}$ is represented by the Feynman di-

agrams shown in Figs. 4.2-4.4. This correction is substantially more complicated, requiring the development of a numerical procedure as well as the derivation of the complete set of formulae. The formulas for contributions $\Delta g_{\text{int}}^{(1)}$ and $\Delta g_{\text{int}}^{(2)}$ are very similar to those for hfs, with the exception that δV is replaced by V^{magn} and a different multiplicative factor is used; for more information, see the Appendix. As a result, the numerical evaluation principles are the same as in the case of hfs. The dual-kinetic-balance (DKB) finite-basis set approach (Shabaev et al., 2004) for the Dirac equation with B-splines as the basis functions (Sapirstein and Johnson, 1996) is used to conduct infinite summations over the complete Dirac spectrum. The number of basis functions is gradually raised from $N = 132$ to $N = 252$ to do the extrapolation $N \rightarrow \infty$ in order to establish a clear convergence pattern of the results. The absolute extrapolation uncertainty is limited to a maximum of 10^{-10} . The partial wave summing over the Dirac quantum number κ is ended at $|\kappa|_{\text{max}} = 16$, and the remainder is approximated with an absolute uncertainty of 3×10^{-11} or less using least-squares inverse polynomial fitting. The numerical evaluation of the two-photon-exchange correction has considerable cancellations between various terms, as well as poor partial-wave expansion convergence. In comparison to Refs. (Volotka et al., 2014; Glazov et al., 2019a), we have significantly improved the numerical integrations over the radial variable x and the virtual-photon energy ω , attaining relative accuracy of 10^{-10} or lower. As a result, all sources of numerical uncertainty have been eliminated, and the two-photon exchange is assured to have a total numerical accuracy of 10^{-10} or better. To ensure the consistency of our implementation, we calculate individual terms of the two-photon exchange correction within the Feynman and Coulomb gauges, and the total results are found to be gauge invariant to a high degree of precision. We also compare the results of the two-photon-exchange correction to those obtained using the Breit approximation. First, the accuracy of the Breit limit of the QED formulas is established by substituting the interelectronic-interaction operator with its frequency-independent counterpart and properly restricting the summing over the intermediate states. Second, the correct behavior of the numerical results is investigated. All of this further confirms the accuracy of the current calculations.

The Breit approximation is used to compute the remaining higher-order contribution $\Delta g_{\text{int},L}^{(3+)}$. We employ the recursive perturbation theory proposed for binding energies in Ref. (Glazov et al., 2017) and extended to the case of external field (g factor, hyperfine splitting) in Refs. (Glazov et al., 2019a; Kosheleva et al., 2020) to achieve this. The DKB finite-basis-set approach (Shabaev et al., 2004; Sapirstein and Johnson, 1996) is also used for numerical computations. Because the many-electron wave function basis set must be considered within this method, the number of basis functions required to be adequate for the available computational resources is much

	Coulomb	CH	KS	DH	DS
Z = 14					
$g^{(0)} - g_C^{(0)}$		348.2661	341.3682	353.1638	329.1102
$\Delta g_{\text{int}}^{(1)}$	321.5903	-33.5491	-25.0951	-39.2815	-11.7598
$\Delta g_{\text{int}}^{(2)}$	-6.8782(1)	0.1362(1)	-1.4838(1)	1.1237(1)	-2.5910(1)
	-6.8787(1) ^a	0.137 ^b			
$\Delta g_{\text{int,L}}^{(3+)}$	0.0934(21)	-0.0443(10)	0.0202(12)	-0.1952(18)	0.0505(12)
	0.0942(4) ^c	-0.046(6) ^b			
$\Delta g_{\text{int,H}}^{(3+)}$	0.0000(74)	0.0000(14)	0.0000(18)	0.0000(12)	0.0000(20)
	0.0000(14) ^a				
Total	314.8055(77)	314.8089(17)	314.8095(22)	314.8107(22)	314.8099(23)
	314.8058(15) ^a				
Z = 20					
$g^{(0)} - g_C^{(0)}$		505.2339	494.1961	513.4290	475.2654
$\Delta g_{\text{int}}^{(1)}$	461.1479	-51.0429	-38.3914	-60.1565	-18.3166
$\Delta g_{\text{int}}^{(2)}$	-6.9338(1)	0.1291(1)	-1.5297(1)	1.1550(1)	-2.6958(1)
	-6.9341(3) ^a	0.129 ^b			
$\Delta g_{\text{int,L}}^{(3+)}$	0.0661(17)	-0.0300(8)	0.0155(12)	-0.1359(13)	0.0388(13)
	0.0695(12) ^c				
$\Delta g_{\text{int,H}}^{(3+)}$	0.0000(108)	0.0000(24)	0.0000(20)	0.0000(20)	0.0000(30)
	0.0000(22) ^a				
Total	454.2802(109)	454.2902(25)	454.2905(24)	454.2915(24)	454.2918(33)
	454.2834(25) ^a				

^a Yerokhin et al., [2021]; ^b Volotka et al., [2014]; ^c Yerokhin et al., [2017]

Table 5.1: Interelectronic-interaction contributions Δg_{int} to the ground-state g factor of $^{28}\text{Si}^{11+}$ and $^{40}\text{Ca}^{17+}$ for various starting potentials: Coulomb, core-Hartree (CH), Kohn-Sham (KS), Dirac-Hartree (DH), and Dirac-Slater (DS), in units of 10^{-6} .

lower than for the two-photon-exchange contribution. Nonetheless, we are able to reach a numerical uncertainty that is lower than that of the currently unknown higher-order part $\Delta g_{\text{int,H}}^{(3+)}$ estimate. The contributions of the third, fourth, and fifth orders of perturbation theory are required at this level. We should also remark that under perturbation theory, we only require a few percent uncertainty for the third-order contribution and considerably more for the fourth and fifth orders to obtain this level of precision. This differs from all-order approaches, such as CI-DFS (Volotka et al., [2014]; Glazov et al., [2004]), which need a numerical uncertainty of $10^{-5} - 10^{-6}$ since they only yield entire result $\Delta g_{\text{int,L}}$ within the Breit approximation.

5.4 INTERELECTRONIC INTERACTION: RESULTS

The results of the interelectronic-interaction correction for Si^{11+} and Ca^{17+} ions are shown in Table [5.1]. In the extended Furry picture, the zeroth-order value minus the Coulomb value, $\Delta g^{(0)}$, makes an important contribution to Δg_{int} . As mentioned in the previous Section [5.3], the one- and two-photon-exchange corrections are calculated

to all orders in αZ to a precision of 10^{-10} or greater. For comparison, the values for the two-photon exchange from Refs. (Volotka et al., 2014; Yerokhin et al., 2021) are provided. Table 5.1 shows that our values are one order of magnitude more accurate than those of Ref. (Volotka et al., 2014), whereas the marginal agreement for the Coulomb potential is found with Ref. (Yerokhin et al., 2021). The results of Refs. (Yerokhin et al., 2021; Yerokhin et al., 2017) obtained using the NRQED method for the Coulomb potential agree well with our results for the third- and higher-order correction $\Delta g_{\text{int,L}}^{(3+)}$ obtained using the Breit approximation.

Before we get to the total results, let us talk about the uncertainty of the higher-order term $\Delta g_{\text{int,H}}^{(3+)}$, which is currently unknown. The three methods of estimate outlined above yield (i) 0.0037, (ii) 0.0013, and (iii) 0.0008, in units of 10^{-6} for the silicon ion and the Coulomb potential. These estimations differ by up to a factor of 5. In this case, which one should be chosen? To make the best decision, we use the following logic. The final results should be the same for all starting potentials once Δg_{int} has been computed to all orders without approximations. As a result, the current differences between the Coulomb, CH, KS, DH, and DS results are due to $\Delta g_{\text{int,H}}^{(3+)}$. To ensure that the results overlap, we chose the first (biggest) uncertainty multiplied by a factor of 2. While, Yerokhin et al., 2021 and Yerokhin et al., 2017 employed the smallest uncertainty (third choice) multiplied by 1.5 (Yerokhin et al., 2017) and 2 (Yerokhin et al., 2021). Their uncertainty is 5 times smaller, and their total result for the Coulomb potential does not overlap with our values for other starting potentials, both for silicon and calcium, as shown in the Table.

Finally, we average our total values from four screening potentials (CH, KS, DH, DS) to get $314.8098(22) \times 10^{-6}$ for $Z = 14$ and $454.2910(24) \times 10^{-6}$ for $Z = 20$ for the interelectronic-interaction correction.

5.5 QED CORRECTIONS: CALCULATION

The QED correction Δg_{QED} to the g factor can be expanded as

$$\Delta g_{\text{QED}} = \Delta g_{\text{QED}}^{(1)} + \Delta g_{\text{QED}}^{(2)} + \Delta g_{\text{QED}}^{(3+)} \quad (5.11)$$

Here the i th order in α is denoted by the superscript i while $\Delta g_{\text{QED}}^{(3+)}$ refers to all higher orders. The first-order contribution $\Delta g_{\text{QED}}^{(1)}$, which is represented by standard radiative diagrams, self-energy, and vacuum polarization in the presence of an external magnetic field, has been rigorously evaluated, for example, by Yerokhin et al., 2004; Glazov et al., 2006; Yerokhin and Harman, 2017; Cakir et al., 2020. The second-order contribution $\Delta g_{\text{QED}}^{(2)}$ can split into two parts: the one-electron

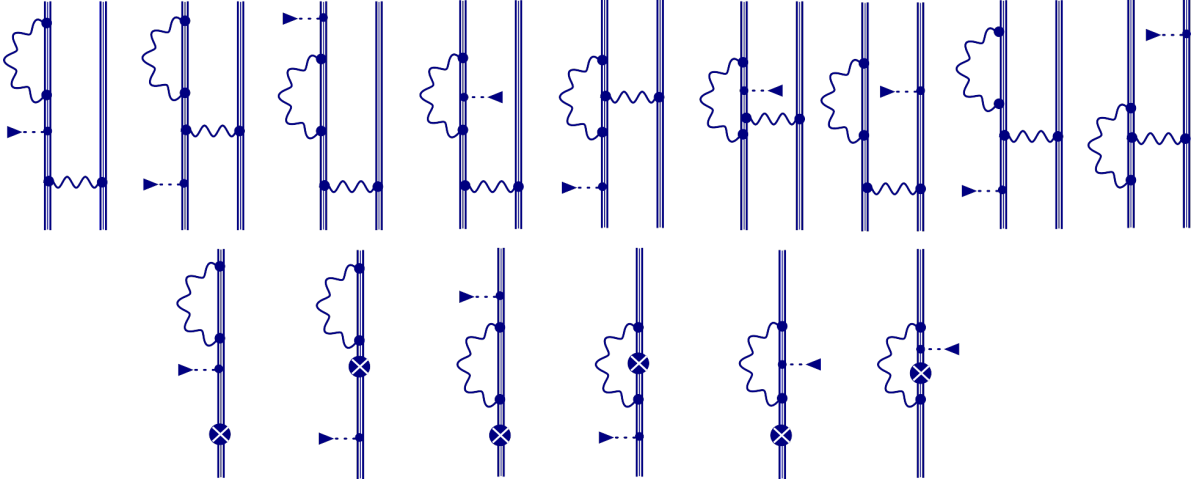


Figure 5.1: Feynman diagrams illustrating the screened self-energy correction to the bound-electron g factor. The counterterm diagrams are shown in the second line. The notations are identical to those shown in Fig. 4.1. The only difference is that now the magnetic interaction δV is equal to the V^{magn} , i.e. $\delta V = V^{\text{magn}}$.

part $\Delta g_{\text{QED-e}}^{(2)}$ (two-loop QED) and the many electron part $\Delta g_{\text{QED-me}}^{(2)}$ (screened QED). The two-electron self-energy diagrams (Fig. 5.1, first line) and two-electron vacuum polarization diagrams (Fig. 5.2, first line) depict the screened QED part $\Delta g_{\text{QED-me}}^{(2)}$. Because we are working within the framework of the extended Furry picture, additional counterterm diagrams appear (see the second line in Figs. 5.1 and 5.2). The screened vacuum-polarization contribution was originally computed in Ref. (Andreev et al., 2012) for the hyperfine interaction as an external field, and then modified in Refs. (Volotka et al., 2014; Cakir et al., 2020) for the g -factor case. Calculating it with the needed accuracy for middle- Z ions is currently not a problem. Volotka et al., 2009; Glazov et al., 2010; Yerokhin et al., 2020 calculated the screened self-energy contribution for the Coulomb potential and Volotka et al., 2014 for the case of screening potentials. Meanwhile, due to the poor basis-set and partial-wave convergence, achieving a high level of numerical accuracy was always a challenge. Therefore, we describe in detail the current improvements to the calculation procedure below. Refs. (Volotka et al., 2014; Volotka et al., 2009; Glazov et al., 2010) contain formal expressions for two-electron self-energy diagrams. The numerical procedure follows the same principles as the two-photon exchange. To achieve the required accuracy, the numerical integrations over the radial variable x and the virtual-photon energy ω have been improved. To begin, we calculate the individual partial wave terms up to $|\kappa|_{\text{max}} = 20$ for various numbers of basis functions N and extrapolate to $N \rightarrow \infty$ to achieve an absolute uncertainty of 10^{-10} or less for each κ . The greater $|\kappa|$, the greater N is required. Then we sum these terms and use least-squares inverse polynomial fitting to estimate the tail of $|\kappa| > |\kappa|_{\text{max}}$. This extrapolation's absolute uncertainty is less than 2×10^{-10} . We should remark that the numerical evaluation

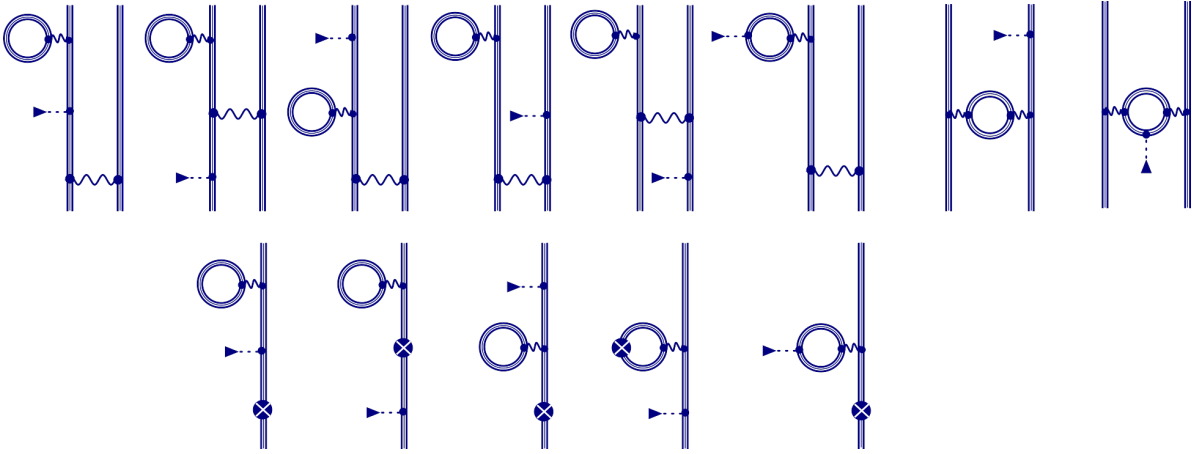


Figure 5.2: Feynman diagrams illustrating the screened vacuum-polarization correction to the bound-electron g factor. The counterterm diagrams are shown in the second line. The notations are identical to those shown in Fig. 4.1. The only difference is that now the magnetic interaction δV is equal to the V^{magn} , i.e. $\delta V = V^{\text{magn}}$.

of screened self-energy correction for the Coulomb potential includes considerable term cancellations, resulting in huge numerical inaccuracy. The use of the screening potential reduces the magnitude of cancellations and increases accuracy significantly. So far, the higher-order QED contributions can only be approximated. Pachucki et al., [2005b]; Pachucki et al., [2005a]; Jentschura, [2009]; Yerokhin and Harman, [2013]; Czarnecki and Szafron, [2016]; Czarnecki et al., [2018]; Czarnecki et al., [2020] calculated the one-electron two-loop term $\Delta g_{\text{QED-1e}}^{(2)}$ within the αZ expansion up to order $\alpha^2(\alpha Z)^5$. We also compute the interelectronic-interaction correction to the two-loop term using two different methods. Within the first approach, we extract the binding part (beyond the free-electron contribution) of this term and multiply it by the "screening coefficient," which is dependent on the screening potential. The binding part of the one-loop term is used to identify this coefficient. In this manner, we obtain the screened values of $\Delta g_{\text{QED-1e}}^{(2)}$ shown in Table 5.2 in the following Section 5.6. In the second approach, we calculate the screening effect on the two-loop contribution by averaging the corresponding term of the effective Hamiltonian from Ref. (Hegstrom, [1973]). The results of these two calculation methods are in perfect agreement with each other. The free-electron part $[(\alpha Z)^0]$ as well as the leading-order $[(\alpha Z)^2]$ correction for the three-loop (and more) one-electron contribution $\Delta g_{\text{QED-1e}}^{(3+)}$ are taken from Aoyama et al., [2019] and Shabaev et al., [2002] respectively.

The effective Hamiltonian from Ref. (Hegstrom, [1973]) is used to compute the higher-order many-electron QED correction $\Delta g_{\text{QED-me,L}}^{(3+)}$. In Refs. (Shabaev et al., [2002]; Glazov et al., [2004]), this approach was proposed and implemented up to the first order in $1/Z$ ($\Delta g_{\text{QED,L}}^{(1)}$ and $\Delta g_{\text{QED-me,L}}^{(2)}$ terms). The multi-recursive perturbation theory scheme was constructed in Ref. (Glazov et al., [2019a]) to effectively evaluate

the contributions of arbitrary order in $1/Z$. This scheme extends the recursive formulation of perturbation theory (Glazov et al., 2017) to the case of Hamiltonian with several effective operators that must be considered at the same time. In this method, $\Delta g_{\text{QED-me,L}}^{(3+)}$ to arbitrary order computations in $1/Z$ were made possible.

5.6 QED CORRECTIONS: RESULTS

The results of the QED corrections, obtained with all five binding potentials for both Si^{11+} and Ca^{17+} ions, are provided in Table . We use the results of Refs. (Yerokhin et al., 2020; Yerokhin et al., 2021) for the Coulomb potential; the values are in the second column. The results of this investigation are shown in the third through sixth columns. Our total values obtained with various screening potentials are close to each other and overlap within their uncertainties, as shown in this Table. The numerical error in $\Delta g_{\text{QED-me}}^{(2)}$ and the estimation of higher-order effects $\Delta g_{\text{QED-me,H}}^{(3+)}$ determine the total uncertainty. The latter is considered to be the biggest value out of three possible estimations, as discussed above in relation to the $\Delta g_{\text{int,H}}^{(3+)}$. Yerokhin et al., 2020; Yerokhin et al., 2021 assessed the uncertainty similarly, but there is still a considerable disagreement between the Coulomb result and the total results for all the screening potentials. The calculation of the term $\Delta g_{\text{QED-me}}^{(2)}$ might be the source of this discrepancy. As shown in Table , it has a far larger contribution for the Coulomb potential than for the screening potentials, and a little change in its value might result in an agreement between the results.

Finally, we take the average of all the screening potentials and present our final QED correction values: $2320.2857(17) \times 10^{-6}$ for silicon and $2321.6601(17) \times 10^{-6}$ for calcium.

5.7 TOTAL RESULTS AND DISCUSSIONS

Table 5.3 summarizes all theoretical contributions to the g factor of Li-like $^{28}\text{Si}^{11+}$ and $^{40}\text{Ca}^{17+}$ ions and compares them to previously reported theoretical and experimental data. We use nuclear recoil contributions from Refs. (Shabaev et al., 2017; Shabaev et al., 2018) in addition to the corrections Δg_{int} and Δg_{QED} calculated in this thesis. For the ions under consideration, the nuclear polarization effect is insignificant. The total uncertainty is still defined by the interelectronic-interaction and QED corrections, as shown in Table 5.3. Figs. 5.3 and 5.4 depicts both the current and previously published theoretical and experimental results from Refs. (Wagner et al., 2013; Köhler

	Coulomb ^a	CH	KS	DH	DS
$Z = 14$					
$\Delta g_{\text{QED}}^{(1)}$	2324.0439	2323.8100	2323.8106	2323.8089	2323.8227
$\Delta g_{\text{QED-1e}}^{(2)}$	-3.5463	-3.5460	-3.5460	-3.5460	-3.5460
$\Delta g_{\text{QED-me}}^{(2)}$	-0.2460(6)	-0.0074(17)	-0.0087(17)	-0.0064(16)	-0.0216(20)
$\Delta g_{\text{QED-1e}}^{(3+)}$	0.0295	0.0295	0.0295	0.0295	0.0295
$\Delta g_{\text{QED-me,L}}^{(3+)}$	0.0099	-0.0003	0.0003	-0.0004	0.0009
$\Delta g_{\text{QED-me,H}}^{(3+)}$	0.0000(6)	0.0000	0.0000(2)	0.0000(1)	0.0000(1)
Total	2320.2910(8)	2320.2858(17)	2320.2857(17)	2320.2856(16)	2320.2855(20)
$Z = 20$					
$\Delta g_{\text{QED}}^{(1)}$	2325.5544	2325.2019	2325.1985	2325.2025	2325.2211
$\Delta g_{\text{QED-1e}}^{(2)}$	-3.5490(3)	-3.5484(3)	-3.5484(3)	-3.5484(3)	-3.5485(3)
$\Delta g_{\text{QED-me}}^{(2)}$	-0.3675(6)	-0.0220(17)	-0.0199(17)	-0.0228(15)	-0.0438(20)
$\Delta g_{\text{QED-1e}}^{(3+)}$	0.0295	0.0295	0.0295	0.0295	0.0295
$\Delta g_{\text{QED-me,L}}^{(3+)}$	0.0105	-0.0003	0.0003	-0.0004	0.0010
$\Delta g_{\text{QED-me,H}}^{(3+)}$	0.0000(12)	0.0000(4)	0.0000	0.0000(7)	0.0000(6)
Total	2321.6779(13)	2321.6607(18)	2321.6600(17)	2321.6604(17)	2321.6593(21)

^a Yerokhin et al., 2020; Yerokhin et al., 2021

Table 5.2: QED corrections Δg_{QED} to the ground-state g factor of $^{28}\text{Si}^{11+}$ and $^{40}\text{Ca}^{17+}$ for various starting potentials: Coulomb, core-Hartree (CH), Kohn-Sham (KS), Dirac-Hartree (DH), and Dirac-Slater (DS), in units of 10^{-6} . Values for the Coulomb potential are taken from Refs. (Yerokhin et al., 2020; Yerokhin et al., 2021).

Effects	$^{28}\text{Si}^{11+}$	$^{40}\text{Ca}^{17+}$
Dirac value	1.998 254 753 3	1.996 426 025 3
e-e interaction	0.000 314 809 8(22)	0.000 454 291 0(24)
QED	0.002 320 285 7(17)	0.002 321 660 1(17)
Nuclear recoil	0.000 000 043 6	0.000 000 066 2
Total theory	2.000 889 892 4(28)	1.999 202 042 6(29)
	2.000 889 893 7(17) ^a	1.999 202 052 9(27) ^a
	2.000 889 896 3(15) ^b	1.999 202 042(13) ^d
	2.000 889 894 4(34) ^c	
Experiment	2.000 889 888 45(14) ^c	1.999 202 040 5(11) ^d
	2.000 889 888 4(19) ^e	

^a Yerokhin et al., 2021; ^b Yerokhin et al., 2020; ^c Glazov et al., 2019a;

^d Köhler et al., 2016; ^e Wagner et al., 2013.

Table 5.3: Theoretical contributions to the ground-state g factor of Li-like $^{28}\text{Si}^{11+}$ and $^{40}\text{Ca}^{17+}$ ions. Total theoretical and experimental values are compared. The numbers in parentheses indicate the uncertainty of the last digit(s). All figures are significant unless an uncertainty is specified.

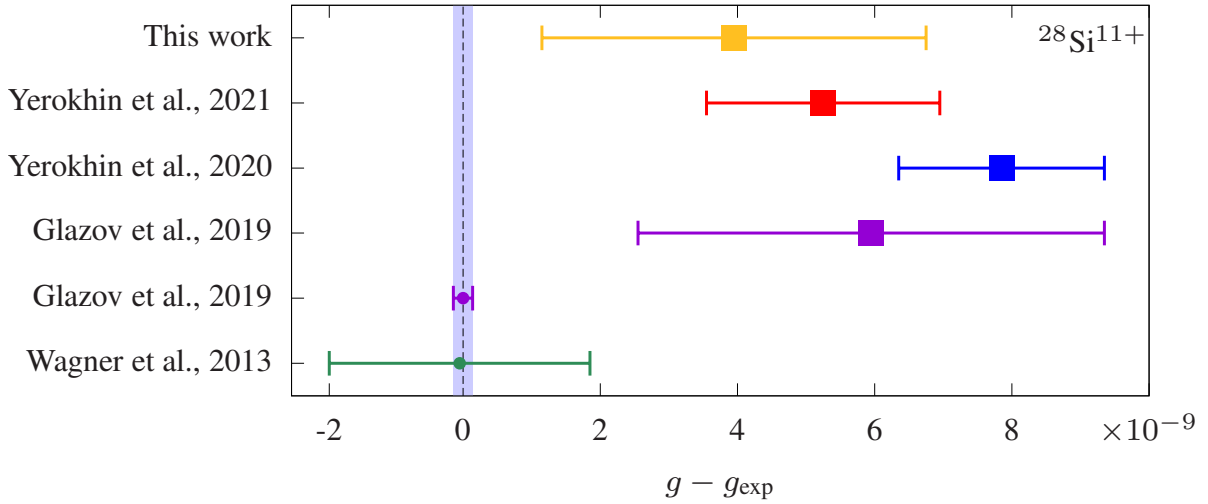


Figure 5.3: Theoretical (squares) and experimental (circles) g -factor values for Li-like silicon reported in this and previously published works.

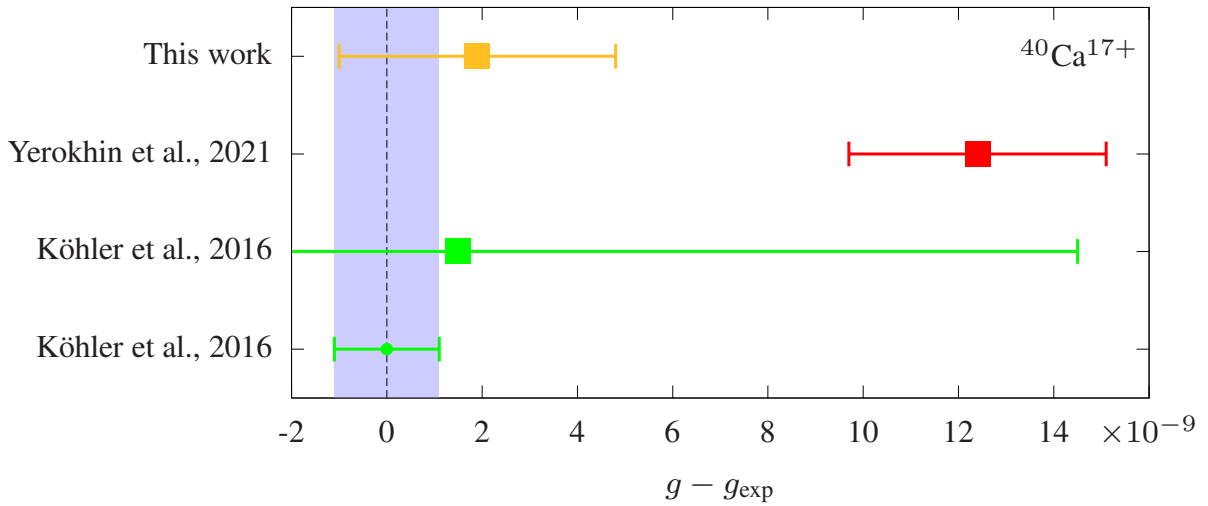


Figure 5.4: Theoretical (squares) and experimental (circles) g -factor values for Li-like calcium reported in this and previously published works.

et al., [2016](#); Glazov et al., [2019a](#); Yerokhin et al., [2020](#); Yerokhin et al., [2021](#)). When compared to Glazov et al., [2019a](#) the silicon result is more precise and closer to the experimental value. When compared to Yerokhin et al., [2021](#) the results agree within the stated uncertainty for $^{28}\text{Si}^{11+}$, however there is a 2.6σ discrepancy for $^{40}\text{Ca}^{17+}$. We should emphasize that the individual contributions, Δg_{int} and Δg_{QED} , disagree even stronger. These discrepancies, however, partially cancel each other out. Yerokhin et al., [2021](#) results for silicon and calcium deviate by 3.1σ and 4.2σ , respectively, from the experimental values. Meanwhile, our results are far closer to the measurements: 1.4σ and 0.6σ deviance, respectively. We believe that the discrepancies identified by Yerokhin et al., [2021](#) are thought to be attributable to an underestimation of the interelectronic-interaction contribution's uncertainty, as well as a probable problem with their computation of the screened QED term.

CONCLUSIONS AND OUTLOOK

We considered the many-electron effects on the hyperfine splitting and g factor of lithiumlike ions in this dissertation. The investigations were performed within the bound-state QED framework. Therefore, first, we laid the foundation of the bound-state QED theory. In Chap. 2 we considered free electron-positron and electromagnetic fields in the presence of the background field of the nucleus.

Then in Chap. 3 we described the QED perturbation theory. To do so, we constructed the time-evolution operator in Sec. 3.2 and presented its Dyson series. In the next Sec. 3.3 we defined the central object of the quantum field theory, the S -matrix. We described the formalism that Gell-Mann, Low, and Sucher first introduced for bound-stated QED perturbation theory, the adiabatic S -matrix approach. And we concluded this chapter by formulating the two-time Green's function formalism which was used in the current dissertation for computations of the QED corrections to the hyperfine splitting and g factor of few-electron ions.

In Chaps. 4 and 5 we investigated the interaction of the bound electron with a magnetic field. Thus, Chap. 4 is devoted to the ground-state hyperfine splitting in lithiumlike ions. In this chapter, we evaluated the interelectronic-interaction contribution to the ground-state hyperfine splitting in Li-like ions for a wide range of nuclear charge numbers. The contributions due to the one- and two-photon-exchange corrections were treated within the framework of the extended Furry picture using a rigorous QED approach. The higher-order interelectronic-interaction contributions were taken into account using the recursive perturbation theory. As a result, the accuracy of the interelectronic-interaction corrections to the ground-state hyperfine splitting in Li-like ions in the $Z = 7 - 82$ range has been significantly improved. These calculations are also necessary for determining the specific difference between H- and Li-like ions, which can be used for high-precision tests of the bound-state QED in a strong nuclear field. As a future task, one can evaluate the screened QED corrections to the hfs in Li-like ions for a wide range of nuclear charge Z to push forward the test of QED with hfs. These findings, when combined with the current rigorous calculations of the interelectronic-interaction correction, would allow one to construct

the specific differences, where the QED effects could be tested via comparison with the experiment.

In Chap. 5 we considered bound-electron g factor of lithiumlike ions. The bound-electron g factor is a physical quantity of great fundamental interest that can be precisely measured and calculated. Many fascinating ideas have been proposed on its basis, such as determining the electron mass and the fine structure constant, investigating nuclear properties, and searching for effects beyond the Standard Model. To realize these ideas, one must first ensure that the QED theory's predictions are correct. Presently, a large discrepancy between theory and experiment exists in the cases of lithiumlike silicon and calcium [D. A. Glazov *et al.*, *Phys. Rev. Lett.* **123**, 173001 (2019); V. A. Yerokhin *et al.*, *Phys. Rev. A* **102**, 022815 (2020); V. A. Yerokhin *et al.*, *Phys. Rev. A* **104**, 022814 (2021)]. In this thesis, we not only improved the theoretical value of the g factor but also explained the reasons for the discrepancy between theory and experiment. As a result, our new theoretical values are much closer to the experiment: the difference is just 1.4σ and 0.6σ for silicon and calcium, respectively.

Quantitatively, in comparison to [D. A. Glazov *et al.*, *Phys. Rev. Lett.* **123**, 173001 (2019)], we have reduced the numerical uncertainty of the two-photon exchange contribution by an order of magnitude. The screened QED correction has been calculated rigorously for different screening potentials, without using extrapolation from high Z as was done in 2019. As a result, we have significantly improved the accuracy of the higher-order contributions. Moreover, we have presented two-fold improvement for calcium in comparison to [F. Köhler *et al.*, *Nat. Commun.* **7**, 10246 (2016)].

As a next step, we propose increasing the accuracy of the total theoretical value of the g factor of lithiumlike silicon and attempting to reach or at least come closer to experimental accuracy. To do so one should rigorously evaluate many-electron QED contributions to the g factor: two-loop many-electron diagrams, particularly the three-photon exchange and the two-photon exchange with a self-energy loop. First and foremost, this can be used to resolve the 1.4σ discrepancy between theory and experiment. Furthermore, the current experimental value has the potential to validate this nontrivial many-electron QED contribution on a few percent level.

BIBLIOGRAPHY

- Andreev, O. V., D. A. Glazov, A. V. Volotka, V. M. Shabaev, and G. Plunien (2012). "Evaluation of the screened vacuum-polarization corrections to the hyperfine splitting of Li-like bismuth." In: *Phys. Rev. A* 85, p. 022510.
- Angeli, I. and K. P. Marinova (2013). "Table of experimental nuclear ground state charge radii: An update." In: *At. Data Nucl. Data Tables* 99, p. 69.
- Aoyama, T., T. Kinoshita, and M. Nio (2019). "Theory of the Anomalous Magnetic Moment of the Electron." In: *Atoms* 7, p. 28.
- Arapoglou, I. et al. (2019). "g Factor of Boronlike Argon $^{40}\text{Ar}^{13+}$." In: *Phys. Rev. Lett.* 122, p. 253001.
- Beier, T. (2000). "The g_j factor of a bound electron and the hyperfine structure splitting in hydrogenlike ions." In: *Phys. Rep.* 339, p. 79.
- Beier, T., I. Lindgren, H. Persson, S. Salomonson, P. Sunnergren, H. Häffner, and N. Hermanspahn (2000). "g_j factor of an electron bound in a hydrogenlike ion." In: *Phys. Rev. A* 62, p. 032510.
- Beiersdorfer, P. et al. (2001). "Hyperfine structure of hydrogenlike thallium isotopes." In: *Phys. Rev. A* 64, p. 032506.
- Berestetsky, V. B., E. M. Lifshitz, and L. P. Pitaevsky (1982). *Quantum Electrodynamics*. Pergamon Press, Oxford.
- Bethe, H. A. (1947). "The Electromagnetic Shift of Energy Levels." In: *Phys. Rev.* 72, pp. 339–341.
- Bjorken, J. and D. Drell (1965). *Relativistic Quantum Fields*. McGraw-Hill, New York.
- Blundell, S. A., K. T. Cheng, and J. Sapirstein (1997). "Radiative corrections in atomic physics in the presence of perturbing potentials." In: *Phys. Rev. A* 55, p. 1857.
- Blundell, S. A., W. R. Johnson, Z. W. Liu, and J. Sapirstein (1989). "Relativistic all-order calculations of energies and matrix elements for Li and Be⁺." In: *Phys. Rev. A* 40, pp. 2233–2246.
- Boucard, S. and P. Indelicato (2000). "Relativistic many-body and QED effects on the hyperfine structure of lithium-like ions." In: *Eur. Phys. J. D* 8, p. 59.
- Bratzev, V. F., G. B. Deyneka, and I. I. Tupitsyn (1977). "Application of the Hartree-Fock method to calculation of relativistic atomic wave functions." In: *Izv. Akad. Nauk SSSR, Ser. Fiz.* 41, 2655 [*Bull. Acad. Sci. USSR, Phys. Ser.* 41, 173].
- Breit, G. (1928). "The Magnetic Moment of the Electron." In: *Nature* 122, p. 649.

- Cakir, H., V. A. Yerokhin, N. S. Oreshkina, B. Sikora, I. I. Tupitsyn, C. H. Keitel, and Z. Harman (2020). "QED corrections to the g factor of Li- and B-like ions." In: *Phys. Rev. A* 101, p. 062513.
- Crespo López-Urrutia, J. R., P. Beiersdorfer, D. W. Savin, and K. Widmann (1996). "Direct observation of the spontaneous emission of the hyperfine transition $F = 4$ to $F = 3$ in ground state hydrogenlike $^{165}\text{Ho}^{66+}$ in an Electron Beam Ion Trap." In: *Phys. Rev. Lett.* 77, p. 826.
- Crespo López-Urrutia, J. R., P. Beiersdorfer, K. Widmann, B. B. Birkett, A.-M. Mårtensson-Pendrill, and M. G. H. Gustavsson (1998). "Nuclear magnetization distribution radii determined by hyperfine transitions in the $1s$ level of H-like ions $^{185}\text{Re}^{74+}$ and $^{187}\text{Re}^{74+}$." In: *Phys. Rev. A* 57, p. 879.
- Czarnecki, A., M. Dowling, J. Piclum, and R. Szafron (2018). "Two-Loop Binding Corrections to the Electron Gyromagnetic Factor." In: *Phys. Rev. Lett.* 120, p. 043203.
- Czarnecki, A., J. Piclum, and R. Szafron (2020). "Logarithmically enhanced Euler-Heisenberg Lagrangian contribution to the electron gyromagnetic factor." In: *Phys. Rev. A* 102, p. 050801.
- Czarnecki, A. and R. Szafron (2016). "Light-by-light scattering in the Lamb shift and the bound electron g factor." In: *Phys. Rev. A* 94, 060501(R).
- Debierre, V., C. Keitel, and Z. Harman (2020). "Fifth-force search with the bound-electron g factor." In: *Phys. Lett. B* 807, p. 135527.
- Debierre, V., B. Sikora, H. Cakir, N. S. Oreshkina, V. A. Yerokhin, C. H. Keitel, and Z. Harman (2021). "Two-loop virtual light-by-light scattering corrections to the bound-electron g factor." In: *Phys. Rev. A* 103, p. L030802.
- Dyson, F. J. (1949a). "The Radiation Theories of Tomonaga, Schwinger, and Feynman." In: *Phys. Rev.* 75, pp. 486–502.
- Dyson, F. J. (1952). "Divergence of Perturbation Theory in Quantum Electrodynamics." In: *Phys. Rev.* 85, pp. 631–632.
- Dyson, F. (1949b). "The S Matrix in Quantum Electrodynamics." In: *Phys. Rev.* 75, p. 1736.
- Dzuba, V. A., V. V. Flambaum, P. G. Silvestrov, and O. P. Sushkov (1987). "Correlation potential method for the calculation of energy levels, hyperfine structure and $E1$ transition amplitudes in atoms with one unpaired electron." In: *J. Phys. B* 20, p. 1399.
- Faustov, R. N. (1970). "Quasipotential method in the bound state problem." In: *Theor. Math. Phys.* 3, p. 478.
- Feynman, R. P. (1949a). "Space-Time Approach to Quantum Electrodynamics." In: *Phys. Rev.* 76, pp. 769–789.
- Feynman, R. P. (1949b). "The Theory of Positrons." In: *Phys. Rev.* 76, pp. 749–759.

- Furry, W. H. (1951). "On Bound States and Scattering in Positron Theory." In: *Phys. Rev.* 81, p. 115.
- Gell-Mann, M. and F. Low (1951). "Bound States in Quantum Field Theory." In: *Phys. Rev.* 84, p. 350.
- Ginges, J. S. M. and A. V. Volotka (2018). "Testing atomic wave functions in the nuclear vicinity: The hyperfine structure with empirically deduced nuclear and quantum electrodynamic effects." In: *Phys. Rev. A* 98, p. 032504.
- Ginges, J. S. M., A. V. Volotka, and S. Fritzsche (2017). "Ground-state hyperfine splitting for Rb, Cs, Fr, Ba⁺, and Ra⁺." In: *Phys. Rev. A* 96, p. 062502.
- Glazov, D. A., F. Köhler-Langes, A. V. Volotka, K. Blaum, F. Heiße, G. Plunien, W. Quint, S. Rau, V. M. Shabaev, S. Sturm, and G. Werth (2019a). "g Factor of Lithiumlike Silicon: New Challenge to Bound-State QED." In: *Phys. Rev. Lett.* 123, p. 173001.
- Glazov, D. A., A. V. Malyshev, A. V. Volotka, V. M. Shabaev, I. I. Tupitsyn, and G. Plunien (2017). "Higher-order perturbative relativistic calculations for few-electron atoms and ions." In: *Nucl. Instr. Meth. Phys. Res. B* 408, p. 46.
- Glazov, D. A. and V. M. Shabaev (2002). "Finite nuclear size correction to the bound-electron g factor in a hydrogenlike atom." In: *Phys. Lett. A* 297, p. 408.
- Glazov, D. A., V. M. Shabaev, I. I. Tupitsyn, A. V. Volotka, V. A. Yerokhin, G. Plunien, and G. Soff (2004). "Relativistic and QED corrections to the g factor of Li-like ions." In: *Phys. Rev. A* 70, p. 062104.
- Glazov, D. A., A. V. Volotka, O. V. Andreev, V. P. Kosheleva, S. Fritzsche, V. M. Shabaev, G. Plunien, and T. Stöhlker (2019b). "Ground-state hyperfine splitting of B-like ions in the high-Z region." In: *Phys. Rev. A* 99, p. 062503.
- Glazov, D. A., A. V. Volotka, V. M. Shabaev, and G. Plunien (2014). "QED Theory of the Bound-Electron Magnetic Moment." In: ed. by W. Quint and M. Vogel, pp. 137–163.
- Glazov, D. A., A. V. Volotka, V. M. Shabaev, I. I. Tupitsyn, and G. Plunien (2006). "Screened QED corrections to the g factor of Li-like ions." In: *Phys. Lett. A* 357, p. 330.
- Glazov, D. A., A. V. Volotka, V. M. Shabaev, I. I. Tupitsyn, and G. Plunien (2010). "Evaluation of the screened QED corrections to the g factor and the hyperfine splitting of lithiumlike ions." In: *Phys. Rev. A* 81, p. 062112.
- Greiner, W. and J. Reinhardt (1996). *Field Quantization*. Springer.
- Hegstrom, R. A. (1973). "Nuclear-mass and anomalous-moment corrections to the Hamiltonian for an atom in a constant external magnetic field." In: *Phys. Rev. A* 7, p. 451.

- Indelicato, P. and J. P. Desclaux (1990). "Multiconfiguration Dirac-Fock calculations of transition energies with QED corrections in three-electron ions." In: *Phys. Rev. A* 42, p. 5139.
- Itzykson, C. and J.-B. Zuber (1980). *Quantum Field Theory*. McGraw-Hill, New York.
- Jentschura, U. D. (2009). "Binding two-loop vacuum-polarization corrections to the bound-electron g factor." In: *Phys. Rev. A* 79, p. 044501.
- Karshenboim, S. G. (2000). "Non-relativistic calculations of the g -factor of a bound electron." In: *Phys. Lett. A* 266, p. 380.
- Karshenboim, S. G., V. G. Ivanov, and V. M. Shabaev (2001). "Some analytic results on the Uehling correction to the g -factor of a bound electron (muon)." In: *Can. J. Phys.* 79, 81 (2001); *Zh. Eksp. Teor. Fiz.* 120, 546 [*Sov. Phys. JETP* 93, 477].
- Kato, T. (1949). "On the Convergence of the Perturbation Method. I." In: *Progress of Theoretical Physics* 4, pp. 514–523.
- Kato, T. (1950a). "On the Convergence of the Perturbation Method, II. 1." In: *Progress of Theoretical Physics* 5, pp. 95–101.
- Kato, T. (1950b). "On the Convergence of the Perturbation Method, II. 2." In: *Progress of Theoretical Physics* 5, pp. 207–212.
- Klaft, I., S. Borneis, T. Engel, B. Fricke, R. Grieser, G. Huber, T. Kühl, D. Marx, R. Neumann, S. Schröder, P. Seelig, and L. Völker (1994). "Precision laser spectroscopy of the ground state hyperfine splitting of hydrogenlike $^{209}\text{Bi}^{82+}$." In: *Phys. Rev. Lett.* 73, p. 2425.
- Koba, Z., T. Tati, and S.-i. Tomonaga (1947a). "On a Relativistically Invariant Formulation of the Quantum Theory of Wave Fields. II: Case of Interacting Electromagnetic and Electron Fields." In: *Progress of Theoretical Physics* 2, pp. 101–116.
- Koba, Z., T. Tati, and S.-i. Tomonaga (1947b). "On a Relativistically Invariant Formulation of the Quantum Theory of Wave Fields. III: Case of Interacting Electromagnetic and Electron Fields." In: *Progress of Theoretical Physics* 2, pp. 198–208.
- Köhler, F., S. Sturm, A. Kracke, G. Werth, W. Quint, and K. Blaum (2015). "The electron mass from g -factor measurements on hydrogen-like carbon $^{12}\text{C}^{5+}$." In: *Journal of Physics B: Atomic, Molecular and Optical Physics* 48, p. 144032.
- Köhler, F. et al. (2016). "Isotope dependence of the Zeeman effect in lithium-like calcium." In: *Nat. Commun.* 7, p. 10246.
- Kosheleva, V. P., A. V. Volotka, D. A. Glazov, and S. Fritzsche (2020). "Many-electron effects in the hyperfine splitting of lithiumlike ions." In: *Phys. Rev. Research* 2, p. 013364.
- Kozhedub, Y. S., D. A. Glazov, A. N. Artemyev, N. S. Oreshkina, V. M. Shabaev, I. I. Tupitsyn, A. V. Volotka, and G. Plunien (2007). "QED calculation of the $2p_{1/2} - 2s$

- and $2p_{3/2} - 2s$ transition energies and the ground-state hyperfine splitting in lithiumlike scandium." In: *Phys. Rev. A* 76, p. 012511.
- Kozhedub, Y. S., A. V. Malyshev, D. A. Glazov, V. M. Shabaev, and I. I. Tupitsyn (2019). "QED calculation of electron-electron correlation effects in heliumlike ions." In: *Phys. Rev. A* 100, p. 062506.
- Kusch, P. and H. M. Foley (1948). "The Magnetic Moment of the Electron." In: *Phys. Rev.* 74, pp. 250–263.
- Labzowsky, L., G. Klimchitskaya, and Y. Dmitriev (1993). *Relativistic Effects in Spectra of Atomic Systems*. IOP Publishing, Bristol.
- Lamb, W. E. and R. C. Retherford (1947). "Fine Structure of the Hydrogen Atom by a Microwave Method." In: *Phys. Rev.* 72, pp. 241–243.
- Latter, R. (1955). "Atomic Energy Levels for the Thomas-Fermi and Thomas-Fermi-Dirac Potential." In: *Phys. Rev.* 99, p. 510.
- Lee, R. N., A. I. Milstein, I. S. Terekhov, and S. G. Karshenboim (2005). "Virtual light-by-light scattering and the g factor of a bound electron." In: *Phys. Rev. A* 71, p. 052501.
- Lindenfels, D. von, M. Wiesel, D. A. Glazov, A. V. Volotka, M. M. Sokolov, V. M. Shabaev, G. Plunien, W. Quint, G. Birkl, A. Martin, and M. Vogel (2013). "Experimental access to higher-order Zeeman effects by precision spectroscopy of highly charged ions in a Penning trap." In: *Phys. Rev. A* 87, p. 023412.
- Lochmann, M. et al. (2014). "Observation of the hyperfine transition in lithium-like bismuth $^{209}\text{Bi}^{80+}$: Towards a test of QED in strong magnetic fields." In: *Phys. Rev. A* 90, 030501(R).
- Logunov, A. A. and A. N. Tavkhelidze (1962). "QUASIOPTICAL APPROACH IN QUANTUM FIELD THEORY." In: *Nuovo Cim.* 29, p. 380.
- Malyshev, A. V., D. A. Glazov, A. V. Volotka, I. I. Tupitsyn, V. M. Shabaev, G. Plunien, and T. Stöhlker (2017a). "Ground-state ionization energies of boronlike ions." In: *Phys. Rev. A* 96, p. 022512.
- Malyshev, A. V., V. M. Shabaev, D. A. Glazov, and I. I. Tupitsyn (2017b). "Nuclear Recoil Effect on the g-Factor of Heavy Ions: Prospects for Tests of Quantum Electrodynamics in a New Region." In: *Pis'ma Zh. Eksp. Teor. Fiz.* 106, 731 [*JETP Lett.* 106, 765].
- Malyshev, A. V., A. V. Volotka, D. A. Glazov, I. I. Tupitsyn, V. M. Shabaev, and G. Plunien (2014). "QED calculation of the ground-state energy of berylliumlike ions." In: *Phys. Rev. A* 90, p. 062517.
- Mohr, P. J. and J. Sapirstein (2000). "Evaluation of two-photon exchange graphs for excited states of highly charged heliumlike ions." In: *Phys. Rev. A* 62, p. 052501.

- Nefiodov, A. V., G. Plunien, and G. Soff (2002). "Nuclear-Polarization Correction to the Bound-Electron g Factor in Heavy Hydrogenlike Ions." In: *Phys. Rev. Lett.* 89, p. 081802.
- Nörtershäuser, W. et al. (2019). "The hyperfine puzzle of strong-field bound-state QED." In: *Hyperfine Interact.* 240, p. 51.
- Oreshkina, N. S., D. A. Glazov, A. V. Volotka, V. M. Shabaev, I. I. Tupitsyn, and G. Plunien (2008). "Radiative and interelectronic-interaction effects on the hyperfine splitting in highly charged B-like ions." In: *Phys. Lett. A* 372, p. 675.
- Oreshkina, N. S., A. V. Volotka, D. A. Glazov, I. I. Tupitsyn, V. M. Shabaev, and G. Plunien (2007). "Hyperfine structure of lithium-like scandium." In: *Opt. Spektrosk.* 102, 889 [*Opt. Spectrosc.* 102, 815].
- Pachucki, K., A. Czarnecki, U. D. Jentschura, and V. A. Yerokhin (2005a). "Complete two-loop correction to the bound-electron g factor." In: *Phys. Rev. A* 72, p. 022108.
- Pachucki, K., U. D. Jentschura, and V. A. Yerokhin (2005b). "Nonrelativistic QED Approach to the Bound-Electron g Factor." In: *Phys. Rev. Lett.* 93, 150401 (2004); *ibid* 94, 229902.
- Persson, H., S. Salomonson, P. Sunnergren, and I. Lindgren (1997). "Radiative corrections to the electron g -factor in H-like ions." In: *Phys. Rev. A* 56, R2499.
- Peskin, M. E. and D. V. Schroeder (1995). *An Introduction to Quantum Field Theory*. Westview Press.
- Sánchez, R. et al. (2017). "Laser spectroscopy measurement of the $2s$ -hyperfine splitting in lithium-like bismuth." In: *J. Phys. B* 50, p. 085004.
- Sapirstein, J. (1998). "Theoretical methods for the relativistic atomic many-body problem." In: *Rev. Mod. Phys.* 70, p. 55.
- Sapirstein, J. and K. T. Cheng (2001). "Hyperfine splitting in lithiumlike bismuth." In: *Phys. Rev. A* 63, p. 032506.
- Sapirstein, J. and K. T. Cheng (2002). "Calculation of the Lamb shift in neutral alkali metals." In: *Phys. Rev. A* 66, p. 042501.
- Sapirstein, J. and K. T. Cheng (2003). "Calculation of radiative corrections to hyperfine splittings in the neutral alkali metals." In: *Phys. Rev. A* 67, p. 022512.
- Sapirstein, J. and K. T. Cheng (2006). "Calculation of radiative corrections to hyperfine splitting in $p_{1/2}$ states." In: *Phys. Rev. A* 74, p. 042513.
- Sapirstein, J. and K. T. Cheng (2008). "Calculation of radiative corrections to hyperfine splitting in $p_{3/2}$ states." In: *Phys. Rev. A* 78, p. 022515.
- Sapirstein, J. and W. R. Johnson (1996). "The use of basis splines in theoretical atomic physics." In: *J. Phys. B* 29, p. 5213.
- Schweber, S. S. (1961). *An Introduction to Relativistic Quantum Field Theory*. Harper and Row, New York.

- Schwinger, J. (1948a). "On Quantum-Electrodynamics and the Magnetic Moment of the Electron." In: *Phys. Rev.* 73, pp. 416–417.
- Schwinger, J. (1948b). "Quantum Electrodynamics. I. A Covariant Formulation." In: *Phys. Rev.* 74, pp. 1439–1461.
- Schwinger, J. (1949a). "Quantum Electrodynamics. II. Vacuum Polarization and Self-Energy." In: *Phys. Rev.* 75, pp. 651–679.
- Schwinger, J. (1949b). "Quantum Electrodynamics. III. The Electromagnetic Properties of the Electron—Radiative Corrections to Scattering." In: *Phys. Rev.* 76, pp. 790–817.
- Seelig, P. et al. (1998). "Ground state hyperfine splitting of hydrogenlike $^{207}\text{Pb}^{81+}$ by laser excitation of a bunched ion beam in the GSI Experimental Storage Ring." In: *Phys. Rev. Lett.* 81, p. 4824.
- Shabaev, V. M. (1994). "Hyperfine structure of hydrogen-like ions." In: *J. Phys. B* 27, p. 5825.
- Shabaev, V. M. (2002). "Two-time Green's function method in quantum electrodynamics of high-Z few-electron atoms." In: *Phys. Rep.* 356, p. 119.
- Shabaev, V. M., A. N. Artemyev, V. A. Yerokhin, O. M. Zhrebtsov, and G. Soff (2001). "Towards a test of QED in investigations of the hyperfine splitting in heavy ions." In: *Phys. Rev. Lett.* 86, p. 3959.
- Shabaev, V. M., D. A. Glazov, A. V. Malyshev, and I. I. Tupitsyn (2017). "Recoil Effect on the g Factor of Li-Like Ions." In: *Phys. Rev. Lett.* 119, p. 263001.
- Shabaev, V. M., D. A. Glazov, A. V. Malyshev, and I. I. Tupitsyn (2018). "Nuclear recoil effect on the g factor of highly charged Li-like ions." In: *Phys. Rev. A* 98, p. 032512.
- Shabaev, V. M., D. A. Glazov, N. S. Oreshkina, A. V. Volotka, G. Plunien, H.-J. Kluge, and W. Quint (2006). "g-factor of heavy ions: a new access to the fine structure constant." In: *Phys. Rev. Lett.* 96, p. 253002.
- Shabaev, V. M., D. A. Glazov, M. B. Shabaeva, V. A. Yerokhin, G. Plunien, and G. Soff (2002). "g factor of high-Z lithiumlike ions." In: *Phys. Rev. A* 65, p. 062104.
- Shabaev, V. M., M. B. Shabaeva, and I. I. Tupitsyn (1995). "Hyperfine structure of hydrogenlike and lithiumlike atoms." In: *Phys. Rev. A* 52, p. 3686.
- Shabaev, V. M., M. B. Shabaeva, and I. I. Tupitsyn (1997a). "Hyperfine structure of lithium-like ions." In: *Astron. Astrophys. Trans.* 12, p. 243.
- Shabaev, V. M., M. B. Shabaeva, I. I. Tupitsyn, V. A. Yerokhin, A. N. Artemyev, T. Kühl, M. Tomaselli, and O. M. Zhrebtsov (1998). "Transition energy and lifetime for the ground-state hyperfine splitting of high-Z lithiumlike ions." In: *Phys. Rev. A* 57, p. 149.

- Shabaev, V. M., M. Tomaselli, T. Kühl, A. N. Artemyev, and V. A. Yerokhin (1997b). "Ground-state hyperfine splitting of high-Z hydrogenlike ions." In: *Phys. Rev. A* 56, p. 252.
- Shabaev, V. M., I. I. Tupitsyn, V. A. Yerokhin, G. Plunien, and G. Soff (2004). "Dual kinetic balance approach to basis-set expansions for the Dirac equation." In: *Phys. Rev. Lett.* 93, p. 130405.
- Shabaev, V. M. and V. A. Yerokhin (2002). "Recoil correction to the bound-electron g factor in H-like atoms to all orders in αZ ." In: *Phys. Rev. Lett.* 88, p. 091801.
- Sikora, B., V. A. Yerokhin, N. S. Oreshkina, H. Cakir, C. H. Keitel, and Z. Harman (2020). "Theory of the two-loop self-energy correction to the g factor in nonperturbative Coulomb fields." In: *Phys. Rev. Research* 2, p. 012002.
- Skripnikov, L. V., S. Schmidt, J. Ullmann, C. Geppert, F. Kraus, B. Kresse, W. Nörtershäuser, A. F. Privalov, B. Scheibe, V. M. Shabaev, M. Vogel, and A. V. Volotka (2018). "New Nuclear Magnetic Moment of ^{209}Bi : Resolving the Bismuth Hyperfine Puzzle." In: *Phys. Rev. Lett.* 120, p. 093001.
- Soguel, R. N., A. V. Volotka, E. V. Tryapitsyna, D. A. Glazov, V. P. Kosheleva, and S. Fritzsche (2021). "Redefined vacuum approach and gauge-invariant subsets in two-photon-exchange diagrams for a closed-shell system with a valence electron." In: *Phys. Rev. A* 103, p. 042818.
- Sturm, S., F. Köhler, J. Zatorski, A. Wagner, Z. Harman, G. Werth, W. Quint, C. H. Keitel, and K. Blaum (2014). "High-precision measurement of the atomic mass of the electron." In: *Nature* 506, p. 467.
- Sturm, S., A. Wagner, M. Kretschmar, W. Quint, G. Werth, and K. Blaum (2013). " g -factor measurement of hydrogenlike $^{28}\text{Si}^{13+}$ as a challenge to QED calculations." In: *Phys. Rev. A* 87, 030501(R).
- Sturm, S., A. Wagner, B. Schabinger, J. Zatorski, Z. Harman, W. Quint, G. Werth, C. H. Keitel, and K. Blaum (2011). " g factor of hydrogenlike $^{28}\text{Si}^{13+}$." In: *Phys. Rev. Lett.* 107, p. 023002.
- Sucher, J. (1957). "S-Matrix Formalism for Level-Shift Calculations." In: *Phys. Rev.* 107, p. 1448.
- Sucher, J. (1980). "Foundations of the relativistic theory of many-electron atoms." In: *Phys. Rev. A* 22, p. 348.
- Sz-Nagy, B. (1946). "Perturbations des transformations autoadjointes dans l'espace de Hilbert." In: *Commentarii Mathematici Helvetici* 19, 347–366.
- Tomonaga, S. (1946). "On a Relativistically Invariant Formulation of the Quantum Theory of Wave Fields*." In: *Progress of Theoretical Physics* 1, pp. 27–42.
- Tupitsyn, I. I., A. V. Loginov, and V. M. Shabaev (2002). "Calculations of hyperfine splitting constants taking into account the volume distribution of the nuclear

- magnetic moment. I. Computational procedure as applied to hydrogen-like ions." In: *Opt. Spektrosk.* **93**, 389 [*Opt. Spectrosc.* **93**, 357].
- Ullmann, J. et al. (2015). "An improved value for the hyperfine splitting of hydrogen-like $^{209}\text{Bi}^{82+}$." In: *J. Phys. B* **48**, p. 144022.
- Ullmann, J. et al. (2017). "High precision hyperfine measurements in Bismuth challenge bound-state strong-field QED." In: *Nat. Commun.* **8**, p. 15484.
- Volotka, A. V., D. A. Glazov, O. V. Andreev, V. M. Shabaev, I. I. Tupitsyn, and G. Plunien (2012). "Test of many-electron QED effects in the hyperfine splitting of heavy high-Z ions." In: *Phys. Rev. Lett.* **108**, p. 073001.
- Volotka, A. V., D. A. Glazov, V. M. Shabaev, I. I. Tupitsyn, and G. Plunien (2009). "Screened QED corrections in lithiumlike heavy ions in the presence of magnetic fields." In: *Phys. Rev. Lett.* **103**, p. 033005.
- Volotka, A. V., D. A. Glazov, V. M. Shabaev, I. I. Tupitsyn, and G. Plunien (2014). "Many-electron QED corrections to the g factor of lithiumlike ions." In: *Phys. Rev. Lett.* **112**, p. 253004.
- Volotka, A. V., D. A. Glazov, I. I. Tupitsyn, N. S. Oreshkina, G. Plunien, and V. M. Shabaev (2008). "Ground-state hyperfine structure of H-, Li-, and B-like ions in the intermediate-Z region." In: *Phys. Rev. A* **78**, p. 062507.
- Volotka, A. V. and G. Plunien (2014). "Nuclear polarization study: New frontiers for tests of QED in heavy highly charged ions." In: *Phys. Rev. Lett.* **113**, p. 023002.
- Wagner, A., S. Sturm, F. Köhler, D. A. Glazov, A. V. Volotka, G. Plunien, W. Quint, G. Werth, V. M. Shabaev, and K. Blaum (2013). "g factor of lithiumlike silicon $^{28}\text{Si}^{11+}$." In: *Phys. Rev. Lett.* **110**, p. 033003.
- Weinberg, S. (2005). *The Quantum theory of fields. Vol. 1: Foundations*. Cambridge University Press.
- Wick, G. (1950). "The Evaluation of the Collision Matrix." In: *Phys. Rev.* **80**, p. 268.
- Yerokhin, V. A. (2008). "Hyperfine structure of S states in Li and Be^+ ." In: *Phys. Rev. A* **77**, p. 020501.
- Yerokhin, V. A., A. N. Artemyev, T. Beier, V. M. Shabaev, and G. Soff (1998). "Direct evaluation of the two-electron self-energy corrections to the ground state energy of lithium-like ions." In: *J. Phys. B* **31**, p. L691.
- Yerokhin, V. A., E. Berseneva, Z. Harman, I. I. Tupitsyn, and C. H. Keitel (2016). "Weighted difference of g factors of light Li-like and H-like ions for an improved determination of the fine-structure constant." In: *Phys. Rev. A* **94**, p. 022502.
- Yerokhin, V. A. and Z. Harman (2013). "Two-loop QED corrections with closed fermion loops for the bound-electron g factor." In: *Phys. Rev. A* **88**, p. 042502.
- Yerokhin, V. A. and Z. Harman (2017). "One-loop electron self-energy for the bound-electron g factor." In: *Phys. Rev. A* **95** (6), 060501(R).

- Yerokhin, V. A., P. Indelicato, and V. M. Shabaev (2002). "Self-Energy Correction to the Bound-Electron g Factor in H-like Ions." In: *Phys. Rev. Lett.* 89, p. 143001.
- Yerokhin, V. A., P. Indelicato, and V. M. Shabaev (2004). "Evaluation of the self-energy correction to the g factor of S states in H-like ions." In: *Phys. Rev. A* 69, p. 052503.
- Yerokhin, V. A., C. H. Keitel, and Z. Harman (2021). "Two-photon-exchange corrections to the g factor of Li-like ions." In: *Phys. Rev. A* 104, p. 022814.
- Yerokhin, V. A., K. Pachucki, M. Puchalski, Z. Harman, and C. H. Keitel (2017). "Electron-correlation effects in the g factor of light Li-like ions." In: *Phys. Rev. A* 95 (6), p. 062511.
- Yerokhin, V. A., K. Pachucki, M. Puchalski, C. H. Keitel, and Z. Harman (2020). "Self-energy screening effects in the g factor of Li-like ions." In: *Phys. Rev. A* 102, p. 022815.
- Zatorski, J., B. Sikora, S. G. Karshenboim, S. Sturm, F. Köhler-Langes, K. Blaum, C. H. Keitel, and Z. Harman (2017). "Extraction of the electron mass from g -factor measurements on light hydrogenlike ions." In: *Phys. Rev. A* 96 (1), p. 012502.
- Zherebtsov, O. M. and V. M. Shabaev (2000). "Higher order interelectronic-interaction corrections to the ground-state hyperfine splitting in lithiumlike ions." In: *Can. J. Phys.* 78, p. 701.

APPENDIX

In Appendix we provide the expressions for the two-photon exchange correction $X_a^{(2)}$ to the hyperfine splitting of lithiumlike ions, see Eq. (4.31). We note that via changing the multiplicative factor G_a to $-\frac{2}{eBm_a}$ and T_z to V^{magn} , in formulas given below, one can get the corresponding contributions for the case of bound-electron g factor

$$X_a^{(2)} \xrightarrow[\substack{T_z \rightarrow V^{\text{magn}} \\ G_a \rightarrow -\frac{2}{eBm_a}}]{\longrightarrow} \Delta g_{\text{int}}^{(2)}. \quad (7.1)$$

Here operator T_z is z component of operator \mathbf{T} (4.2), V^{magn} is defined by Eq. (5.1), and G_a is given by Eq. (4.9).

7.1 THREE-ELECTRON CONTRIBUTION $X_{3\text{el}}^{(2)}$

The irreducible parts of the three-electron contribution $X_{3\text{el}}^{(2)}$, see Fig. 4.2 is given by the following expression

$$X_{3\text{el}}^{(2)} = X_{3\text{el},A}^{(2)} + X_{3\text{el},B}^{(2)} + X_{3\text{el},C}^{(2)} + X_{3\text{el},D}^{(2)}, \quad (7.2)$$

where

$$\begin{aligned} X_{3\text{el},A}^{(2)} = & 2G_a \sum_{b_1, b_2} \sum_{P, Q} (-1)^{P+Q} \sum_n' \left\{ \frac{\langle PaPb_2 | I(\Delta_{Pa a}) | \xi_a n \rangle \langle nb_1 | I(\Delta_{b_1 Q b_1}) | Qb_2 Qb_1 \rangle}{\varepsilon_{b_2} - \varepsilon_n} \right. \\ & + \frac{\langle Pb_2 Pa | I(\Delta_{Pb_2 b_2}) | \xi_{b_2} n \rangle \langle nb_1 | I(\Delta_{b_1 Q b_1}) | Qa Qb_1 \rangle}{\varepsilon_a - \varepsilon_n} \\ & + \frac{\langle Pb_2 Pb_1 | I(\Delta_{Pb_2 b_2}) | \xi_{b_2} n \rangle \langle na | I(\Delta_{a Q a}) | Qb_1 Qa \rangle}{\varepsilon_{b_1} - \varepsilon_n} \\ & \left. + \frac{\langle Pa Pb_1 | I(\Delta_{Pa b_2}) | \xi_{b_2} n \rangle \langle nb_2 | I(\Delta_{b_2 Q b_1}) | Qa Qb_1 \rangle}{\varepsilon_a + \varepsilon_{b_1} - \varepsilon_{b_2} - \varepsilon_n} \right\} \end{aligned}$$

$$+ \frac{1}{2} \left\langle \frac{\langle \text{Pb}_2 \text{Pb}_1 | I(\Delta_{\text{Pb}_2 \text{a}}) | \xi_{\text{a}} \mathbf{n} \rangle \langle \mathbf{n} \mathbf{a} | I(\Delta_{\text{a} \text{Qb}_1}) | \text{Qb}_2 \text{Qb}_1 \rangle}{\varepsilon_{\text{b}_1} + \varepsilon_{\text{b}_2} - \varepsilon_{\text{a}} - \varepsilon_{\text{n}}} \right\rangle, \quad (7.3)$$

$$\begin{aligned} X_{3\text{el},\text{B}}^{(2)} &= 2G_{\text{a}} \sum_{\text{b}_1, \text{b}_2} \sum_{\text{P}, \text{Q}} (-1)^{\text{P}+\text{Q}} \sum_{\mathbf{n}} \left\{ \frac{\langle \xi_{\text{Pa}} \text{Pb}_2 | I(\Delta_{\text{Pa a}}) | \mathbf{a} \mathbf{n} \rangle \langle \mathbf{n} \mathbf{b}_1 | I(\Delta_{\text{b}_1 \text{Qb}_1}) | \text{Qb}_2 \text{Qb}_1 \rangle}{\varepsilon_{\text{b}_2} - \varepsilon_{\text{n}}} \right. \\ &+ \frac{\langle \xi_{\text{Pb}_2} \text{Pa} | I(\Delta_{\text{Pb}_2 \text{b}_2}) | \mathbf{b}_2 \mathbf{n} \rangle \langle \mathbf{n} \mathbf{b}_1 | I(\Delta_{\text{b}_1 \text{Qb}_1}) | \text{Qa} \text{Qb}_1 \rangle}{\varepsilon_{\text{a}} - \varepsilon_{\text{n}}} \\ &+ \frac{\langle \xi_{\text{Pb}_2} \text{Pb}_1 | I(\Delta_{\text{Pb}_2 \text{b}_2}) | \mathbf{b}_2 \mathbf{n} \rangle \langle \mathbf{n} \mathbf{a} | I(\Delta_{\text{a} \text{Qa}}) | \text{Qb}_1 \text{Qa} \rangle}{\varepsilon_{\text{b}_1} - \varepsilon_{\text{n}}} \\ &+ \frac{\langle \xi_{\text{Pa}} \text{Pb}_1 | I(\Delta_{\text{Pa b}_2}) | \mathbf{b}_2 \mathbf{n} \rangle \langle \mathbf{n} \mathbf{b}_2 | I(\Delta_{\text{b}_2 \text{Qb}_1}) | \text{Qa} \text{Qb}_1 \rangle}{\varepsilon_{\text{a}} + \varepsilon_{\text{b}_1} - \varepsilon_{\text{b}_2} - \varepsilon_{\text{n}}} \\ &\left. + \frac{1}{2} \left\langle \frac{\langle \xi_{\text{Pb}_2} \text{Pb}_1 | I(\Delta_{\text{Pb}_2 \text{a}}) | \mathbf{a} \mathbf{n} \rangle \langle \mathbf{n} \mathbf{a} | I(\Delta_{\text{a} \text{Qb}_1}) | \text{Qb}_2 \text{Qb}_1 \rangle}{\varepsilon_{\text{b}_1} + \varepsilon_{\text{b}_2} - \varepsilon_{\text{a}} - \varepsilon_{\text{n}}} \right\rangle \right\}, \quad (7.4) \end{aligned}$$

$$\begin{aligned} X_{3\text{el},\text{C}}^{(2)} &= G_{\text{a}} \sum_{\text{b}_1, \text{b}_2} \sum_{\text{P}, \text{Q}} (-1)^{\text{P}+\text{Q}} \sum_{\mathbf{n}_1, \mathbf{n}_2} \left\{ \right. \\ &\left\{ \frac{\langle \text{Pb}_2 \text{Pa} | I(\Delta_{\text{Pb}_2 \text{b}_2}) | \mathbf{b}_2 \mathbf{n}_1 \rangle \langle \mathbf{n}_1 | \text{V}^{\text{magn}} | \mathbf{n}_2 \rangle \langle \mathbf{n}_2 \mathbf{b}_1 | I(\Delta_{\text{b}_1 \text{Qb}_1}) | \text{Qa} \text{Qb}_1 \rangle}{(\varepsilon_{\text{a}} - \varepsilon_{\mathbf{n}_1})(\varepsilon_{\text{a}} - \varepsilon_{\mathbf{n}_2})} \right. \\ &+ 2 \frac{\langle \text{Pb}_2 \text{Pb}_1 | I(\Delta_{\text{Pb}_2 \text{b}_2}) | \mathbf{b}_2 \mathbf{n}_1 \rangle \langle \mathbf{n}_1 | \text{V}^{\text{magn}} | \mathbf{n}_2 \rangle \langle \mathbf{n}_2 \mathbf{a} | I(\Delta_{\text{a} \text{Qa}}) | \text{Qb}_1 \text{Qa} \rangle}{(\varepsilon_{\text{b}_1} - \varepsilon_{\mathbf{n}_1})(\varepsilon_{\text{b}_1} - \varepsilon_{\mathbf{n}_2})} \\ &+ \frac{\langle \text{Pa} \text{Pb}_1 | I(\Delta_{\text{Pa b}_2}) | \mathbf{b}_2 \mathbf{n}_1 \rangle \langle \mathbf{n}_1 | \text{V}^{\text{magn}} | \mathbf{n}_2 \rangle \langle \mathbf{n}_2 \mathbf{b}_2 | I(\Delta_{\text{b}_2 \text{Qb}_1}) | \text{Qa} \text{Qb}_1 \rangle}{(\varepsilon_{\text{a}} + \varepsilon_{\text{b}_1} - \varepsilon_{\text{b}_2} - \varepsilon_{\mathbf{n}_1})(\varepsilon_{\text{a}} + \varepsilon_{\text{b}_1} - \varepsilon_{\text{b}_2} - \varepsilon_{\mathbf{n}_2})} \\ &\left. + \frac{1}{2} \left\langle \frac{\langle \text{Pb}_2 \text{Pb}_1 | I(\Delta_{\text{Pb}_2 \text{a}}) | \mathbf{a} \mathbf{n}_1 \rangle \langle \mathbf{n}_1 | \text{V}^{\text{magn}} | \mathbf{n}_2 \rangle \langle \mathbf{n}_2 \mathbf{a} | I(\Delta_{\text{a} \text{Qb}_1}) | \text{Qb}_2 \text{Qb}_1 \rangle}{(\varepsilon_{\text{b}_1} + \varepsilon_{\text{b}_2} - \varepsilon_{\text{a}} - \varepsilon_{\mathbf{n}_1})(\varepsilon_{\text{b}_1} + \varepsilon_{\text{b}_2} - \varepsilon_{\text{a}} - \varepsilon_{\mathbf{n}_2})} \right\rangle \right\}, \quad (7.5) \end{aligned}$$

$$\begin{aligned} X_{3\text{el},\text{D}}^{(2)} &= 2G_{\text{a}} \sum_{\text{b}_1, \text{b}_2} \sum_{\text{P}, \text{Q}} (-1)^{\text{P}+\text{Q}} \sum_{\mathbf{n}} \left\{ \frac{\langle \text{Pa} \xi_{\text{Pb}_2} | I(\Delta_{\text{Pa a}}) | \mathbf{a} \mathbf{n} \rangle \langle \mathbf{n} \mathbf{b}_1 | I(\Delta_{\text{b}_1 \text{Qb}_1}) | \text{Qb}_2 \text{Qb}_1 \rangle}{\varepsilon_{\text{b}_2} - \varepsilon_{\text{n}}} \right. \\ &+ \frac{\langle \text{Pb}_2 \xi_{\text{Pa}} | I(\Delta_{\text{Pb}_2 \text{b}_2}) | \mathbf{b}_2 \mathbf{n} \rangle \langle \mathbf{n} \mathbf{b}_1 | I(\Delta_{\text{b}_1 \text{Qb}_1}) | \text{Qa} \text{Qb}_1 \rangle}{\varepsilon_{\text{a}} - \varepsilon_{\text{n}}} \\ &+ \frac{\langle \text{Pb}_2 \xi_{\text{Pb}_1} | I(\Delta_{\text{Pb}_2 \text{b}_2}) | \mathbf{b}_2 \mathbf{n} \rangle \langle \mathbf{n} \mathbf{a} | I(\Delta_{\text{a} \text{Qa}}) | \text{Qb}_1 \text{Qa} \rangle}{\varepsilon_{\text{b}_1} - \varepsilon_{\text{n}}} \\ &+ \frac{\langle \text{Pa} \xi_{\text{Pb}_1} | I(\Delta_{\text{Pa b}_2}) | \mathbf{b}_2 \mathbf{n} \rangle \langle \mathbf{n} \mathbf{b}_2 | I(\Delta_{\text{b}_2 \text{Qb}_1}) | \text{Qa} \text{Qb}_1 \rangle}{\varepsilon_{\text{a}} + \varepsilon_{\text{b}_1} - \varepsilon_{\text{b}_2} - \varepsilon_{\text{n}}} \\ &\left. + \frac{1}{2} \left\langle \frac{\langle \text{Pb}_2 \xi_{\text{Pb}_1} | I(\Delta_{\text{Pb}_2 \text{a}}) | \mathbf{a} \mathbf{n} \rangle \langle \mathbf{n} \mathbf{a} | I(\Delta_{\text{a} \text{Qb}_1}) | \text{Qb}_2 \text{Qb}_1 \rangle}{\varepsilon_{\text{b}_1} + \varepsilon_{\text{b}_2} - \varepsilon_{\text{a}} - \varepsilon_{\text{n}}} \right\rangle \right\}. \quad (7.6) \end{aligned}$$

Hereinafter, the prime over the sum means that terms with vanishing denominators should be omitted in the summation. Notation $\Delta_{n_1 n_2} = \varepsilon_{n_1} - \varepsilon_{n_2}$, ε_n denotes one-electron energies, b denotes the $1s$ state, and the sum over b takes into account two possible projections $m_b = \pm 1/2$ of total angular momentum j_b , a refers to the valence-electron $2s$ state. The interelectronic-interaction operator $I(\omega)$ is given by Eq. (2.21), P and Q are permutation operators, giving rise to the sign $(-1)^P$ and $(-1)^Q$, respectively. The modified wave function $|\xi\rangle$ is defined by

$$|\xi_a\rangle = \sum_n^{\varepsilon_n \neq \varepsilon_a} \frac{|n\rangle \langle n | T_Z | a\rangle}{\varepsilon_a - \varepsilon_n}. \quad (7.7)$$

7.2 TWO-ELECTRON CONTRIBUTION $X_{2\text{el}}^{(2)}$

The irreducible parts of the two-electron diagrams depicted in Fig. 4.3 yield

$$X_{2\text{el}}^{(2)} = X_{2\text{el},\text{lad-W}}^{(2)} + X_{2\text{el},\text{cr-W}}^{(2)} + X_{2\text{el},\text{lad-S}}^{(2)} + X_{2\text{el},\text{cr-S}'}^{(2)} \quad (7.8)$$

where

$$\begin{aligned} X_{2\text{el},\text{lad-W}}^{(2)} &= G_a \sum_b \sum_{P,Q} (-1)^{P+Q} \frac{i}{\pi} \int_{-\infty}^{\infty} d\omega \\ &\times \sum_{n_1, n_2} ' \frac{\langle PaPb | I(\omega) | n_1 n_2 \rangle \langle n_1 n_2 | I(\omega + \Delta_{PaQa}) | \xi_{Qa} Qb \rangle}{(\varepsilon_{Pa} + \omega - u\varepsilon_{n_1})(\varepsilon_{Qb} - \omega - \Delta_{PaQa} - u\varepsilon_{n_2})}, \end{aligned} \quad (7.9)$$

$$\begin{aligned} X_{2\text{el},\text{cr-W}}^{(2)} &= G_a \sum_b \sum_{P,Q} (-1)^{P+Q} \frac{i}{\pi} \int_{-\infty}^{\infty} d\omega \\ &\times \sum_{n_1, n_2} ' \frac{\langle Pan_2 | I(\omega) | n_1 Qb \rangle \langle \xi_{Pb} n_1 | I(\omega - \Delta_{PaQa}) | n_2 Qa \rangle}{(\varepsilon_{Pa} - \omega - u\varepsilon_{n_1})(\varepsilon_{Qb} - \omega - u\varepsilon_{n_2})}, \end{aligned} \quad (7.10)$$

$$\begin{aligned} X_{2\text{el},\text{lad-S}}^{(2)} &= G_a \sum_b \sum_{P,Q} (-1)^{P+Q} \frac{i}{2\pi} \int_{-\infty}^{\infty} d\omega \sum_{n_1, n_2, n_3} ' \frac{i}{2\pi} \\ &\times [\langle PaPb | I(\omega) | n_1 n_2 \rangle \langle n_2 | T_Z | n_3 \rangle \langle n_1 n_3 | I(\omega + \Delta_{PaQa}) | Qa Qb \rangle] \\ &\times [(\varepsilon_{Pa} + \omega - u\varepsilon_{n_1})(\varepsilon_{Qb} - \omega - \Delta_{PaQa} - u\varepsilon_{n_2}) \\ &\times (\varepsilon_{Qb} - \omega - \Delta_{PaQa} - u\varepsilon_{n_3})]^{-1}, \end{aligned} \quad (7.11)$$

$$\begin{aligned}
\chi_{2\text{el,cr-S}}^{(2)} &= G_a \sum_b \sum_{P,Q} (-1)^{P+Q} \int d\omega \sum_{n_1, n_2, n_3} ' \frac{i}{2\pi} \\
&\times \frac{\langle P a n_2 | I(\omega) | n_1 Q b \rangle \langle n_3 | T_z | n_2 \rangle \langle P b n_1 | I(\omega - \Delta_{PaQa}) | n_3 Q a \rangle}{(\varepsilon_{Pa} - \omega - u\varepsilon_{n_1})(\varepsilon_{Qb} - \omega - u\varepsilon_{n_2})(\varepsilon_{Qb} - \omega - u\varepsilon_{n_3})}, \quad (7.12)
\end{aligned}$$

where the prime on the sums indicates that in the summation we omit the reducible and infrared-divergent terms, namely, those with $\varepsilon_{n_1} + \varepsilon_{n_2} = \varepsilon_a + \varepsilon_b$ in the ladder-W diagrams, with $\varepsilon_{n_1} = \varepsilon_{Pa}$, $\varepsilon_{n_2} = \varepsilon_{Qb}$ in the direct parts of the cross-W diagrams, with $\varepsilon_{n_1} = \varepsilon_{n_2} = \varepsilon_a, \varepsilon_b$ in the exchange parts of the cross-W diagrams, with $\varepsilon_{n_1} + \varepsilon_{n_2} = \varepsilon_a + \varepsilon_b$ and $\varepsilon_{n_1} + \varepsilon_{n_3} = \varepsilon_a + \varepsilon_b$ and $\varepsilon_{n_2} = \varepsilon_{n_3} = \varepsilon_{Qb} - \Delta_{PaQa}$ in the ladder-S diagrams, with $\varepsilon_{n_1} = \varepsilon_{Pa}$, $\varepsilon_{n_2} = \varepsilon_{Qb}$ and $\varepsilon_{n_1} = \varepsilon_{Pa}$, $\varepsilon_{n_3} = \varepsilon_{Qb}$ and $\varepsilon_{n_2} = \varepsilon_{n_3} = \varepsilon_{Qb}$ in the direct parts of the cross-S diagrams, with $\varepsilon_{n_1} = \varepsilon_{n_2} = \varepsilon_a, \varepsilon_b$ and $\varepsilon_{n_1} = \varepsilon_{n_3} = \varepsilon_a, \varepsilon_b$ and $\varepsilon_{n_2} = \varepsilon_{n_3} = \varepsilon_a, \varepsilon_b$ in the exchange parts of the cross-S diagrams. Here, $u = 1 - i\delta$, $\delta > 0$ keeps the electron propagators' poles properly treated.

7.3 REDUCIBLE CONTRIBUTION $\chi_{\text{RED}}^{(2)}$

In turn, the reducible parts of the two-electron diagrams are given by the following expression

$$\chi_{\text{red}}^{(2)} = \chi_{\text{red, E}}^{(2)} + \chi_{\text{red, F}}^{(2)} + \chi_{\text{red, G}}^{(2)} + \chi_{\text{red, 2-el}}^{(2)}, \quad (7.13)$$

where

$$\begin{aligned}
\chi_{\text{red, E}}^{(2)} &= G_a \sum_{a_1} \langle a_1 | T_z | a \rangle \sum_{b_1, b_2} \sum_P (-1)^P \sum_n ' \left\{ - \frac{\langle b_1 a | I(0) | b_1 n \rangle \langle n b_2 | I(\Delta_{b_2 P b_2}) | P a_1 P b_2 \rangle}{(\varepsilon_a - \varepsilon_n)^2} \right. \\
&+ \frac{\langle a b_1 | I(\Delta_1) | b_1 n \rangle \langle n b_2 | I(\Delta_{b_2 P b_2}) | P a_1 P b_2 \rangle}{(\varepsilon_a - \varepsilon_n)^2} - 2 \frac{\langle a b_1 | I'(\Delta_1) | b_1 n \rangle \langle n b_2 | I(\Delta_{b_2 P b_2}) | P a_1 P b_2 \rangle}{\varepsilon_a - \varepsilon_n} \\
&- 2 \frac{\langle b_2 a | I'(\Delta_2) | a_1 n \rangle \langle n b_1 | I(\Delta_{b_1 P b_1}) | P b_2 P b_1 \rangle}{\varepsilon_{b_2} - \varepsilon_n} + \frac{\langle b_1 b_2 | I(\Delta_1) | a_1 n \rangle \langle n a | I(\Delta_{a P b_2}) | P b_1 P b_2 \rangle}{(\varepsilon_{b_1} + \varepsilon_{b_2} - \varepsilon_a - \varepsilon_n)^2} \\
&+ 2 \frac{\langle b_1 b_2 | I'(\Delta_1) | a_1 n \rangle \langle n a | I(\Delta_{a P b_2}) | P b_1 P b_2 \rangle}{\varepsilon_{b_1} + \varepsilon_{b_2} - \varepsilon_a - \varepsilon_n} + \frac{\langle b_1 a | I(\Delta_{21}) | b_2 n \rangle \langle n b_2 | I(\Delta_{b_2 P b_1}) | P a_1 P b_1 \rangle}{(\varepsilon_a + \varepsilon_{b_1} - \varepsilon_{b_2} - \varepsilon_n)^2} \\
&- \frac{\langle a b_1 | I(\Delta_2) | b_2 n \rangle \langle n b_2 | I(\Delta_{b_2 P b_1}) | P a_1 P b_1 \rangle}{(\varepsilon_a + \varepsilon_{b_1} - \varepsilon_{b_2} - \varepsilon_n)^2} + 2 \frac{\langle a b_1 | I'(\Delta_2) | b_2 n \rangle \langle n b_2 | I(\Delta_{b_2 P b_1}) | P a_1 P b_1 \rangle}{\varepsilon_a + \varepsilon_{b_1} - \varepsilon_{b_2} - \varepsilon_n} \left. \right\} \\
&+ G_a \sum_{b_1, b_2, b_3} \langle b_2 | T_z | b_3 \rangle \sum_P (-1)^P \sum_n ' \left\{ - 2 \frac{\langle b_1 b_3 | I(0) | b_1 n \rangle \langle n a | I(\Delta_{a P a}) | P b_2 P a \rangle}{(\varepsilon_{b_2} - \varepsilon_n)^2} \right. \\
&+ 2 \frac{\langle b_3 b_1 | I(\Delta_{21}) | b_1 n \rangle \langle n a | I(\Delta_{a P a}) | P b_2 P a \rangle}{(\varepsilon_{b_2} - \varepsilon_n)^2} + 2 \frac{\langle b_3 a | I'(\Delta_2) | a n \rangle \langle n b_1 | I(\Delta_{b_1 P b_1}) | P b_2 P b_1 \rangle}{\varepsilon_{b_2} - \varepsilon_n}
\end{aligned}$$

$$\begin{aligned}
& + 2 \frac{\langle ab_3 | I'(\Delta_2) | b_2 n \rangle \langle n b_1 | I(\Delta_{b_1 P b_1}) | P a P b_1 \rangle}{\varepsilon_a - \varepsilon_n} - \frac{\langle b_1 b_3 | I(\Delta_1) | a n \rangle \langle n a | I(\Delta_{a P b_2}) | P b_1 P b_2 \rangle}{(\varepsilon_{b_1} + \varepsilon_{b_2} - \varepsilon_a - \varepsilon_n)^2} \\
& + \frac{\langle b_3 b_1 | I(\Delta_2) | a n \rangle \langle n a | I(\Delta_{a P b_2}) | P b_1 P b_2 \rangle}{(\varepsilon_{b_1} + \varepsilon_{b_2} - \varepsilon_a - \varepsilon_n)^2} + 2 \frac{\langle b_3 b_1 | I'(\Delta_2) | a n \rangle \langle n a | I(\Delta_{a P b_2}) | P b_1 P b_2 \rangle}{\varepsilon_{b_1} + \varepsilon_{b_2} - \varepsilon_a - \varepsilon_n} \\
& + \frac{\langle b_3 a | I(\Delta_{21}) | b_1 n \rangle \langle n b_1 | I(\Delta_{b_1 P b_2}) | P a P b_2 \rangle}{(\varepsilon_a + \varepsilon_{b_2} - \varepsilon_{b_1} - \varepsilon_n)^2} - \frac{\langle a b_3 | I(\Delta_1) | b_1 n \rangle \langle n b_1 | I(\Delta_{b_1 P b_2}) | P a P b_2 \rangle}{(\varepsilon_a + \varepsilon_{b_2} - \varepsilon_{b_1} - \varepsilon_n)^2} \\
& - \frac{\langle b_1 a | I(\Delta_{21}) | b_2 n \rangle \langle n b_3 | I(\Delta_{b_2 P b_1}) | P a P b_1 \rangle}{(\varepsilon_a + \varepsilon_{b_1} - \varepsilon_{b_2} - \varepsilon_n)^2} + \frac{\langle a b_1 | I(\Delta_2) | b_2 n \rangle \langle n b_3 | I(\Delta_{b_2 P b_1}) | P a P b_1 \rangle}{(\varepsilon_a + \varepsilon_{b_1} - \varepsilon_{b_2} - \varepsilon_n)^2} \\
& - 2 \frac{\langle a b_1 | I'(\Delta_2) | b_2 n \rangle \langle n b_3 | I(\Delta_{b_2 P b_1}) | P a P b_1 \rangle}{\varepsilon_a + \varepsilon_{b_1} - \varepsilon_{b_2} - \varepsilon_n} \Bigg\}. \tag{7.14}
\end{aligned}$$

Hereinafter a_1 denotes the $2s$ state, the sum over a_1 takes into account two possible projections $m_{a_1} = \pm 1/2$ of total angular momentum $j_{a_1} = j_a$. Similarly, b_1 , b_2 , and b_3 denote $1s$ state, the sum over b_1 , b_2 , and b_3 takes into account two possible projections of total angular momentum $j_{b_1} = j_{b_2} = j_{b_3} = j_b$, $m_{b_1} = \pm 1/2$, $m_{b_2} = \pm 1/2$, and $m_{b_3} = \pm 1/2$, respectively.

$$\begin{aligned}
X_{\text{red, F}}^{(2)} = & G_a \sum_{a_1} \sum_{b_1, b_2} \left\{ -2\langle \xi_a b_1 | I'(\Delta) | b_2 a_1 \rangle \langle a_1 b_2 | I(\Delta) | b_1 a \rangle - 2\langle a \xi_{b_1} | I'(\Delta) | b_2 a_1 \rangle \langle a_1 b_2 | I(\Delta) | b_1 a \rangle \right. \\
& - 2\langle a_1 \xi'_{b_2} | I(\Delta) | b_1 a \rangle \langle a b_1 | I(\Delta) | b_1 a \rangle + \sum_P (-1)^P \left[-2\langle b_2 \xi'_a | I(0) | b_2 a_1 \rangle \langle a_1 b_1 | I(\Delta_{b_1 P b_1}) | P a P b_1 \rangle \right. \\
& + 2\langle \xi'_a b_2 | I(\Delta_2) | b_2 a_1 \rangle \langle a_1 b_1 | I(\Delta_{b_1 P b_1}) | P a P b_1 \rangle - 2\langle \xi_a b_2 | I'(\Delta_2) | b_2 a_1 \rangle \langle a_1 b_1 | I(\Delta_{b_1 P b_1}) | P a P b_1 \rangle \\
& \left. - 2\langle a \xi_{b_2} | I'(\Delta_2) | b_2 a_1 \rangle \langle a_1 b_1 | I(\Delta_{b_1 P b_1}) | P a P b_1 \rangle + 2\langle a b_1 | I'(\Delta) | \xi_{b_2} a_1 \rangle \langle a b_2 | I(\Delta_{b_2 P b_1}) | P a P b_1 \rangle \right] \\
& + \left[-2\langle b_2 \xi_a | I(0) | b_2 a_1 \rangle + 2\langle \xi_a b_2 | I(\Delta_2) | b_2 a_1 \rangle + 2\langle a \xi_{b_2} | I(\Delta_2) | b_2 a_1 \rangle - 2\langle \xi_{b_2} a | I(0) | b_2 a_1 \rangle \right] \\
& \times \langle a_1 b_1 | I'(\Delta_1) | b_1 a \rangle \left. \right\} + G_a \sum_{b_1, b_2, b_3} \left\{ -2\langle b_2 \xi'_{b_1} | I(0) | b_2 b_3 \rangle \langle b_3 a | I(\Delta_{a P a}) | P b_1 P a \rangle \right. \\
& + 2\langle \xi'_{b_1} b_2 | I(\Delta_{21}) | b_2 b_3 \rangle \langle b_3 a | I(\Delta_{a P a}) | P b_1 P a \rangle \\
& + \left[2\langle b_2 \xi_{b_1} | I(0) | b_2 b_3 \rangle - 2\langle \xi_{b_1} b_2 | I(\Delta_{21}) | b_2 b_3 \rangle + 2\langle \xi_{b_2} b_1 | I(0) | b_2 b_3 \rangle \right. \\
& \left. - 2\langle b_1 \xi_{b_2} | I(\Delta_{21}) | b_2 b_3 \rangle \right] \langle b_3 a | I'(\Delta_1) | a b_1 \rangle + \sum_P (-1)^P \left[2\langle b_2 \xi_a | I'(\Delta_2) | a b_3 \rangle \right. \\
& \left. - 2\langle a \xi'_{b_2} | I(0) | a b_3 \rangle + 2\langle \xi'_{b_2} a | I(\Delta_2) | a b_3 \rangle + 2\langle \xi_{b_2} a | I'(\Delta_2) | a b_3 \rangle \right] \langle b_3 b_1 | I(\Delta_{b_1 P b_1}) | P b_2 P b_1 \rangle \left. \right\} \\
& + G_a \sum_{a_1, a_2} \sum_{b_1, b_2} \left\{ 2\langle b_1 \xi_a | I(0) | b_2 a_1 \rangle - 2\langle \xi_a b_1 | I(\Delta) | b_2 a_1 \rangle - 2\langle a b_1 | I(\Delta) | \xi_{b_2} a_1 \rangle \right. \\
& \left. - 2\langle a \xi_{b_1} | I(\Delta) | b_2 a_1 \rangle \right\} \langle a_1 b_2 | I'(\Delta) | b_1 a_2 \rangle \\
& + G_a \sum_{a_1} \sum_{b_1, b_2} \sum'_n -2 \frac{\langle b_1 a | I(0) | b_2 n \rangle \langle n | T_z | a_1 \rangle \langle a_1 b_2 | I(\Delta) | b_1 a \rangle}{(\varepsilon_a - \varepsilon_n)^2} \\
& + G_a \sum_{a_1} \sum_{b_1, b_2} \sum_P (-1)^P \sum'_n \left\{ -2 \frac{\langle a b_1 | I(\Delta) | b_2 n \rangle \langle n | T_z | a_1 \rangle \langle a_1 b_2 | I(\Delta_{a P a}) | P a P b_1 \rangle}{(\varepsilon_a - \varepsilon_n)^2} \right. \\
& + 2 \frac{\langle a b_1 | I'(\Delta) | b_2 n \rangle \langle n | T_z | a_1 \rangle \langle a_1 b_2 | I(\Delta_{a P a}) | P a P b_1 \rangle}{\varepsilon_a - \varepsilon_n} \\
& \left. + 2 \frac{\langle a b_1 | I'(\Delta) | b_2 a_1 \rangle \langle a_1 | T_z | n \rangle \langle n b_2 | I(\Delta_{b_2 P b_1}) | P a P b_1 \rangle}{\varepsilon_a - \varepsilon_n} \right\}, \tag{7.15}
\end{aligned}$$

where

$$I''(\omega) = d^2 I(\omega) / d\omega^2, \quad |\xi_a\rangle = \sum_n \frac{|n\rangle \langle n | T_z | a \rangle}{\varepsilon_a - \varepsilon_n}, \quad |\xi'_a\rangle = \frac{\partial}{\partial \varepsilon_a} |\xi_a\rangle. \tag{7.16}$$

$$\begin{aligned}
X_{\text{red}, G}^{(2)} = & \frac{1}{2} G_a \sum_{a_1} \sum_{b_1, b_2} \left\{ \langle b_2 | T_z | b_2 \rangle \langle a b_1 | I''(\Delta) | b_2 a_1 \rangle \langle a_1 b_2 | I(\Delta) | b_1 a \rangle \right. \\
& + 2 \langle b_2 | T_z | b_2 \rangle \langle a b_1 | I'(\Delta) | b_2 a_1 \rangle \langle a_1 b_2 | I'(\Delta) | b_1 a \rangle \\
& + \langle b_2 | T_z | b_2 \rangle \langle a b_1 | I(\Delta) | b_2 a_1 \rangle \langle a_1 b_2 | I''(\Delta) | b_1 a \rangle \\
& - \langle b_2 | T_z | b_2 \rangle \langle b_1 a | I(0) | b_2 a_1 \rangle \langle a_1 b_2 | I''(\Delta) | b_1 a \rangle \\
& + \langle a | T_z | a \rangle \langle a b_1 | I''(\Delta) | b_2 a_1 \rangle \langle a_1 b_2 | I(0) | a b_1 \rangle \\
& - \langle a | T_z | a \rangle \langle a b_1 | I''(\Delta) | b_2 a_1 \rangle \langle a_1 b_2 | I(\Delta) | b_1 a \rangle \\
& - 2 \langle a | T_z | a \rangle \langle a b_1 | I'(\Delta) | b_2 a_1 \rangle \langle a_1 b_2 | I'(\Delta) | b_1 a \rangle \\
& - \langle a | T_z | a \rangle \langle a b_1 | I(\Delta) | b_2 a_1 \rangle \langle a_1 b_2 | I''(\Delta) | b_1 a \rangle \\
& - \langle b_1 | T_z | b_1 \rangle \langle b_1 a | I(0) | b_2 a_1 \rangle \langle a_1 b_2 | I''(\Delta) | b_1 a \rangle \\
& + \langle a | T_z | a \rangle \langle b_1 a | I(0) | b_2 a_1 \rangle \langle a_1 b_2 | I''(\Delta) | b_1 a \rangle \\
& + \langle b_1 | T_z | b_1 \rangle \langle a b_1 | I''(\Delta) | b_2 a_1 \rangle \langle a_1 b_2 | I(\Delta) | b_1 a \rangle \\
& + 2 \langle b_1 | T_z | b_1 \rangle \langle a b_1 | I'(\Delta) | b_2 a_1 \rangle \langle a_1 b_2 | I(\Delta) | b_1 a \rangle \\
& + \langle b_1 | T_z | b_1 \rangle \langle a b_1 | I(\Delta) | b_2 a_1 \rangle \langle a_1 b_2 | I''(\Delta) | b_1 a \rangle \\
& + \langle a b_1 | I''(\Delta) | b_2 a_1 \rangle \langle a_1 | T_z | a_1 \rangle \langle a_1 b_2 | I(0) | a b_1 \rangle \\
& - \langle a b_1 | I''(\Delta) | b_2 a_1 \rangle \langle a_1 | T_z | a_1 \rangle \langle a_1 b_2 | I(\Delta) | b_1 a \rangle \\
& - 2 \langle a b_1 | I'(\Delta) | b_2 a_1 \rangle \langle a_1 | T_z | a_1 \rangle \langle a_1 b_2 | I'(\Delta) | b_1 a \rangle \\
& - \langle a b_1 | I(\Delta) | b_2 a_1 \rangle \langle a_1 | T_z | a_1 \rangle \langle a_1 b_2 | I''(\Delta) | b_1 a \rangle \\
& + \left. \langle b_1 a | I(0) | b_2 a_1 \rangle \langle a_1 | T_z | a_1 \rangle \langle a_1 b_2 | I''(\Delta) | b_1 a \rangle \right\} \\
& + G_a \sum_{b_1, b_2} \left\{ \langle a | T_z | a \rangle \langle a b_2 | I'(\Delta_2) | b_2 a \rangle \langle a b_1 | I'(\Delta_1) | b_1 a \rangle \right. \\
& - \langle b_2 | T_z | b_2 \rangle \langle a b_2 | I'(\Delta_2) | b_2 a \rangle \langle a b_1 | I'(\Delta_1) | b_1 a \rangle \\
& - \sum_P (-1)^P \left[\langle a | T_z | a \rangle \langle a b_2 | I''(\Delta_2) | b_2 a \rangle \langle a b_1 | I(\Delta_{aPa}) | PaPb_1 \rangle \right. \\
& + \langle b_2 | T_z | b_2 \rangle \langle a b_2 | I''(\Delta_2) | b_2 a \rangle \langle a b_1 | I(\Delta_{aPa}) | PaPb_1 \rangle \\
& + \left. \langle b_2 | T_z | b_2 \rangle \langle b_2 b_1 | I''(\Delta_{21}) | b_2 b_2 \rangle \langle b_2 a | I(\Delta_{b_1 P b_1}) | Pb_1 Pa \rangle \right] \left. \right\} \\
& + G_a \sum_{b_1, b_2, b_3} \sum_P (-1)^P \left\{ \langle a | T_z | a \rangle \langle a b_2 | I''(\Delta_2) | b_3 a \rangle \langle b_3 a | I(\Delta_{b_2 P b_2}) | Pb_2 Pb_1 \rangle \right. \\
& - \langle b_3 | T_z | b_3 \rangle \langle b_3 b_1 | I''(\Delta_{21}) | b_1 b_2 \rangle \langle b_2 a | I(\Delta_{b_2 P b_2}) | Pb_3 Pa \rangle \\
& - \left. \langle b_3 | T_z | b_3 \rangle \langle b_3 a | I''(\Delta_2) | a b_2 \rangle \langle b_2 b_1 | I(\Delta_{b_2 P b_2}) | Pb_3 Pb_1 \rangle \right\}, \tag{7.17}
\end{aligned}$$

$$X_{\text{red}, 2\text{-el}}^{(2)} = -\frac{i}{\pi} G_a \sum_b \sum_{n_1, n_2} \int_{-\infty}^{\infty} d\omega \frac{\langle b n_2 | I(\omega) | n_1 b \rangle \langle n_1 \xi_a | I(\omega + \Delta) | a n_2 \rangle}{(\varepsilon_b - \omega - u\varepsilon_{n_1})(\varepsilon_b - \omega - u\varepsilon_{n_2})}$$

$$\begin{aligned}
& + \frac{i}{\pi} G_a \sum_b \sum_{n_1, n_2} \int_{-\infty}^{\infty} d\omega \frac{\langle b n_2 | I(\omega) | n_1 b \rangle \langle n_1 a | I(\omega + \Delta) | a n_2 \rangle \langle a | T_z | a \rangle}{(\varepsilon_b - \omega - u\varepsilon_{n_1})(\varepsilon_b - \omega - u\varepsilon_{n_2})} \\
& \times \left[\frac{1}{\varepsilon_b - \omega - u\varepsilon_{n_1}} + \frac{1}{\varepsilon_b - \omega - u\varepsilon_{n_2}} \right] \\
& + \frac{i}{\pi} G_a \sum_b \sum_{n_1, n_2} \int_{-\infty}^{\infty} d\omega \frac{\langle b n_2 | I'(\omega) | n_1 b \rangle \langle n_1 a | I(\omega + \Delta) | a n_2 \rangle \langle a | T_z | a \rangle}{(\varepsilon_b - \omega - u\varepsilon_{n_1})(\varepsilon_b - \omega - u\varepsilon_{n_2})} \\
& - \frac{i}{\pi} G_a \sum_b \sum_{n_1, n_2, n_3} \int_{-\infty}^{\infty} d\omega \frac{\langle b n_2 | I(\omega) | n_1 b \rangle \langle n_3 | T_z | n_2 \rangle \langle n_1 a | I(\omega + \Delta) | a n_3 \rangle}{(\varepsilon_b - \omega - u\varepsilon_{n_1})(\varepsilon_b - \omega - u\varepsilon_{n_2})(\varepsilon_b - \omega - u\varepsilon_{n_3})} \\
& - \frac{i}{\pi} G_a \sum_b \sum_{n_1, n_2} \int_{-\infty}^{\infty} d\omega \frac{\langle a n_2 | I(\omega) | n_1 a \rangle \langle n_1 \xi_b | I(\omega + \Delta) | b n_2 \rangle}{(\varepsilon_a + \omega - u\varepsilon_{n_1})(\varepsilon_a + \omega - u\varepsilon_{n_2})} \\
& + \frac{i}{2\pi} G_a \sum_b \sum_{n_1, n_2} \int_{-\infty}^{\infty} d\omega \frac{\langle a n_2 | I(\omega) | n_1 a \rangle \langle n_1 b | I'(\omega + \Delta) | b n_2 \rangle \langle b | T_z | b \rangle}{(\varepsilon_a + \omega - u\varepsilon_{n_1})(\varepsilon_a + \omega - u\varepsilon_{n_2})} \\
& + \frac{i}{\pi} G_a \sum_b \sum_{n_1, n_2} \int_{-\infty}^{\infty} d\omega \frac{\langle a b | I(\omega) | n_1 n_2 \rangle \langle n_1 n_2 | I(\omega + \Delta) | b \xi_a \rangle}{(\varepsilon_a + \omega - u\varepsilon_{n_1})^2} \\
& - \frac{i}{\pi} G_a \sum_b \sum_{n_1, n_2} \int_{-\infty}^{\infty} d\omega \langle a b | I(\omega) | n_1 n_2 \rangle \left[\frac{\langle n_1 n_2 | I(\omega + \Delta) | b a \rangle}{(\varepsilon_a + \omega - u\varepsilon_{n_1})^3} \right. \\
& \left. - \frac{\langle n_1 n_2 | I'(\omega + \Delta) | b a \rangle}{(\varepsilon_a + \omega - u\varepsilon_{n_1})^2} \right] \langle a | T_z | a \rangle \\
& - \frac{1}{2} G_a \sum_{a_1} \sum_{b_1, b_2} \left\{ \langle a b_2 | I(0) | a_1 b_1 \rangle \langle a_1 b_1 | I''(\Delta) | b a \rangle \langle a | T_z | a \rangle \right. \\
& \left. - \langle a b_2 | I(\Delta) | b_1 a_1 \rangle \langle b_1 a_1 | I''(0) | b a \rangle \langle a | T_z | a \rangle \right\} \\
& + \frac{i}{\pi} G_a \sum_b \sum_{\substack{(\varepsilon_{n_1}, \varepsilon_{n_2}) \neq (\varepsilon_a, \varepsilon_b) \\ n_1, n_2}} \int_{-\infty}^{\infty} d\omega \left[\frac{\langle a b | I(\omega) | n_1 n_2 \rangle \langle n_1 n_2 | I(\omega + \Delta) | b a \rangle}{(\varepsilon_a + \omega - u\varepsilon_{n_1})^2 (\varepsilon_b - \omega - u\varepsilon_{n_2})} \right. \\
& \left. - \frac{\langle a b | I(\omega) | n_1 n_2 \rangle \langle n_1 n_2 | I'(\omega + \Delta) | b a \rangle}{(\varepsilon_a + \omega - u\varepsilon_{n_1})(\varepsilon_b - \omega - u\varepsilon_{n_2})} \right] \langle a | T_z | a \rangle \\
& + \frac{i}{\pi} G_a \sum_b \sum_{\substack{(\varepsilon_{n_1}, \varepsilon_{n_3}) \neq (\varepsilon_a, \varepsilon_b) \\ n_1, n_2, n_3}} \int_{-\infty}^{\infty} d\omega \frac{\langle a b | I(\omega) | n_1 n_2 \rangle \langle n_2 | T_z | n_3 \rangle \langle n_1 n_3 | I(\omega + \Delta) | b a \rangle}{(\varepsilon_a + \omega - u\varepsilon_{n_1})^2 (\varepsilon_b - \omega - u\varepsilon_{n_3})} \\
& + \frac{i}{\pi} G_a \sum_b \sum_{\substack{(\varepsilon_{n_1}, \varepsilon_{n_2}) \neq (\varepsilon_a, \varepsilon_b) \\ n_1, n_2, n_3}} \int_{-\infty}^{\infty} d\omega \frac{\langle a b | I(\omega) | n_1 n_2 \rangle \langle n_2 | T_z | n_3 \rangle \langle n_1 n_3 | I(\omega + \Delta) | b a \rangle}{(\varepsilon_a + \omega - u\varepsilon_{n_1})^2 (\varepsilon_b - \omega - u\varepsilon_{n_2})} \\
& - \frac{i}{\pi} G_a \sum_{b_1, b_2} \sum_{\substack{\varepsilon_n \neq \varepsilon_a \\ n}} \int_{-\infty}^{\infty} d\omega \frac{\langle a b_2 | I(\omega) | n b_1 \rangle \langle b_1 | T_z | b_1 \rangle \langle n b_1 | I(\omega + \Delta) | b_2 a \rangle}{(\varepsilon_a + \omega - u\varepsilon_{n_1})(\omega - i0)^2} \\
& - \frac{i}{\pi} G_a \sum_b \sum_{n_1, n_2, n_3} \int_{-\infty}^{\infty} d\omega \frac{\langle a b | I(\omega) | n_1 n_2 \rangle \langle n_2 | T_z | n_3 \rangle \langle n_1 n_3 | I(\omega + \Delta) | b a \rangle}{(\varepsilon_a + \omega - u\varepsilon_{n_1})^3}
\end{aligned}$$

$$\begin{aligned}
& + G_a \sum_{a_1} \sum_{b_1, b_2} \langle ab_2 | I(\Delta) | b_1 a_1 \rangle \langle a_1 | T_z | a_1 \rangle \langle b_1 a_1 | I''(0) | b_2 a \rangle \\
& + \frac{i}{\pi} G_a \sum_b \sum_{n_1, n_2} \int_{-\infty}^{\infty} d\omega \frac{\langle ab | I(\omega) | n_2 n_1 \rangle \langle n_2 n_1 | I(\omega + \Delta) | \xi_b a \rangle}{(\varepsilon_b - \omega - u\varepsilon_{n_1})^2} \\
& + \frac{i}{2\pi} G_a \sum_b \sum_{n_1, n_2} \int_{-\infty}^{\infty} d\omega \left[\frac{\langle ab | I(\omega) | n_2 n_1 \rangle \langle n_2 n_1 | I(\omega + \Delta) | ba \rangle \langle b | T_z | b \rangle}{(\varepsilon_b - \omega - u\varepsilon_{n_1})^3} \right. \\
& + \left. \frac{\langle ab | I'(\omega) | n_2 n_1 \rangle \langle n_2 n_1 | I(\omega + \Delta) | ba \rangle \langle b | T_z | b \rangle}{(\varepsilon_b - \omega - u\varepsilon_{n_1})^2} \right] \\
& + \frac{1}{2} G_a \sum_{a_1} \sum_{b_1, b_2} \left[\langle ab_1 | I(0) | a_1 b_2 \rangle \langle a_1 b_2 | I''(\Delta) | b_1 a \rangle \langle b_1 | T_z | b_1 \rangle \right. \\
& + \left. \langle ab_1 | I(\Delta) | b_2 a_1 \rangle \langle b_2 a_1 | I''(0) | b_1 a \rangle \langle b_1 | T_z | b_1 \rangle \right] \\
& - \frac{i}{2\pi} G_a \sum_b \sum_{\substack{(\varepsilon_{n_1}, \varepsilon_{n_2}) \neq (\varepsilon_a, \varepsilon_b) \\ n_1, n_2}} \int_{-\infty}^{\infty} d\omega \left[\frac{\langle ab | I'(\omega) | n_2 n_1 \rangle \langle n_2 n_1 | I(\omega + \Delta) | ba \rangle \langle b | T_z | b \rangle}{(\varepsilon_b - \omega - u\varepsilon_{n_1})(\varepsilon_a + \omega - u\varepsilon_{n_2})} \right. \\
& - \left. \frac{\langle ab | I(\omega) | n_2 n_1 \rangle \langle n_2 n_1 | I(\omega + \Delta) | ba \rangle \langle b | T_z | b \rangle}{(\varepsilon_b - \omega - u\varepsilon_{n_1})(\varepsilon_a + \omega - u\varepsilon_{n_2})^2} \right] \\
& - \frac{i}{\pi} G_a \sum_b \sum_{n_1, n_2} \int_{-\infty}^{\infty} d\omega \frac{\langle ab | I(\omega) | n_2 n_1 \rangle \langle n_2 n_1 | I(\omega) | \xi_a b \rangle}{(\varepsilon_a + \omega - u\varepsilon_{n_2})^2} \\
& - \frac{i}{\pi} G_a \sum_b \sum_{\substack{(\varepsilon_{n_1}, \varepsilon_{n_2}) \neq (\varepsilon_a, \varepsilon_b) \\ n_1, n_2}} \int_{-\infty}^{\infty} d\omega \frac{\langle ab | I(\omega) | n_2 n_1 \rangle \langle n_2 n_1 | I(\omega) | ab \rangle \langle a | T_z | a \rangle}{(\varepsilon_b - \omega - u\varepsilon_{n_1})(\varepsilon_a + \omega - u\varepsilon_{n_2})^2} \\
& + \frac{i}{\pi} G_a \sum_b \sum_{n_1, n_2} \int_{-\infty}^{\infty} d\omega \frac{\langle ab | I(\omega) | n_2 n_1 \rangle \langle n_2 n_1 | I(\omega) | ab \rangle \langle a | T_z | a \rangle}{(\varepsilon_a + \omega - u\varepsilon_{n_2})^3} \\
& + \frac{i}{\pi} G_a \sum_b \sum_{n_1, n_2} \int_{-\infty}^{\infty} d\omega \frac{\langle n_2 b | I(\omega) | a n_1 \rangle \langle n_1 \xi_a | I(\omega) | b n_2 \rangle}{(\varepsilon_b - \omega - u\varepsilon_{n_1})(\varepsilon_a - \omega - u\varepsilon_{n_2})} \\
& - \frac{i}{\pi} G_a \sum_b \sum_{n_1, n_2} \int_{-\infty}^{\infty} d\omega \frac{\langle n_2 b | I(\omega) | a n_1 \rangle \langle n_1 a | I(\omega) | b n_2 \rangle \langle a | T_z | a \rangle}{(\varepsilon_b - \omega - u\varepsilon_{n_1})(\varepsilon_a - \omega - u\varepsilon_{n_2})^2} \\
& - \frac{i}{\pi} G_a \sum_b \sum_{n_1, n_2} \int_{-\infty}^{\infty} d\omega \frac{\langle ab | I(\omega) | n_1 n_2 \rangle \langle n_1 n_2 | I(\omega) | a \xi_b \rangle}{(\varepsilon_a - \omega - u\varepsilon_{n_1})^2} \\
& - \frac{i}{2\pi} G_a \sum_b \sum_{\substack{(\varepsilon_{n_1}, \varepsilon_{n_2}) \neq (\varepsilon_a, \varepsilon_b) \\ n_1, n_2}} \int_{-\infty}^{\infty} d\omega \frac{\langle ab | I(\omega) | n_1 n_2 \rangle \langle n_1 n_2 | I(\omega) | ab \rangle \langle b | T_z | b \rangle}{(\varepsilon_a - \omega - u\varepsilon_{n_1})(\varepsilon_b + \omega - u\varepsilon_{n_2})^2} \\
& - \frac{i}{2\pi} G_a \sum_b \sum_{n_1, n_2} \int_{-\infty}^{\infty} d\omega \frac{\langle ab | I(\omega) | n_1 n_2 \rangle \langle n_1 n_2 | I(\omega) | ab \rangle \langle b | T_z | b \rangle}{(\varepsilon_a - \omega - u\varepsilon_{n_1})^3} \\
& + \frac{i}{2\pi} G_a \sum_b \sum_{n_1, n_2, n_3} \int_{-\infty}^{\infty} d\omega \frac{\langle n_2 a | I(\omega) | b n_1 \rangle \langle n_3 | T_z | n_2 \rangle \langle n_1 b | I(\omega) | a n_3 \rangle}{(\varepsilon_a - \omega - u\varepsilon_{n_1})(\varepsilon_b - \omega - u\varepsilon_{n_2})(\varepsilon_b - \omega - u\varepsilon_{n_3})}
\end{aligned}$$

$$\begin{aligned}
& - \frac{i}{2\pi} G_a \sum_b \sum_{\substack{(\varepsilon_{n_1}, \varepsilon_{n_2}) \neq (\varepsilon_a, \varepsilon_b) \\ n_1, n_2, n_3}} \int_{-\infty}^{\infty} d\omega \frac{\langle ab|I(\omega)|n_1 n_2\rangle \langle n_2|T_z|n_3\rangle \langle n_1 n_3|I(\omega)|ab\rangle}{(\varepsilon_a - \omega - u\varepsilon_{n_1})^2 (\varepsilon_b + \omega - u\varepsilon_{n_2})} \\
& - \frac{i}{2\pi} G_a \sum_b \sum_{\substack{(\varepsilon_{n_1}, \varepsilon_{n_3}) \neq (\varepsilon_a, \varepsilon_b) \\ n_1, n_2, n_3}} \int_{-\infty}^{\infty} d\omega \frac{\langle ab|I(\omega)|n_1 n_2\rangle \langle n_2|T_z|n_3\rangle \langle n_1 n_3|I(\omega)|ab\rangle}{(\varepsilon_a - \omega - u\varepsilon_{n_1})^2 (\varepsilon_b + \omega - u\varepsilon_{n_3})} \\
& + \frac{i}{2\pi} G_a \sum_{b_1, b_2} \sum_{\substack{\varepsilon_n \neq \varepsilon_a \\ n}} \int_{-\infty}^{\infty} d\omega \frac{\langle ab_2|I(\omega)|nb_1\rangle \langle b_1|T_z|b_1\rangle \langle nb_1|I(\omega)|ab_2\rangle}{(\varepsilon_a - \omega - u\varepsilon_{n_1})(\omega + i0)^2} \\
& + \frac{i}{2\pi} G_a \sum_b \sum_{n_1, n_2, n_3} \int_{-\infty}^{\infty} d\omega \frac{\langle ab|I(\omega)|n_1 n_2\rangle \langle n_2|T_z|n_3\rangle \langle n_1 n_3|I(\omega)|ab\rangle}{(\varepsilon_a - \omega - u\varepsilon_{n_1})^3} \\
& + \frac{i}{\pi} G_a \sum_b \sum_{n_1, n_2} \int_{-\infty}^{\infty} d\omega \frac{\langle n_2 a|I(\omega)|bn_1\rangle \langle n_1 \xi_b|I(\omega)|an_2\rangle}{(\varepsilon_a - \omega - u\varepsilon_{n_1})(\varepsilon_b - \omega - u\varepsilon_{n_2})} \\
& - \frac{i}{2\pi} G_a \sum_b \sum_{n_1, n_2} \int_{-\infty}^{\infty} d\omega \frac{\langle n_2 a|I(\omega)|bn_1\rangle \langle n_1 b|I(\omega)|an_2\rangle \langle b|T_z|b\rangle}{(\varepsilon_a - \omega - u\varepsilon_{n_1})(\varepsilon_b - \omega - u\varepsilon_{n_2})^2} \\
& - \frac{i}{2\pi} G_a \sum_b \sum_{\substack{(\varepsilon_{n_1}, \varepsilon_{n_3}) \neq (\varepsilon_a, \varepsilon_b) \\ n_1, n_2, n_3}} \int_{-\infty}^{\infty} d\omega \frac{\langle ab|I(\omega)|n_2 n_1\rangle \langle n_2|T_z|n_3\rangle \langle n_3 n_1|I(\omega)|ab\rangle}{(\varepsilon_a + \omega - u\varepsilon_{n_2})^2 (\varepsilon_a + \omega - u\varepsilon_{n_3})} \\
& - \frac{i}{2\pi} G_a \sum_b \sum_{\substack{(\varepsilon_{n_1}, \varepsilon_{n_2}) \neq (\varepsilon_a, \varepsilon_b) \\ n_1, n_2, n_3}} \int_{-\infty}^{\infty} d\omega \frac{\langle ab|I(\omega)|n_2 n_1\rangle \langle n_2|T_z|n_3\rangle \langle n_3 n_1|I(\omega)|ab\rangle}{(\varepsilon_a + \omega - u\varepsilon_{n_2})(\varepsilon_a + \omega - u\varepsilon_{n_3})^2} \\
& + \frac{i}{2\pi} G_a \sum_{a_1} \sum_b \sum_{\substack{\varepsilon_n \neq \varepsilon_b \\ n}} \int_{-\infty}^{\infty} d\omega \frac{\langle ab|I(\omega)|a_1 n\rangle \langle a_1|T_z|a_1\rangle \langle a_1 n|I(\omega)|ab\rangle}{(\varepsilon_b + \omega - u\varepsilon_n)(-\omega + i0)^2} \\
& - \frac{i}{2\pi} G_a \sum_b \sum_{n_1, n_2, n_3} \int_{-\infty}^{\infty} d\omega \frac{\langle ab|I(\omega)|n_2 n_1\rangle \langle n_2|T_z|n_3\rangle \langle n_3 n_1|I(\omega)|ab\rangle}{(\varepsilon_a + \omega - u\varepsilon_{n_2})^3} \\
& + \frac{i}{2\pi} G_a \sum_b \sum_{n_1, n_2, n_3} \int_{-\infty}^{\infty} d\omega \frac{\langle n_2 b|I(\omega)|an_1\rangle \langle n_3|T_z|n_2\rangle \langle n_1 a|I(\omega)|bn_3\rangle}{(\varepsilon_b - \omega - u\varepsilon_{n_1})(\varepsilon_a - \omega - u\varepsilon_{n_2})(\varepsilon_b - \omega - u\varepsilon_{n_3})} \\
& + G_a \sum_b \left\{ \frac{i}{2\pi} \sum_{\substack{(\varepsilon_{n_1}, \varepsilon_{n_2}) \neq (\varepsilon_a, \varepsilon_b) \\ n_1, n_2}} \int_{-\infty}^{\infty} d\omega \left[\frac{\langle ab|I(\omega)|n_1 n_2\rangle \langle n_1 n_2|I'(\Delta - \omega)|ba\rangle}{(\varepsilon_a - \omega - u\varepsilon_{n_1})(\varepsilon_b + \omega - u\varepsilon_{n_2})} \right. \right. \\
& - \left. \frac{\langle ab|I(\omega)|n_1 n_2\rangle \langle n_1 n_2|I(\Delta - \omega)|ba\rangle}{(\varepsilon_a - \omega - u\varepsilon_{n_1})^2 (\varepsilon_b + \omega - u\varepsilon_{n_2})} \right] \\
& - \frac{i}{2\pi} \sum_{n_1, n_2} \int_{-\infty}^{\infty} d\omega \left[\frac{\langle ab|I(\omega)|n_1 n_2\rangle \langle n_1 n_2|I'(\Delta - \omega)|ba\rangle}{(\varepsilon_a - \omega - u\varepsilon_{n_1})^2} \right. \\
& - \left. \frac{\langle ab|I(\omega)|n_1 n_2\rangle \langle n_1 n_2|I(\Delta - \omega)|ba\rangle}{(\varepsilon_a - \omega - u\varepsilon_{n_1})^3} \right] \\
& + \frac{i}{2\pi} \sum_{n_1, n_2} \int_{-\infty}^{\infty} d\omega \left[\frac{\langle an_2|I(\omega)|n_1 a\rangle \langle n_1 b|I'(\Delta - \omega)|bn_2\rangle}{(\varepsilon_a - \omega - u\varepsilon_{n_1})(\varepsilon_a - \omega - u\varepsilon_{n_2})} \right.
\end{aligned}$$

$$\begin{aligned}
& - \frac{\langle a n_2 | I(\omega) | n_1 a \rangle \langle n_1 b | I(\Delta - \omega) | b n_2 \rangle}{(\varepsilon_a - \omega - u \varepsilon_{n_1})(\varepsilon_a - \omega - u \varepsilon_{n_2})} \left(\frac{1}{\varepsilon_a - \omega - u \varepsilon_{n_1}} + \frac{1}{\varepsilon_a - \omega - u \varepsilon_{n_2}} \right) \Bigg] \\
& + \frac{i}{2\pi} \sum_{n_1, n_2}^{(\varepsilon_{n_1}, \varepsilon_{n_2}) \neq (\varepsilon_a, \varepsilon_b)} \int_{-\infty}^{\infty} d\omega \frac{\langle a b | I(\omega) | n_1 n_2 \rangle \langle n_2 n_1 | I(\omega) | b a \rangle}{(\varepsilon_a - \omega - u \varepsilon_{n_1})^2 (\varepsilon_b + \omega - u \varepsilon_{n_2})} \\
& - \frac{i}{2\pi} \sum_{n_1, n_2} \int_{-\infty}^{\infty} d\omega \frac{\langle a b | I(\omega) | n_1 n_2 \rangle \langle n_2 n_1 | I(\omega) | b a \rangle}{(\varepsilon_a - \omega - u \varepsilon_{n_1})^3} \\
& + \frac{i}{2\pi} \sum_{n_1, n_2} \int_{-\infty}^{\infty} d\omega \frac{\langle a n_1 | I(\omega) | n_2 b \rangle \langle b n_2 | I(\omega) | n_1 a \rangle}{(\varepsilon_b - \omega - u \varepsilon_{n_1})(\varepsilon_a - \omega - u \varepsilon_{n_2})^2} \Bigg\} \langle a | T_Z | a \rangle. \tag{7.18}
\end{aligned}$$

Here, the $(\varepsilon_{n_1}, \varepsilon_{n_2}) \neq (\varepsilon_a, \varepsilon_b)$ means that terms with energies $\varepsilon_{n_1} + \varepsilon_{n_2} = \varepsilon_a + \varepsilon_b$ should be omitted in the summation.

7.4 COUNTERTERM CONTRIBUTION $\chi_{\text{CT}}^{(2)}$

The formal expressions for the contribution of the counterterm diagrams shown in Fig. 4.4 are given by

$$\chi_{\text{ct}}^{(2)} = \chi_{\text{ct-1}}^{(2)} + \chi_{\text{ct-2}}^{(2)}, \tag{7.19}$$

where

$$\begin{aligned}
\chi_{\text{ct-1}}^{(2)} = & 2 G_a \sum_b \left[\langle \xi_a \eta_b | I(0) | a b \rangle - \langle \eta_b \xi_a | I(\Delta) | a b \rangle + \langle \eta_a \xi_b | I(0) | a b \rangle - \langle \xi_b \eta_a | I(\Delta) | a b \rangle \right. \\
& + \langle \xi_a b | I(0) | \eta_a b \rangle - \langle b \xi_a | I(\Delta) | \eta_a b \rangle + \langle a \xi_b | I(0) | a \eta_b \rangle - \langle \xi_b a | I(\Delta) | a \eta_b \rangle \\
& + \langle \xi_a b | I(0) | a \eta_b \rangle - \langle \xi_b a | I(\Delta) | \eta_a b \rangle + \langle \eta_a b | I(0) | a \xi_b \rangle - \langle \eta_b a | I(\Delta) | \xi_a b \rangle \\
& + \left(\langle a b | I(0) | a b \rangle - \langle b a | I(\Delta) | a b \rangle \right) \left(\langle \xi'_a | V^{\text{scr}} | a \rangle + \langle \xi'_b | V^{\text{scr}} | b \rangle \right) - \langle b a | I'(\Delta) | a b \rangle \\
& \times \left(\langle \xi_a | V^{\text{scr}} | a \rangle - \langle \xi_b | V^{\text{scr}} | b \rangle \right) - \langle a | T_Z | a \rangle \langle \eta_b a | I'(\Delta) | a b \rangle + \langle b | T_Z | b \rangle \langle b \eta_a | I'(\Delta) | a b \rangle \\
& - \langle a | V^{\text{scr}} | a \rangle \langle \xi_b a | I'(\Delta) | a b \rangle + \langle b | V^{\text{scr}} | b \rangle \langle b \xi_a | I'(\Delta) | a b \rangle - \frac{1}{2} \langle b a | I''(\Delta) | a b \rangle \\
& \times \left(\langle a | T_Z | a \rangle - \langle b | T_Z | b \rangle \right) \left(\langle a | V^{\text{scr}} | a \rangle - \langle b | V^{\text{scr}} | b \rangle \right) \\
& + (-1)^P \sum_P \left(\langle \xi_a | V^{\text{scr}} | \zeta_{b|P_a P_b} \rangle + \langle \xi_b | V^{\text{scr}} | \zeta_{a|P_b P_a} \rangle + \langle \eta_a | T_Z | \zeta_{b|P_a P_b} \rangle \right. \\
& + \langle \eta_b | T_Z | \zeta_{a|P_b P_a} \rangle + \langle a | T_Z | a \rangle \langle a | V^{\text{scr}} | \zeta'_{b|P_a P_b} \rangle + \langle b | T_Z | b \rangle \langle b | V^{\text{scr}} | \zeta'_{a|P_b P_a} \rangle \\
& \left. + \langle a | V^{\text{scr}} | a \rangle \langle a | T_Z | \zeta'_{b|P_a P_b} \rangle + \langle b | V^{\text{scr}} | b \rangle \langle b | T_Z | \zeta'_{a|P_b P_a} \rangle \right), \tag{7.20}
\end{aligned}$$

corresponds to the five diagrams in the first line of Fig. 4.4 and

$$\begin{aligned} \chi_{\text{ct-2}}^{(2)} = & G_a \left(2\langle \xi_a | V^{\text{scr}} | \eta_a \rangle + 2\langle \xi'_a | V^{\text{scr}} | a \rangle \langle a | V^{\text{scr}} | a \rangle + \langle \eta_a | T_z | \eta_a \rangle \right. \\ & \left. + \langle \eta'_a | V^{\text{scr}} | a \rangle \langle a | T_z | a \rangle \right) \end{aligned} \quad (7.21)$$

stays for the two diagrams in second line of Fig. 4.4. The employed functions are defined by Eq. 4.28).

EHRENWÖRTLICHE ERKLÄRUNG

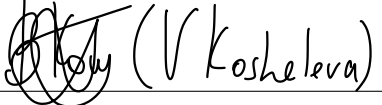
Ich erkläre hiermit ehrenwörtlich, dass ich die vorliegende Arbeit selbstständig, ohne unzuässige Hilfe dritter und ohne Benutzung anderer als der angegebenen Hilfsmittel und Literatur angefertigt habe. Die aus anderen Quellen direkt oder indirekt übernommenen Daten und Konzepte sind unter Angabe der Quelle gekennzeichnet. Bei der Anfertigung dieser Arbeit haben mir meine Betreuer und die Koautoren oben genannter Publikationen geholfen.

Weitere Personen waren an der inhaltlich-materiellen Erstellung der vorliegenden Arbeit nicht beteiligt. Insbesondere habe ich hierfür nicht die entgeltliche Hilfe von Vermittlungs- bzw. Beratungsdiensten (Promotionsberater oder andere Personen) in Anspruch genommen.

Niemand hat von mir unmittelbar oder mittelbar geldwerte Leistungen für Arbeiten erhalten, die im Zusammenhang mit dem Inhalt der vorgelegten Dissertation stehen. Die Arbeit wurde bisher weder im In- noch im Ausland in gleicher oder ähnlicher Form einer anderen Prüfungsbehörde vorgelegt. Die geltende Promotionsordnung der Physikalisch-Astronomischen Fakultät ist mir bekannt.

Ich versichere ehrenwörtlich, dass ich nach bestem Wissen die reine Wahrheit gesagt und nichts verschwiegen habe.

Jena,


Valeriia Kosheleva

CURRICULUM VITAE

PERSONAL INFORMATION

Name Valeriia Kosheleva
Born 14 December 1993 in Arkhangelsk, Russia

SCHOOL EDUCATION

09.2001 - 06.2008 City Gymnasium No. 3, Arkhangelsk, Russia
09.2008 – 06.2012 Arkhangelsk City Lyceum named after M.V. Lomonosov,
Arkhangelsk, Russia

UNIVERSITY EDUCATION

09.2012 - 07.2016 Bachelor of Physics, Physics Department, Saint-Petersburg State University, Russia
09.2016 - 07.2018 Master of Physics, Physics Department, Saint-Petersburg State University, Russia
11.2018 - 03.2022 Promotion, Physikalisch-Astronomische Fakultät, Friedrich-Schiller-Universität Jena, Germany

EMPLOYMENT

03.2019 - 03.2022 Research fellow, Helmholtz Institute Jena, Germany